NASA Contractor Report 172410

Flutter Parametric Studies Of Cantilevered Twin-Engine-Transport Type Wing With And Without Winglet

Volume II. Transonic & Density Effect Investigations

Kumar G. Bhatia, and K.S. Nagaraja

Boeing Commercial Airplane Company

Seattle, Wa.

Contract NAS1-17539

September 1984

National Aeronautics and Space Administration

Langley Research Center
Hampton Virginia 23665

FOREWORD

This document presents results of a recently completed joint Boeing-NASA program to study the effects of winglets on flutter characteristics of twin—engine transport type wings and to verify flutter analysis methodology. This document is one of the two proposed NASA publications dealing with this study and contains details sufficient to permit independent vibration and flutter analysis. A second publication, a NASA Technical Paper (TP), is planned for 1985, and will contain a technical summary. The present document is in two volumes:

Volume I - Low-Speed Investigations
Volume II - Transonic & Density Effect Investigations.

The two volumes are arranged such that each volume may be used independently of the other volume. The foreword and introduction are common to both volumes and are included in each volume along with a complete table of contents covering both volumes.

Mr. C. L. Ruhlin of Configuration Aeroelasticity Branch of NASA Langley Research Center was the test engineer for flutter tests conducted in the NASA Langley 16' Transonic Dynamic Tunnel, and was the contract monitor for preparation of the two NASA documents. The Boeing Commercial Airplane Company personnel who were major contributors to this study are:

K. G. Bhatia	Flutter - Principal Investigator
J. F. Bueno	Structures - Program Manager
A. W. Byrski	Loads & Flutter - Supervisor
W. F. Carver	Loads
M. G. Friend	Model Design
J. J. Hill	Weights
R. G. Kunkel	Model Shop
D. W. Lee, Jr.	Weights
D. J. Marzano	Flutter
J. E. Morrison	Loads
R. M. Nadreau	Structural Dynamics Laboratory
K. S. Nagaraja	Flutter
C R. Pickrel	Structural Dynamics Laboratory
S. Ros	Loads
J. L. Stelma	Flutter
J. H. Thompson	Model Design

LIST OF SYMBOLS

a_c	AERODYNAMIC CENTER
C_{n_α}	SECTIONAL LIFT-CURVE SLOPE PER DEGREE ANGLE OF ATTACK
C_{n_β}	SECTIONAL LIFT-CURVE SLOPE PER DEGREE SIDESLIP ANGLE
C_N	WING (TOTAL) LIFT COEFFICIENT
M	MACH NUMBER
q,Q	DYNAMIC PRESSURE
q_F, Q_F	FLUTTER DYNAMIC PRESSURE

LIST OF CONTENTS

VOLUME II – TRANSONIC & DENSITY EFFECT INVESTIGATIONS

LIST OF TABLES – VOLUME II

LIST OF FIGURES - VOLUME II

LIST OF FIGURES - VOLUME II (Cont'd)

LIST OF FIGURES - VOLUME II (Cont'd)

LIST OF FIGURES - VOLUME II (Concluded)

LIST OF FIGURES - VOLUME II (Cont'd)

LIST OF FIGURES - VOLUME II (Cont'd)

APPENDIX A MODEL GEOMETRY, MASS & STIFFNESS DATA

LIST OF FIGURES - VOLUME II (Cont'd)

APPENDIX B AERODYNAMIC DATA

LIST OF FIGURES - VOLUME II (Cont'd)

APPENDIX B AERODYNAMIC DATA

LIST OF FIGURES - VOLUME II (Concluded)

APPENDIX C VIBRATION FREQUENCIES & NODE LINES

LIST OF CONTENTS
VOLUME I–LOW-SPEED INVESTIGATIONS

LIST OF TABLES – VOLUME I

LIST OF FIGURES – VOLUME I

LIST OF FIGURES – VOLUME I (Cont'd)

LIST OF FIGURES – VOLUME I (Cont'd)

LIST OF FIGURES - VOLUME I (Cont'd)

LIST OF FIGURES – VOLUME I(Cont'd)

APPENDIX

LIST OF FIGURES – VOLUME I (Concluded)

1.0 Summary

Flutter characteristics of a cantilevered high aspect ratio wing with winglet were investigated. The configuration represented a current technology, twin-engine airplane. A low-speed and a high-speed model were used to evaluate compressibility effects through transonic Mach numbers and a wide range of mass-density ratios. The results of the investigation are described in two volumes of this NASA CR and summarized in a forthcoming NASA TP. The results from the test in NASA Langley 16' Transonic Dynamic Tunnel (TDT) and analysis-test correlation are included in this Volume II.

The low-speed model was retested in TDT to determine altitude or mass-density ratio effects. This model had been earlier tested in General Dynamics, Convair Division, San Diego low-speed tunnel, and the results are discussed in Volume I. The mass-density ratio was varied in TDT by testing the low-speed model in both air and freon. The configurations with winglet showed a switch in flutter mode, from nacelle vertical bending to second wing bending, due to decrease in mass-density ratio. The mass-density ratio effects, including the mode switch, were satisfactorily correlated between analysis and test.

The high-speed model was tested in freon for a Mach range of about 0.6 to 0.91 and dynamic pressures up to 200 psf. Four flutter mechanisms were obtained in test, as well as analysis, from various combinations of configuration parameters. The winglet aerodynamic effects were significant and caused reduction in flutter dynamic pressure. The winglet related flutter for the configuration tested, was found to be amenable to the conventional flutter analysis techniques. The analysis showed that coupling between wing tip vertical and chordwise motions has significant effect under some conditions.

2.0 Introduction

The interest in using wing-tip-mounted winglets to reduce drag for transport airplanes was stimulated by the work reported in Reference (1). One of the first applications of winglets was for the KC-135 airplane based on a potential drag reduction of about six percent estimated in Reference (2). The KC-135 Winglet Flight Research and Demonstration Program was formulated to design, fabricate and flight test a set of winglets to prove the drag reduction and other characteristics of the winglet concept. This program included a low-speed wind-tunnel flutter model test and a flight flutter test program (Ref. 3). The critical mode during flight flutter test was a 3.0 Hz low-damped mode occurring with a light fuel loading at 21,500 feet altitude and with zero degree cant angle and -4 degrees incidence winglets. Flight testing for this configuration was terminated at 370 KEAS, rather than the test goal of 395 KEAS, due to low damping ($g = 0.015$). The low damping obtained for this mode was not predicted by flutter analysis. The lack of correlation was judged to be due to limitations of current linearized aerodynamic theory and inability to represent transonic effects. Winglets have also been considered for the B-747 airplane as a part of the NASA Energy Efficient Transport Program (Ref. 4). Two flutter modes were obtained in the low-speed model test for the configuration with winglets. These flutter mechanisms were not present for the baseline configuration without winglets and were shown to result from winglet aerodynamics rather than mass effects. Flutter speeds for the configuration with winglets were significantly lower than the baseline configuration. It was suggested that the flutter mechanisms could be predicted by incorporating static-lift effects as with T-tail type flutter analysis.

A transonic flutter model study of a supercritical wing with winglet for an executive-jet-transport airplane (Ref. 5) reported a good analysis-test correlation. The winglet addition decreased flutter speed by seven percent, of which a five percent decrease was due to the wing-tip mass effect. Thus, there was no significant reduction in flutter speed due to winglet aerodynamics. Results of another application of winglets for the DC-10 airplane, under the NASA Energy Efficient Transport Program, were recently published (Refs 6 and 7). A low-speed flutter model test showed that the winglets had generally detrimental effects on the flutter characteristics with small-to-moderate

degradation in the basic wing flutter mode and a large degradation in a higher frequency wing flutter mode. During the flight test of the DC-10 airplane with winglets, 500 pounds of mass balance was installed in each wing tip to ensure adequate flutter margins for flight testing.

It appears from the available data that winglets generally caused degradation in flutter speed. The actual reduction in flutter speed varied with the configuration. The KC-135 flight test experience of encountering an unexpected low-damped mode highlighted the technical risk involved in flutter assessment of an airplane configuration with winglets. The only transonic wind-tunnel flutter test data available on a scaled airplane wing was for an executivejet-transport wing which showed a small reduction in flutter speed due to addition of a winglet. These considerations led to a joint Boeing/NASA program to develop a flutter methodology for winglet configured wings. A typical, current technology, twin-engine transport wing was selected as the basis for the study. A test program was outlined as follows:

A. Pressure Model Test for Aerodynamic Data Base

B. Low-Speed Test
   - (i) Model Ground Vibration Test (GVT)
   - (ii) Flutter Test and Parametric Studies
   - (iii) Analysis-Test Correlation

C. Test in NASA Langley 16' Transonic Dynamics Tunnel (TDT)
   - (i) Retest of Low-Speed Flutter Model for Mass-Density Ratio Effects
   - (ii) Selection of High-Speed Model Configurations
   - (iii) High-Speed Model GVT
   - (iv) High-Speed Model Flutter Test
   - (v) Analysis-Test Correlation

Cantilevered wing models were used in all three tests. It was judged that once the wing-winglet interaction was adequately represented, the effect of body and empennage on flutter could be accounted for. The pressure model test was designed to collect

aerodynamic data for both loads and flutter analysis. Figure 1 shows the model installation in the Boeing Transonic Wind Tunnel (BTWT). Pressure data was collected for a Mach number–angle of attack grid for the following configurations:

A. (i) Clean wing with nominal tip
   (ii) Clean wing with winglet at 20° cant angle (outboard relative to the vertical)

B. (i) Wing with nacelle and nominal tip
   (ii) Wing with nacelle and
      (a) Winglet at 20° cant
      (b) Winglet at 10° cant
      (c) Winglet at 0° cant

C. Configurations described under B above but with the wing sweep angle increased by 5°

D. Configurations described under B but with the wing sweep angle decreased by 5°

The pressure data was reduced to sectional data. The wing sectional data was linearized with respect to angle of attack to obtain C_{n_α}, and corrected to remove the effect of the model wing flexibility. The wing sectional data was also linearized with respect to the wing sweep angle to obtain C_{n_β}, but was not corrected for the model flexibility effects. The winglet sectional data was similarly linearized without being corrected for the model flexibility. The linearized sectional data was used in the flutter analysis.

The choice of flutter test configurations and parameters was dictated by the task definition, viz., to develop flutter methodology. Therefore, the test was planned to obtain different kinds of flutter modes so that the winglet mass and aerodynamic effects could be separately identified for each of the flutter modes. The low-speed flutter test was designed with a larger number and a wider range of parameters taking advantage of the relative ease of atmospheric low-speed flutter testing compared to high-speed testing. The high-speed flutter test was designed after establishing analysis-test correlation for the low-speed flutter test. Based on the knowledge derived from the low-speed flutter

test, a reduced number of configurations and parameters were selected for testing in the high-speed tunnel. The low-speed flutter test was conducted at the General Dynamics, Convair Division, San Diego wind tunnel facility. The transonic test was conducted in the NASA Langley 16' Transonic Dynamics Tunnel (TDT). A schematic diagram of the wing and the wing tips tested, is shown in figure 2.

The low-speed model wing was of conventional, single-spar construction with wing sections perpendicular to the spar. The configurations for the low-speed flutter model test were:

A. (i) Clean wing (without nacelle)
   (ii) Wing with winglet (without nacelle)
   (iii) Wing with winglet mass simulator (without nacelle)

B. (i) Wing with nacelle
   (ii) Wing with nacelle and winglet
   (iii) Wing with nacelle and winglet mass simulator

C. (i) Wing with nacelle boom
   (ii) Wing with nacelle boom and winglet
   (iii) Wing with nacelle boom and winglet mass simulator

The winglet mass simulator was designed to represent winglet weight, center of gravity and inertia properties to help separate winglet inertia and aerodynamic effects. The results from configurations with nacelle boom were not used due to good correlation obtained for the configurations with nacelle.

The parameters varied were:

a. angle of attack,
b. model yaw angle,
c. wing fuel (0%, 50%, 75%, and 100%),

d. nacelle strut side bending frequency,
e. nacelle strut vertical bending frequency,
f. winglet/simulator cant angle (0°, 10°, 20° relative to the vertical), and
g. winglet/simulator stiffness.

The variation of angle of attack and yaw angle was included to evaluate the static-lift effects. The effect of nacelle side bending frequency was found to be small for the test configuration, and is not discussed further in this document.

The main objective of flutter testing in the NASA Langley TDT was to determine the effects of Mach number on flutter characteristics. However, the flutter points obtained in a variable density, transonic tunnel depend upon the mass-density ratio as well as the Mach effects. Therefore the low-speed model was retested in TDT to determine altitude or mass-density ratio effects at lowspeeds. Only two configurations, empty wing with nominal nacelle and with and without winglet, were tested. The analysis had shown a switch in flutter mode, from nacelle vertical bending to second wing bending, due to decrease in the mass-density ratio. To obtain the mode change in the tunnel, mass-density ratio was varied by testing the configuration with winglet in both air and freon. The strategy was to show that the mass-density ratio effects, for a winglet configured wing, could be predicted at low Mach numbers. The flutter correlation at higher Mach numbers could then be evaluated on the basis of compressibility and transonic effects. The high-speed model was tested in freon for a Mach range of about 0.6 to 0.91 and dynamic pressures up to 200 psf.

The high-speed model was constructed primarily of fiberglass sandwich components with ribs, spars, stringers and skin representing a modern transport wing. Wing fuel was simulated by water. The model was instrumented with 20 accelerometers, 23 pressure transducers in two chordwise arrays, and strain gages to monitor wing and winglet loads. The following configurations were selected for testing:

A. Wing with nacelle and nominal tip
B. Wing with nacelle and ballasted tip
C. Wing with nacelle and winglet

The ballasted tip configuration was selected to determine the effect of winglet weight separately from winglet aerodynamics. A winglet mass simulator similar to that used on the low-speed model, would have introduced unknown aerodynamic effects at high speeds. Therefore, the ballast weight was incorporated inside the wing contour resulting in a wing tip aerodynamically identical to the nominal tip. The test parameters selected were:

a. wing fuel (empty and full),
b. nacelle strut vertical bending frequency,
c. winglet cant angle (0° and 20° relative to the vertical), and
d. angle of attack.

Two nacelle strut vertical bending springs were used. The nominal strut vertical bending spring (nominal nacelle) and the softer strut vertical bending spring (soft nacelle) gave rise to different flutter characteristics due to differences in coupling of nacelle motion with inboard wing torsion. A series of high angle of attack runs, within the model load limits, was run to verify that there were no single-degree-of-freedom instabilities at transonic speeds.

This volume pertains to the flutter test conducted in the NASA Langley tunnel. The highlights are covered in the main body. Appendices A, B and C contain sufficient data, in the form of figures and tables, to allow an independent analysis. Appendix D contains procedure used to modify calculated stiffness matrix. A summary of experimental results is tabulated in Appendix E.

3.0 Mass-Density Ratio Effects at Low Mach Numbers

The low-speed model tested earlier in the Convair tunnel, was retested in the TDT. Only two configurations, empty wing with nominal nacelle and with and without winglet, were tested. The configurations tested were identical to the similar configurations tested earlier at Convair except for the following:

(a) The model was wall mounted and supported from the balance in the TDT. The body fairing of the high-speed model was used. In the Convair tunnel, the model was mounted on a stiffened body supported by an A-frame bolted to the tunnel floor at the centerline of the tunnel. The model test frequencies did not change significantly between the two installations. Table 1 lists the two sets of frequencies and the analyatical frequencies for the configuration with winglet. Figure 3 shows a photograph of the low-speed model installed in TDT.

(b) The model tested in the Convair tunnel had shims installed in the wing sections to simulate the wing twist distribution for most of the runs. The model was installed in the TDT, without any shims. The effects of wing twist for the winglet configuration with 75% fuel case was evaluated in the Convair test and is summarized below:

TUNNEL	WING TIP	SHIMS	SPEED (KTAS)	FLUTTER DYN PR (PSF)	FREQ (Hz)
CONVAIR	WINGLET	YES	90.9	27.4	8.7
CONVAIR	WINGLET	NO	88.8	25.8	8.6
CONVAIR	NOMINAL	YES	97.9	31.7	8.7
CONVAIR	NOMINAL	NO	96.6	30.8	8.6

Since the repeatability of flutter speed was determined tc be within 1 KTAS, there appears to be a small drop in the flutter speed due to removal of the shims from the wing sections for the configuration with winglet. The repeatability of flutter speeds between the Convair and TDT (air) for the two empty fuel configurations is summarized below:

TUNNEL	WING TIP	SHIMS	DENSITY (SLUGS/ FT^3)x 10^3	SPEED (KTAS)	FLUTTER DYN PRESS (lb/ft^2)	FREQ (Hz)
CONVAIR	WINGLET	YES	2.329	89.2	26.4	8.8
TDT	WINGLET	NO	2.309	86.0	24.3	9.0
CONVAIR	NOMINAL	YES	2.322	96.5	30.8	8.7
TDT	NOMINAL	NO	2.349	91.2	27.8	9.0

The difference in the flutter speed for the configuration without winglet is about 5%, and is higher than the configuration with winglet. The higher difference in flutter speeds for configuration with nominal tip was not looked into in detail as more emphasis was placed on the configuration with winglet. The mass-density ratio effects were obtained and analyzed in more detail for the configuration with winglet as described below.

The analysis had shown a switch in flutter mode, from nacelle vertical bending to second wing bending, due to decrease in the mass–density ratio. The range of mass–density ratio, to affect the mode change in the tunnel, was achieved by testing the configuration with winglet in both air and freon. Figure 4a shows the analysis-test correlation as a function of mass–density ratio for all test points. In Figure 4b, the data points are shown for mass–density ratios up to 50 to show more clearly the switching of flutter modes. The analysis is able to predict the trend correctly and shows good correlation with the test results. The switch in the flutter mode occurred at higher mass–density ratio in the test than shown by analysis. A small difference in actual and predicted damping could explain this difference. The analytical results were calculated using the post-test model described in Section 6 of Volume I except that the analysis frequencies were adjusted to match the model GVT. This adjustment is equivalent to about 1.5 KTAS increase in analytical flutter speed. It was concluded that the mass–density ratio effects can be predicted with acceptable accuracy for winglet configured wings at low Mach numbers.

4.0 Description of High-Speed Test

The model was installed in the NASA Langley TDT as shown in Figure 5. The model was supported on the NASA balance mounted on the wall turntable. A ballasted wing tip was fabricated such that it could replace the nominal wing tip. The weight and Body Station coordinate of center-of-gravity location of the ballasted tip were similar to the winglet:

	WEIGHT (LBS)	CG LOCATION (INCHES IN WRP RELATIVE TO LEADING EDGE OF WING TIP) AFT	OUTBOARD
BALLASTED TIP	0.350	5.00	0.40
WINGLET	0.378	5.36	1.17
NOMINAL TIP	0.0198	3.96	0.30

The nominal and ballasted tips were aerodynamically identical to each other. Each one of the three tips could be attached to two hard points in the wing tip structure.

The nominal nacelle configuration was a strut - spring combination corresponding to cantilevered nacelle vertical bending frequency of 24.7 Hz. The soft nacelle configuration was a strut - spring combination corresponding to a cantilevered nacelle vertical bending frequency of 15.99 Hz. The nominal winglet configuration was a 20° cant winglet with a cantilevered winglet frequency of 93.0 Hz.

The test procedure adopted reflects the emphasis on flutter correlation rather than flutter clearance. A comprehensive model GVT was conducted in the Boeing Structures Dynamics Laboratory (SDL) prior to the wind tunnel test. The model frequencies were also determined for the tunnel installation. The model responses were monitored during the test. Some of the highlights of the test procedure are described below.

The cantilevered model configurations tested in the SDL for mode shapes were:

	SUPPORT	BODY SHELL	WING FUEL	NACELLE	WINGLET
a)	STEEL PLATE	OFF	EMPTY	OFF	OFF
b)	NASA BALANCE	OFF	EMPTY	OFF	OFF
c)	NASA BALANCE	ON	EMPTY	OFF	OFF
d)	NASA BALANCE	ON	EMPTY	NOMINAL	OFF
e)	NASA BALANCE	ON	EMPTY	NOMINAL	NOMINAL
f)	NASA BALANCE	ON	FULL	NOMINAL	OFF
g)	NASA BALANCE	ON	FULL	NOMINAL	NOMINAL
h)	NASA BALANCE	ON	EMPTY	OFF	NOMINAL

The steel plate as well as the NASA Balance were supported from a strongback. A hammer test for wing-nacelle-winglet configuration was conducted in the SDL and it was decided that the hammer test, instead of shaker, will be used in the tunnel to obtain model frequencies in still air. An instrumented hammer was used for exciting the model to obtain its frequency response. The frequency spectrum of each configuration in the tunnel was examined to verify that the model was not damaged and the tunnel installation was proper. This procedure allowed detection of anomalies in the model and helped in isolation and correction of the cause of any differences.

Figure 6 shows the tunnel characteristics for freon operation. The total pressure (H) curves roughly correspond to constant stagnation density lines in the tunnel. The most efficient tunnel operation is achieved in a tunnel "run" by operating the tunnel along constant H curves which results in a simultaneous increase in the Mach number and dynamic pressure. A run was terminated if one of the following four conditions was reached: (i) Mach 0.91, or (ii) dynamic pressure of 200 psf, or (iii) excessive model response amplitudes either due to buffet or low damping, or (iv) onset of flutter. The maximum Mach number, dynamic pressure and other tunnel parameters as well as the frequencies of significant responses and reason for terminating the run were recorded. This procedure was followed throughout the test. The results of pre-test analysis were

used to select the tunnel runs. For a typical predicted flutter boundary example, also shown in Figure 6, runs might be made along H = 300, 400 and 600 psf. If the test flutter points obtained were judged to correlate with the prediction, no further runs were regarded as necessary for that particular configuration; otherwise additional runs were made. A decision was made to not spend the tunnel time in precisely defining the transonic bucket. Instead, the limited tunnel time was utilized to test as many configurations as possible. This strategy proved to be successful based on the number of configurations tested and flutter points obtained in the tunnel.

During each run the model responses were monitored by strip chart traces, and reduced to power spectra, "damping indicator", and cascade plots. The acceleration power spectrum of either the wing tip vertical and fore-aft accelerometers (or both) were displayed in real time with updates every second. The inverse of the amplitude of the highest peak of the power spectrum, for wing tip vertical accelerometer, was plotted, also in real time, versus Mach number. This was called a "damping indicator" or "relative damping" plot. The cascade power spectra were plotted for almost every run and were available within a few minutes after the run.

Two DRAS (Dynamic Response Actuated Switch) units were employed to safeguard against excessive model acceleration amplitudes. One of the DRAS units was set to actuate opening of the four tunnel by-pass valves for quick shutdown at a preset, sustained amplitude. The second unit was set up to switch a red warning light at a fixed percent of the shut-off amplitude. The hook up of the DRAS units was initially permitted by NASA on a trial basis. There was a concern about DRAS unit repeatedly shutting-off the tunnel prematurely. The system worked well in practice and the DRAS unit remained in the shut-off loop throughout the test.

5.0 Analytical Representation

The analytical representation used was identical to the low-speed model (Volume 1). The built-up, high-speed model wing was structurally represented by finite beam elements (elastic axis) as if the wing were of single-spar co struction. The nacelle and strut were

attached as rigid, lump-masses to the wing elastic axis. The winglet and ballasted tip were represented as separate substructures using branch mode representation. The cantilevered nacelle strut and winglet test frequencies and mode shapes were input as assumed modes. The mass distributions of the model wing and winglet were calculated, and the total mass and inertias were individually verified with the measured values. The nominal and ballasted tip mass and inertia properties were measured. The calibrated model stiffness properties were used to improve correlation with the results of the model GVT. This data is included in Appendix A to allow independent analysis.

The aerodynamic representation for flutter analysis was based on the strip-theory aerodynamics (AF1 program-Ref 8). The sectional aerodynamics data was derived, from two wind tunnel tests, for Mach numbers of 0.4, 0.65, 0.80, 0.88, and 0.91. There were minor differences between the pressure model and the high-speed flutter model. Therefore, an earlier wind tunnel test for wing-nacelle configuration was used as a basis for sectional aerodynamics data. To obtain the sectional data for configurations with winglet, the difference due to winglet from the later test was algebraically added to the sectional data from the earlier test. The sectional data for the five selected Mach numbers is included in Appendix B. In order to get a theoretical sectional aerodynamic data, DUBLAT (doublet lattice program - from Ref 8) was used for steady flow. The theoretical sectional data obtained are also included in Appendix B. The nacelle C_{n_α} and C_{y_β} values used were 0.052 and 0.042 respectively at M = .4 and changed very little at high Mach number.

The flutter solutions were obtained at Mach numbers of 0.4, 0.65, 0.80, 0.88, and 0.91 and five densities for each configuration. The flutter dynamic pressures were plotted on tunnel charts. The match-point solutions were determined, for each flutter mode, corresponding to structural damping (g) of 0.0 and 0.03.

6.0 Correlation With Model GVT Results

The model GVT results were used to modify the analytical model to improve correlation with the test mode shapes and frequencies. The GVT results for the clean wing (without

nacelle and with nominal tip) configuration were used to modify the analytical representation. Assuming the analytical mode shapes to exactly match the test mode shapes for the clean wing, the analytical stiffness matrix was modified based on matching the frequencies. Table 2 lists the frequencies for the clean wing. The node line plots for mode shapes from the modified analysis and the test are included in Appendix C for clean wing, wing-nacelle, and wing-nacelle-winglet configurations. The procedure for modifying the stiffness matrix is described in Appendix D.

The modified stiffness matrix was used for all configurations. This was possible because of the modeling approach described in Section 5. Tables 3 and 4 list the frequencies for wing-nacelle, wing-nacelle-ballasted tip and wing-nacelle-winglet configurations for empty and full wing fuel. The differences in GVT frequencies between model installation in the Structures Dynamics Laboratory (SDL) and the tunnel are attributed to the tunnel turntable. The frequencies for empty wing configurations with soft nacelle are shown in Table 5.

The modal correlation between the analysis and GVT was considered to be reasonably good specially when considering the difficulties involved in stiffness calibration. The only significant difference in the modal correlation was found to be for the wing (full)- nacelle (nominal)- winglet (20 deg) configuration for the "chordwise" mode. For this mode, the wing fore-aft motion is dominant with significant coupling with outboard wing bending and torsion. The analytical frequency is about 2 Hz nigher than the frequency of 20.7 Hz obtained during tunnel GVT. In the post-test analysis, this difference was found to be significant for some flutter modes. This is further discussed in Section 9.

7.0 Flutter Test Results and Correlation

The test results obtained are shown in figures 7a to 7e. There was a significant reduction in flutter dynamic pressure (Q_F) due to the winglet aerodynamic effects. For the configuration with nominal nacelle strut and empty fuel (fig. 7b), the effect of the ballasted tip was to slightly lower the flutter boundary except at higher Mach numbers.

However, for the configuration with the nominal nacelle strut and full fuel (fig. 7c), the effect of the ballasted tip was to cause a low-damped mode to occur at a slightly lower dynamic pressure. The reduction in Q_F due to winglet aerodynamic effects was more pronounced for this case. The configuration with the soft nacelle strut and empty fuel (fig. 7d) showed trends similar to the configuration with nominal nacelle strut. The effect of winglet cant angle shown in figure 7e, was found to be similar to that for the low-speed model. The differences in the effects of winglet aerodynamics on different configurations were primarily due to the flutter modes. The four flutter modes encountered were similar to the four flutter mechanisms found for the low-speed model. The flutter test results are summarized in a tabular form in Appendix E. An angle-of-attack variation series was run, within model load limits, over a Q-M range representative of scaled flight envelope for the wing (empty)- nacelle (nominal)-winglet (20 deg) configuration. The model load limits were -80 lbs to 180 lbs. No single degree-of-freedom instability was found to exist.

The analysis-test correlation obtained is shown in figures 8-11. A short discussion related to each configuration is presented below.

(a) Wing (Empty)-Nacelle (Nominal) configuration results are shown in Figure 8a. The nacelle vertical bending mode was found to flutter. The analysis also predicts the flutter to occur in the nacelle vertical bending mode. The analytical Q_F-M flutter boundary appears to have similar shape as the test, but the analysis is conservative.

(b) Wing (Empty)-Nacelle (Nominal)-Ballasted Tip configuration results are shown in Figure 8b. The flutter still occurs in the nacelle vertical bending mode. However, the analysis is slightly unconservative rather than conservative as for the nominal tip configuration.

(c) Wing (Empty)-Nacelle (Nominal)-Winglet (Nominal) configuration results are shown in Figure 8c. At the two higher Mach numbers, M = 0.77 and .828, the flutter occurred in nacelle vertical bending mode. At Mach .66, the model response showed high amplitude in 17.6 Hz nacelle vertical bending mode and 22.3 Hz second wing bending mode.

The ratio of acceleration amplitude squared, of the 22.3 Hz to the 17.6 Hz mode is 1.37. This ratio is based on a spectrum derived from exponential averaging, with overlap processing, of ten ensembles of five seconds each. The corresponding ratio of displacement amplitudes is 0.72. Therefore, it is possible to classify the flutter mode as a second wing bending mode based on acceleration response, or as a nacelle vertical bending mode based on displacement response. However, since acceleration response is generally used in flutter testing, the flutter mode was designated as second wing bending mode. The analysis–test correlation for nacelle vertical bending mode is satisfactory. The correlation at M = 0.66 is also satisfactory, since the test point is interpreted as being a combination of nacelle vertical bending - second wing bending response.

(d) Wing (Full)-Nacelle (Nominal) configuration results are shown in Figure 9a. The wing chordwise bending mode disappears at higher damping (g). Two runs were made and one flutter point for wing tip mode was obtained. The analysis-test correlation is satisfactory.

(e) Wing (Full)-Nacelle (Nominal)-Ballasted Tip configuration results are shown in Figure 9b. Two runs were made. No flutter points were obtained although the pass at higher dynamic pressure resulted in some low damped response in second wing bending mode.

(f) Wing (Full)-Nacelle (Nominal)-Winglet (Nominal) configuration results are shown in Figure 9c. This is the most complicated configuration in terms of sorting out the flutter modes. Three flutter modes (nacelle vertical bending, wing chordwise bending and wing tip) were observed. At Mach .856, there was distinct beating between the 18.5 Hz (nacelle vertical bending) and the 19.1 Hz (wing chordwise bending) modes. At Mach .79, response in both these modes is apparent. The higher frequency wing tip mode was observed for the test points at Mach .73 and .644. The analytical results match fairly well for the nacelle vertical bending and wing chordwise mode at the two higher Mach numbers.

However, the analysis appears too conservative for the wing chordwise mode and unconservative for the wing tip mode. Considerable analytical effort was devoted in understanding the sensitivities of the wing chordwise and tip modes. The results are discussed in Section 9.

(g) Wing (Empty)–Nacelle (Soft) configuration results are shown in Figure 10a. At the higher Mach numbers, low-damped response at several frequencies was observed. The flutter obtained was in second wing bending mode. The analysis-test correlation is satisfactory. The area included in the $g = 0$ boundary for the nacelle vertical bending mode is the region of instability for that mode.

(h) Wing (Empty)–Nacelle (Soft)–Ballasted Tip configuration results are shown in Figure 10b. The flutter characteristics and the nature of correlation is similar to case (g) above.

(i) Wing (Empty)–Nacelle (Soft)–Winglet (Nominal) configuration results are shown in Figure 10c. The flutter speeds are lower compared to cases (g) and (h) above. The analysis–test correlation is satisfactory. An interesting feature is that both analysis and test, show presence of the nacelle vertical bending and second wing bending modes in close proximity to each other.

(j) Wing (Empty)–Nacelle (Nominal)-Winglet (0° cant) configuration results are shown in Figure 11. The flutter characteristics did not show a significant difference due to change of winglet cant angle from 20° to 0°.

The effect of the winglet was to reduce the flutter dynamic pressure. In order to get a quantitative effect, the analytical flutter results for wing (empty)-nacelle (nominal) with the three wing tips are shown in Figures 12a to 12c for a density of 1.11×10^{-3} slugs/cu ft. For the nacelle vertical bending mode at $M = .88$, the effect of the tip weight is to increase the flutter dynamic pressure ($g = .03$) by 7% relative to the nominal tip configuration. The aerodynamic effect of winglet is to reduce the flutter dynamic pressure ($g = .03$) by 14% relative to the ballasted tip configuration. Thus the net

reduction in the analytical flutter dynamic pressure due to the combined effect of winglet weight and aerodynamics is relatively small for the empty fuel configuration. For different wing configurations, different fuel conditions or different modes, the effect of the winglet weight and aerodynamics will obviously be different.

8.0 Reduction of Test Data

The data obtained during the test was critically evaluated after the test. The reason for stopping each run was reviewed by examining the strip charts and cascade plots. Also post-test data reduction was done for selected runs. The post-test data reduction consisted of:

(a) Plotting of calibrated $1/A^2$ (from power spectrums) versus Mach number for maximum amplitude in each of the three selected frequency bands.

(b) Calibrated time histories for eight seconds near end of the run with the maximum response near the middle of the eight seconds.

(c) Flutter modes were derived from Fourier analysis of one second of maximum response described in (b). The wing tip response was used as a reference in defining the phase relations.

Figures 13, 14, and 15 present examples of the information provided by (a), (b), and (c), respectively. The following observations were made from review of the test data.

(a) The flutter dynamic pressure and Mach number recorded in the tunnel did not warrant much of an adjustment. The "damping indicator" versus Mach number plots could be used to extrapolate to a Mach number corresponding to a selected level of $1/A^2$. It is not feasible to extrapolate to a $1/A^2 = 0$ corresponding to flutter because of (i) some scatter in the "damping indicator" versus Mach plots, (ii) the accuracy of .01 associated with determination of the tunnel Mach number and (iii) the accuracy associated with reading the recorded

analog voltage signal corresponding to the Mach number. It was confirmed that the tunnel was stopped at about the same level of acceleration response for most of the flutter runs. Therefore, no modification was made to flutter Mach numbers and dynamic pressures recorded during the test.

(b) Comparisons of time traces approaching flutter for runs where the response frequencies were significantly different, do not indicate significant differences in phase relationship of one accelerometer to the other. From the low-speed model responses, it was possible to identify different phase characteristics for different flutter modes. This is much more difficult to do from the high-speed model responses. Possible reasons could be that (i) the higher turbulence associated with higher dynamic pressures excites many of the lower frequency modes, and (ii) the sustained oscillations are not maintained for a sufficient time to clean up the response. Therefore, the response frequency remains the primary means of identifying the flutter mode.

9.0 Analytical Sensitivity Studies

An analytical sensitivity study was conducted to evaluate the effect of selected parameters on analysis-test correlation. The primary configuration for the sensitivity study was the wing (full)-nacelle (nominal)- winglet (nominal) configuration. This was judged to be the most interesting configuration tested since three flutter mechanisms were observed. In addition, this configuration was found to be sensitive to the characteristics of the wing chordwise bending mode as described later in this section.

The following parametric variations resulted in small changes to the flutter results, and were judged to be not significant:

(a) Wing elastic axis location was varied as shown in Figure 16.

(b) Number of aerodynamic strips in the AF1 program were varied.

(c) The static-lift effect was included in the flutter analysis using SLOAEF program.

(d) The modification of stiffness matrix (Appendix D).

The flutter speeds were found to be sensitive to the following parameters:

(a) Structural - Wing chordwise bending, and

(b) aerodynamic - spanwise distribution of static lift-curve slope and aerodynamic center.

The sensitivity to wing chordwise bending was considered to be somewhat unusual, and is believed to be brought about by the combination of winglet and fuel. The importance of the wing chordwise bending mode can be seen from plots of flutter dynamic pressure versus wing chordwise bending frequency for Mach (density) combinations of 0.65 (3.50 X 10^{-3} slugs/cu ft.) and 0.88 (1.11 X 10^{-3} slugs/cu ft.) in Figures 17a and 17b. The wing chordwise bending mode has a significant wing tip vertical motion component which accounts for its effect on flutter speeds.

The chordwise bending stiffness was modified (see Figure A2) to evaluate the effect of change in stiffness distribution. The modified stiffness probably was a better representation of the model. The chordwise bending stiffness has significant effect on the frequencies of wing chordwise and torsion modes. The resulting wing chordwise bending and torsion frequencies for the wing (full)- nacelle (nominal)-winglet (nominal) were 20.3 Hz and 40.3 Hz, respectively. The corresponding frequencies for the reference analysis were 22.87 Hz and 41.89 Hz (Figure C5). The corresponding test frequencies were 20.7 Hz and 42.8 Hz (TDT installation), respectively. Thus the modification to the wing chordwise bending stiffness improved the GVT frequency correlation for the chordwise mode with some deterioration for the torsion mode. The sensitivity of flutter dynamic pressure to chordwise bending stiffness, along with other parameters, is discussed below.

The flutter dynamic pressure (Q_F) at selected Mach number - density combinations is compared in Taole 6. Four Mach number - density combinations were selected mainly based on their proximity to the test points obtained. These were Mach = 0.4, 0.65, 0.80, and 0.88 and corresponding densities of 1.11 X 10^{-3}, 3.50 X 10^{-3}, 1.50 X 10^{-3} and 1.11 X 10^{-3} slugs/cu ft, respectively. The Q_F for reference analysis is tabulated for comparison. The base for sensitivity analysis is different from the reference analysis in the chordwise bending stiffness.

Variation 1 shows the effect of "tuned" frequencies. The analytical frequencies were "tuned" to match the GVT frequencies. The effect is primarily due to the wing torsion mode frequency change from 40.3 Hz to 42.8 Hz, and results in increasing Q_F of the tip mode. In Variation 2, there is a 10% increase in wing C_{n_α} for η = .538 to 1.0. There is a drop in Q_F for all three modes. The effect of shift in wing aerodynamic center (η= .538 to 1.0) by .05C and .10C forward, is also seen to be significant from results tabulated under Variations 3 and 4. As expected, Q_F drops for all three modes. The stiffness Variation 5, shows the effect of including the stiffness matrix modification based on the cantilevered wing only frequencies. There appears to be a further drop in Q_F for the nacelle vertical bending and wing chordwise bending modes. This requires further evaluation to understand the reasons for the significant effect.

The effect of using doublet-lattice aerodynamics program (DUBLAT) rather than the strip theory program (AF1) was evaluated. No empirical corrections were used. The results tabulated under Variation 6 should be compared to Variation 2 for M = .4 and .65, and to Variation 1 for M = .8. The reason being that the test C_{n_α} sectional distributions used for M = .4 and .65 are about 10% lower than the corresponding theoretical DUBLAT distributions. For M = .8, the test and theoretical C_{n_α} distributions are similar. It is not surprising that the flutter dynamic pressure predicted by DUBLAT at M = .88 is significantly higher than the AF1 results as well as the test results. The DUBLAT results at Mach 0.4 and 0.65 appear to be in the right range. However, the reason for DUBLAT predicted flutter dynamic pressure at M = .80 being significantly higher than the results from the base run, needs to be investigated.

The effect of chordwise mode shape appears to be significant based on preliminary assessment. As described earlier, there is a significant wing bending and torsion motion associated with the wing chordwise bending mode for the wing (full)–nacelle (nominal)–winglet (nominal) configuration. An attempt to use experimentally measured mode shape was initiated, but has not been completed. It was found that the wing twist could not be reliably reduced from the measured data as it was sensitive to small changes in accelerometer readings. The error bounds for the accelerometers are not known with sufficient accuracy to enable evaluation of the quality of wing twist information obtained from the displacement data.

The application of compressibility correction or "C_c correction" was compared to direct solution using AF1 with empirical sectional data for appropriate Mach numbers. The flutter at any Mach number, ($^{Q}F_{M}$), may be determined as

$$Q_{F_M} = \frac{\left(C_{N_\alpha}\right)_{M_1}}{\left(C_{N_\alpha}\right)_{M}} Q_{F_{M_1}} = C_C^2 \, Q_{F_{M_1}}$$

where C_c^2 is generally determined from the wind tunnel test data, and M_1 is selected to be incompressible Mach number. It has been customary to use $M_1 = 0.4$. Figures 18a to 18d show comparisons of two methods of solutions for wing–nacelle and wing–nacelle–winglet configurations at a density of 1.11×10^{-3} slugs/cu ft. The comparison is shown for two flutter modes, nacelle vertical bending and second wing bending mode. For the wing–nacelle configuration, the C_c correction resulted in higher Q_F at transonic Mach numbers for both modes. However, the nacelle mode is softer at higher Mach numbers using actual Mach solution compared to the solution obtained with C_c correction. For the wing–nacelle–winglet configuration, the C_c solution approximated fairly well the actual Mach solution. These comparisons have been made for specific configurations and altitude. No general conclusions are warranted except one. The "C_c correction" may give

results different from the actual Mach solution, and may not be always conservative. However, the simple approach may be useful for preliminary evaluation of test configurations for the purpose of planning the test.

10. Conclusions and Recommendations

The test program has been successful in creating the data base for flutter characteristics of winglet configured wing for a twin-engine configuration. The four flutter mechanisms predicted by analysis were obtained in the tunnel. The number of flutter test points for the ten high-speed configurations and two low-speed configurations, obtained in the tunnel cover a wide range of altitudes and Mach numbers. This provides an excellent reference for evaluation of analytical correlation for a configuration with and without winglet.

The mass-density ratio effects at low Mach numbers were correlated (analysis vs. test) satisfactorily over a wide range. The application of conventional analysis proved to be satisfactory through the transonic Mach regime. It was not surprising to find that theoretical doublet-lattice analysis gave unconservative answers at M = .8 and .88. It was concluded that the flutter characteristics of a winglet configured high aspect ratio wing can be satisfactorily predicted with careful application of existing methods for a twin-engine airplane configuration. The wing chordwise bending mode for certain configurations can be expected to have significant wing bending and torsion motion. It is indicated by the present study that this coupling effect is important.

It is recommended that the experimental and analytical data base established in this program be used to advantage. The number and diversity of flutter test points and the correlation established with simple methods, should be used to evaluate state-of-the-art transonic codes. There are many examples published where two or three degrees-of-freedom systems or simplified representations have been studied for transonic effects using very expensive codes. It is believed that the time has come to make a real effort using the data from a realistic configuration to determine the advantages and costs of applying transonic codes.

9.0 References

1) Whitcomb,R.T., "A Design Approach and Selected Wind-Tunnel Results at High Subsonic Speeds for Wing-Tip Mounted Winglets," NASA TND-8260, July 1976.

2) Ishimitsu, K.K., "Aerodynamic Design and Analysis of Winglets," AIAA Paper 76-940, September 1976.

3) Kehoe, M.W., "KC-135 Winglet Program Review", NASA CP2211, 1982.

4) Boeing Company, "Selected Advanced Aerodynamics and Active Controls Technology Concept Development on a Derivative B-747 Aircraft," NASA CR 3164, February 1980.

5) Ruhlin, C.L.; Rauch, F.J.; and Waters, C., "Transonic Flutter Model Study of a Supercritical Wing and Winglet," J. Aircraft, Vol. 20, No. 8, August 1983.

6) Schollenberger, C.A.; Humphreys, J.W.; Heiberger, F.S.; and Pearson, R.M., "Results of Winglet Development Studies for DC-10 Derivatives," NASA CR 3677, March 1983.

7) Douglas Aircraft Company, "DC-10 Winglet Flight Evaluation" NASA CR 3704, June 1983.

8) Dreisbach, R.L. (Editor), "ATLAS - An Integrated Structural Analysis and Design System, ATLAS User's Guide," NASA CR-159041, 1979.

9) Jennings, W.B.; and Berry, M.A., "Effect of Stabilizer Dihedral and Static Lift on T-Tail Flutter," J. Aircraft, Vol. 14, No. 4, April 1977.

TABLE 1. LOW-SPEED MODEL FREQUENCIES
EFFECT DUE TO TUNNEL INSTALLATION
WING(EMPTY) – NACELLE (NOMINAL) – WINGLET (20 DEG)

MODE	MODEL FREQUENCIES (Hz) FOR INSTALLATION IN		
	CONVAIR TUNNEL	NASA TDT	ANALYSIS
1st WING BENDING	3.93	4.0	3.78
NACELLE SIDE BENDING	-	8.0	7.83
NACELLE VERTICAL BENDING	9.45	9.5	9.13
WING CHORDWISE BENDING	11.74	13.49	12.4
2nd WING BENDING	12.19	13.0	11.93
NACELLE ROLL	17.88	-	-
1st WING CHORDWISE BENDING + O/B WING TORSION	23.46	24.6	22.85
O/B WING TORSION + WING CHORDWISE BENDING	23.80	24.17	25.6
1st WING TORSION	27.00	26.6	31.73

TABLE 2: HIGH SPEED MODEL, CORRELATION OF ANALYSIS AND TEST VIBRATION FREQUENCIES (HZ) FOR CLEAN WING (EMPTY)

MODE	TEST		ANALYSIS	
	RIGID PLATE	NASA BALANCE	NASA BALANCE	WITH STIFFNESS MOD
1st Wing Bending	7.81	7.80	7.61	7.80
2nd Wing Bending	25.00	24.70	23.93	24.70
1st Wing Chordwise Bending	34.00	32 02	34.90	32.02
3rd Wing Bending	52.68	52.12	52.61	52.12
1st Wing Torsion	58.42	58.08	57.70	58.08
Higher Mode	86.7	85.88	90.83	85.88
Higher Mode	96.10	94.12	95.91	94.12

TABLE 3

HIGH SPEED MODEL, CORRELATION OF ANALYSIS AND TEST VIBRATION FREQUENCIES (Hz) FOR WING (EMPTY)-NACELLE (NOMINAL)

MODE	NOMINAL TIP			BALLASTED TIP		WINGLET (NOM) TIP		
	GVT (SDL)	GVT (TUNNEL)	ANALYSIS	GVT (TUNNEL)	ANALYSIS	GVT (SDL)	GVT (TUNNEL)	ANALYSIS
1st WING BENDING	7.72	7.5	7.76	6.8	6.84	6.84	6.6	6.72
NACELLE SIDE BENDING	15.14	15.0	15.26	15.0	15.20	15.23	14.8	15.19
NACELLE VERTICAL BENDING	19.82	19.2	18.60	19.2	18.56	19.82	19.1	18.54
2nd WING BENDING	24.02	23.5	24.15	21.3	21.80	21.09	20.7	21.08
NACELLE ROLL	29.49	27.8	29.80	28.2-31.0	30.08	29.69	28.0	29.98
1st WING CHORDWISE BENDING	30.47	----	32.07	27.0	27.92	27.64	26.7	26.64
3rd WING BENDING	43.75	42.2	42.76	40.3	40.58	40.33	39.1	38.91
1st WING TORSION	55.51	54.3	57.19	52.6	55.2	46.88	46.7	47.01

TABLE 4

HIGH SPEED MODEL, CORRELATION OF ANALYSIS AND TEST VIBRATION FREQUENCIES (Hz) FOR WING(FULL)-NACELLE (NOMINAL)

MODE	NOMINAL TIP			BALLASTED TIP		WINGLET (NOM) TIP		
	GVT (SDL)	GVT (TUNNEL)	ANALYSIS	GVT (TUNNEL)	ANALYSIS	GVT (SDL)	GVT (TUNNEL)	ANALYSIS
1st WING BENDING	6.06	6.0	6.06	5.7	5.64	5.66	5.5	5.59
NACELLE SIDE BENDING	15.04	14.8	14.98	15.8	15.86	15.62	15.5	15.75
NACELLE VERTICAL BENDING	19.14	18.5	19.06	18.8	18.71	19.04	18.8	18.65
2nd WING BENDING	17.19	16.9	16.80	14.8	14.28	14.45	14.3	14.04
NACELLE ROLL	29.20	27.7	29.93	29.8	30.56	29.68	28.5	30.26
1st WING CHORDWISE BENDING	22.36	----	25.20	21.5	23.39	21.48	20.7	22.87
3rd WING BENDING	32.03	31.2	32.41	28.1	29.37	28.61	27.5	28.73
1st WING TORSION	46.39	45.8	46.63	43.9	46.15	43.06	42.8	41.89

TABLE 5

HIGH SPEED MODEL, CORRELATION OF ANALYSIS AND TEST VIBRATION FREQUENCIES (Hz) FOR WING (EMPTY) - NACELLE (SOFT)

MODE	NOMINAL TIP		BALLASTED TIP		WINGLET (NOM) TIP	
	GVT (TUNNEL)	ANALYSIS	GVT (TUNNEL)	ANALYSIS	GVT (TUNNEL)	ANALYSIS
1st WING BENDING	7.5	7.5	6.8	6.8	6.8	6.7
NACELLE VERTICAL BENDING	14.5	14.5	14.4	14.1	14.5	14.1
NACELLE SIDE BENDING	15.4	15.4	15.3	15.3	15.5	15.3
2nd WING BENDING	23.5	23.0	21.1	21.5	20.7	20.8
1st WING CHORDWISE BENDING	27.6	30.0	26.2	27.9	26.8	26.6
NACELLE ROLL	28.7	31.5	27.8	30.1	31.6	30.0
3rd WING BENDING	40.8	38.8	38.5	37.9	38.4	36.7
1st WING TORSION	53.5	54.5	50.3	53.2	46.3	46.6

TABLE 6 - SUMMARY OF SENSITIVITY STUDIES, WING(FULL)-NACELLE(NOMINAL)-WINGLET(20^{o})

			REFERENCE		BASE		VARIATION 1		VARIATION 2		VARIATION 3		VARIATION 4		VARIATION 5		VARIATION 6	
STIFF MATRIX MOD			YES		NO		NO		NO		NO		NO		YES		NO	
ΔCB STIFF DIST			NOMINAL		ADJUSTED		ADJUSTED		ADJUSTED		ADJUSTED		ADJUSTED		ADJUSTED		ADJUSTED	
VIBRATION FREQS			TUNED WCB		UNTUNED		TUNED		TUNED		TUNED		TUNED		TUNED		TUNED	
n_a DIST			TEST		TEST		TEST		10% INCREASE		10% INCREASE		10% INCREASE		10% INCREASE		THEORETICAL	
a_c DIST			TEST		TEST		TEST		TEST		5% FORWARD		10% FORWARD		10% FORWARD		THEORETICAL	
AERODYNAMIC PROGRAM			AF1		AF1		AF1		AF1		AF1		AF1		AF1		DUBLAT	
MACH NO.	DENSITY SLUGS/ FT.^{3} X 10^3	FLUTTER MODE	FLUTTER Q_F (PSF) g = 0.0	0.03	FLUTTER Q_F (PSF) g = 0.0	0.03	FLUTTER Q_F (PSF) g = 0.0	0.03	FLUTTER Q_F (PSF) g = 0.0	0.03	FLUTTER Q_F (PSF) g = 0.0	0.03	FLUTTER Q_F (PSF) g = 0.0	0.03	FLUTTER Q_F (PSF) g = 0.0	0.03	FLUTTER Q_F (PSF) g = 0.0	0.03
.4	1.11	NVB	-	-	209	-	-	-	-	-	170	-	143	153	134	148	275	372
		WCB	153	172	198	209	198	220	187	193	176	177	160	167	148	162	148	182
		WT	275	-	257	266	275	288	247	256	221	235	204	-	209	-	207	227
.65	3.50	NVB	511	-	-	-	437	496	422	575	375	543	161	-	152	-	-	-
		WCB	152	174	202	217	207	232	183	202	169	183	161	165	144	161	152	192
		WT	248	259	238	248	259	270	227	237	207	209	190	197	183	197	222	238
.80	1.50	NVB	115	125	130	146	130	-	115	-	106	-	97	106	93	106	340	370
		WCB	106	118	130	141	135	146	115	123	111	123	106	114	97	111	146	166
		WT	174	192	163	168	174	183	157	163	111	149	130	138	130	143	212	221
.88	1.11	NVB	109	117	123	130	125	128	109	-	101	109	91	97	89	93	-	-
		WCB	97	113	130	136	134	141	115	117	107	117	103	117	93	-	148	160
		WT	165	185	155	162	-	-	148	153	134	141	125	130	125	139	204	212

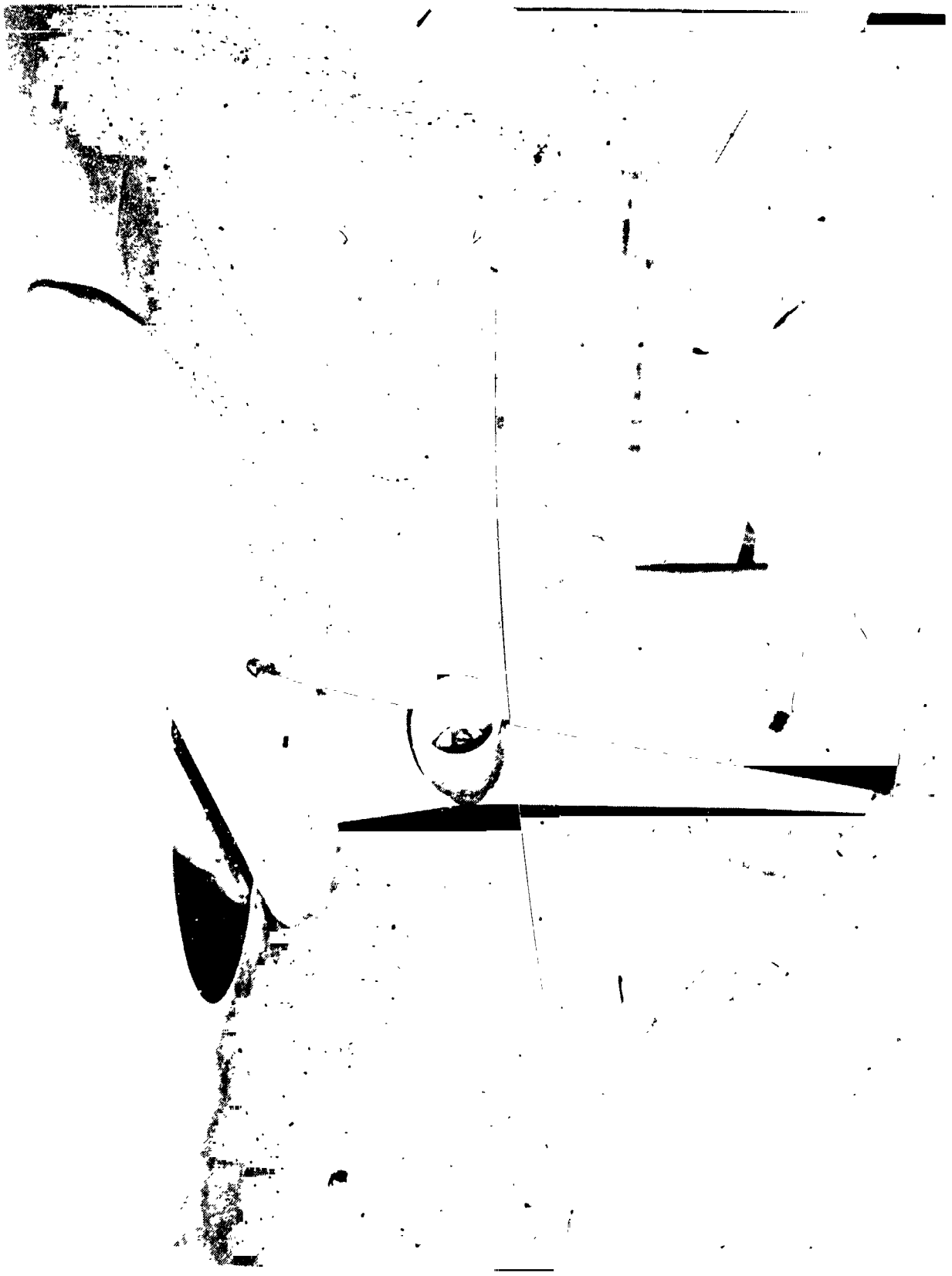

FIG. 1 PRESSURE MODEL INSTALLATION IN BOEING TRANSONIC WIND TUNNEL

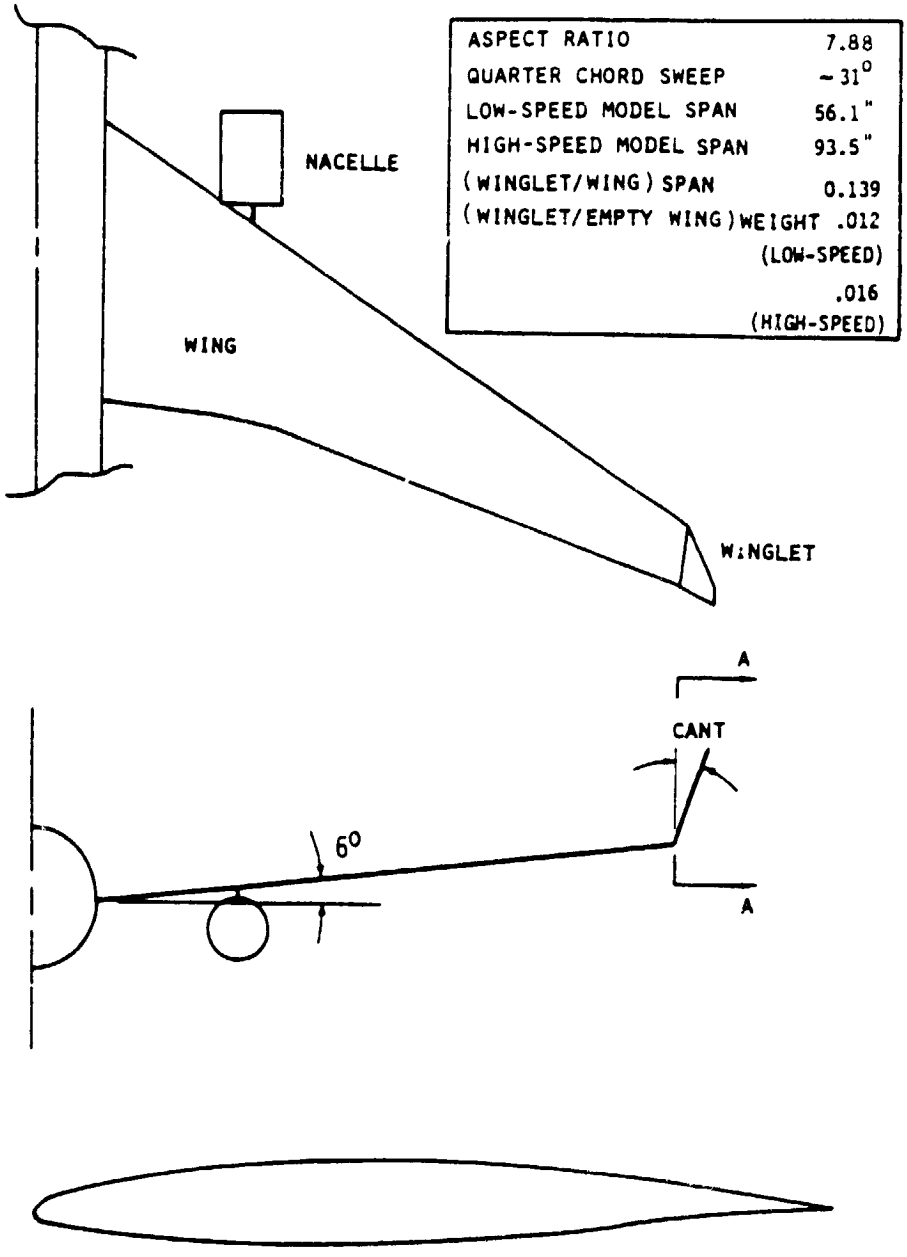

ASPECT RATIO	7.88
QUARTER CHORD SWEEP	-31°
LOW-SPEED MODEL SPAN	56.1"
HIGH-SPEED MODEL SPAN	93.5"
(WINGLET/WING) SPAN	0.139
(WINGLET/EMPTY WING) WEIGHT	.012 (LOW-SPEED)
	.016 (HIGH-SPEED)

TYPICAL MODEL WING SECTION

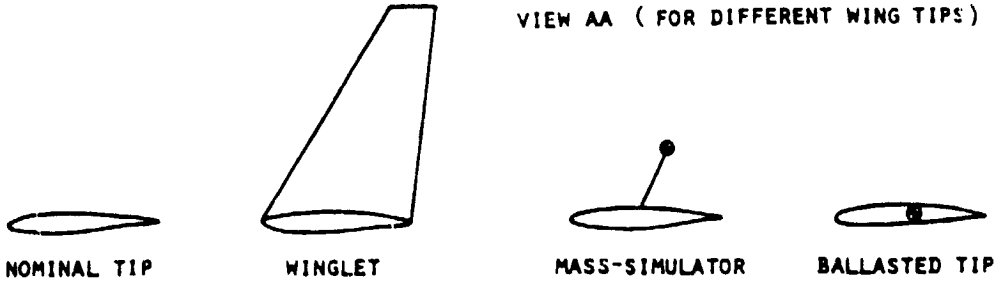

FIG. 2 MODEL WING AND WING TIPS

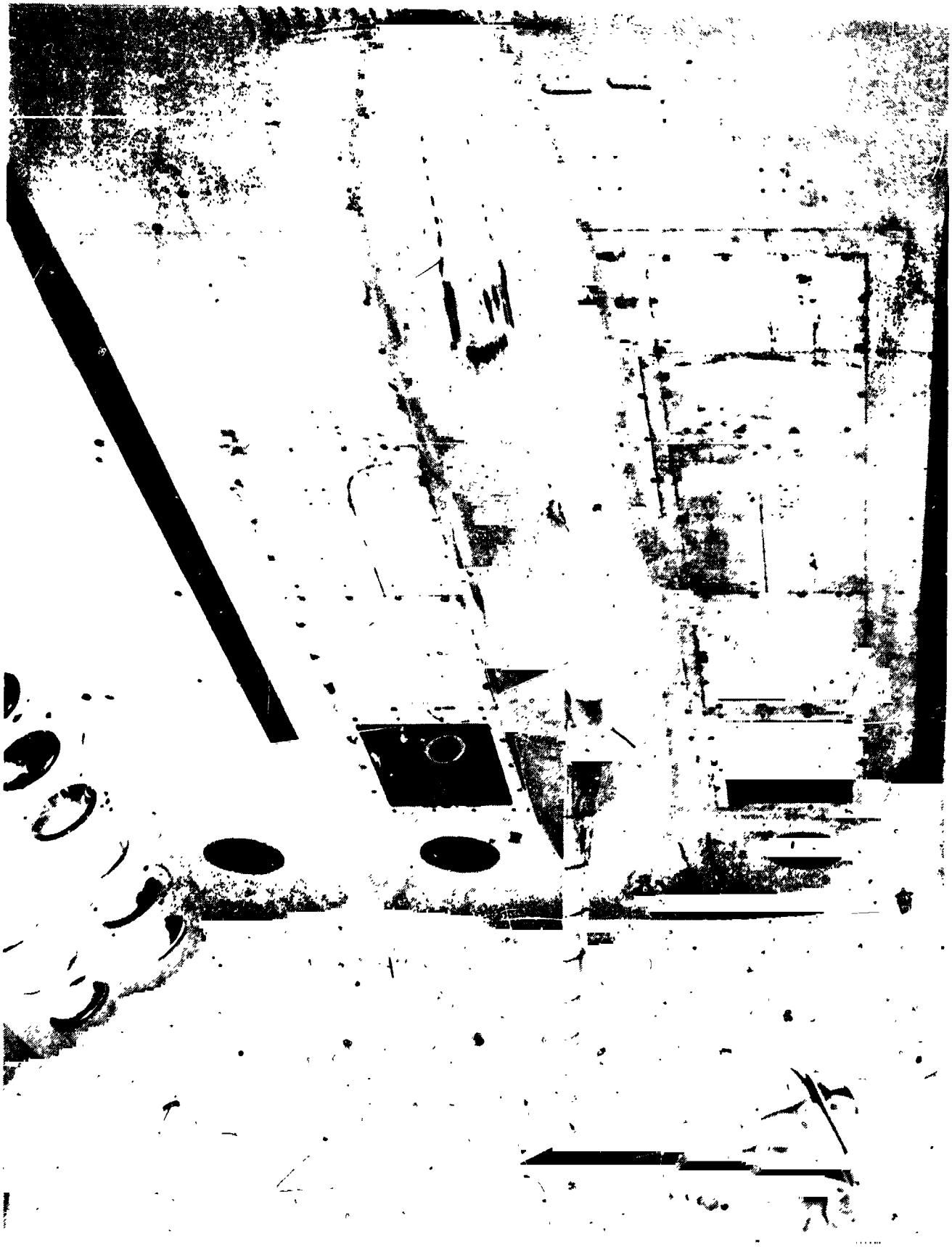

FIGURE 3 LOW-SPEED MODEL SET-UP IN LANGLEY TUNNEL

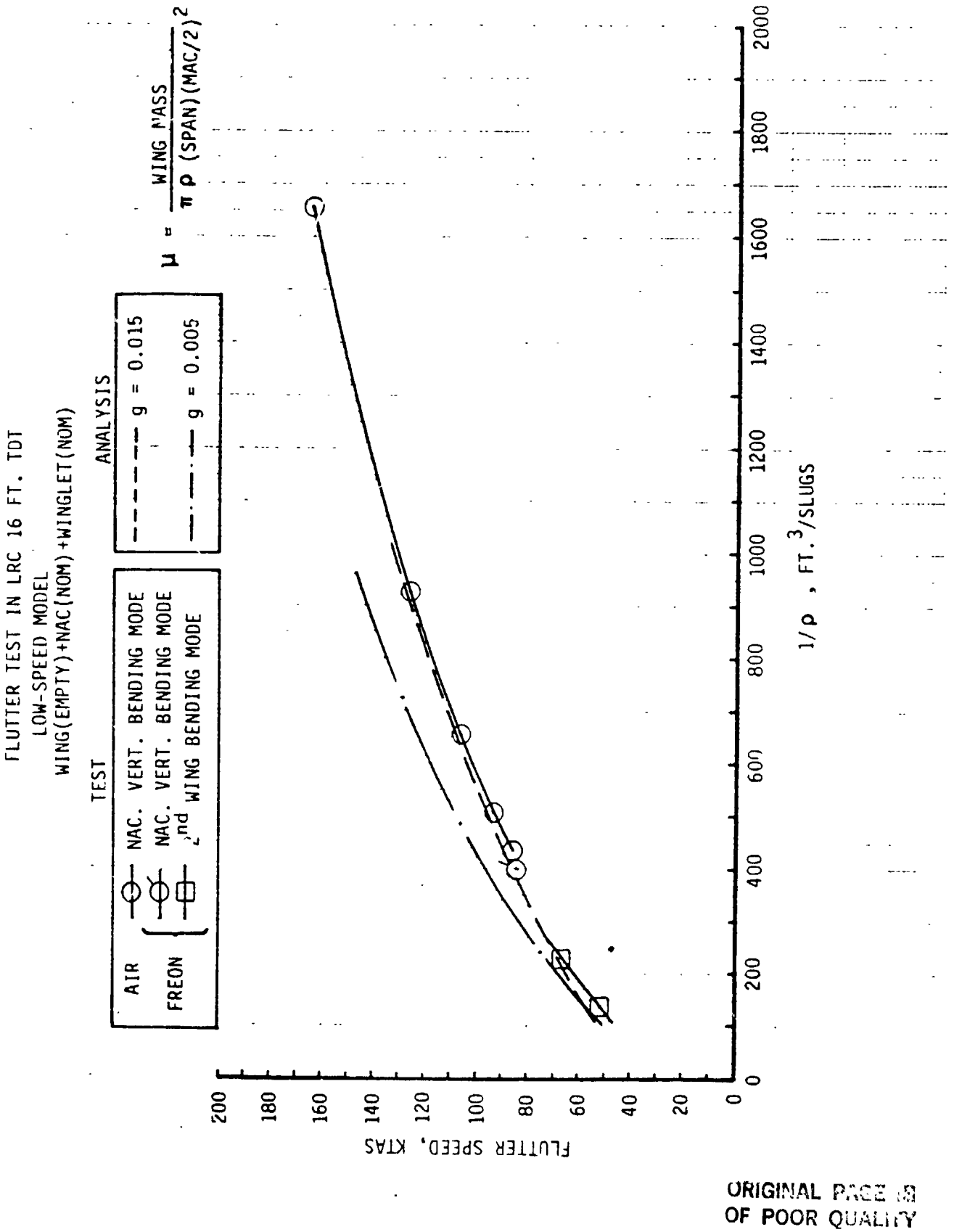

ORIGINAL PAGE IS
OF POOR QUALITY

FIGURE 4a MASS-DENSITY RATIO EFFECTS ON FLUTTER

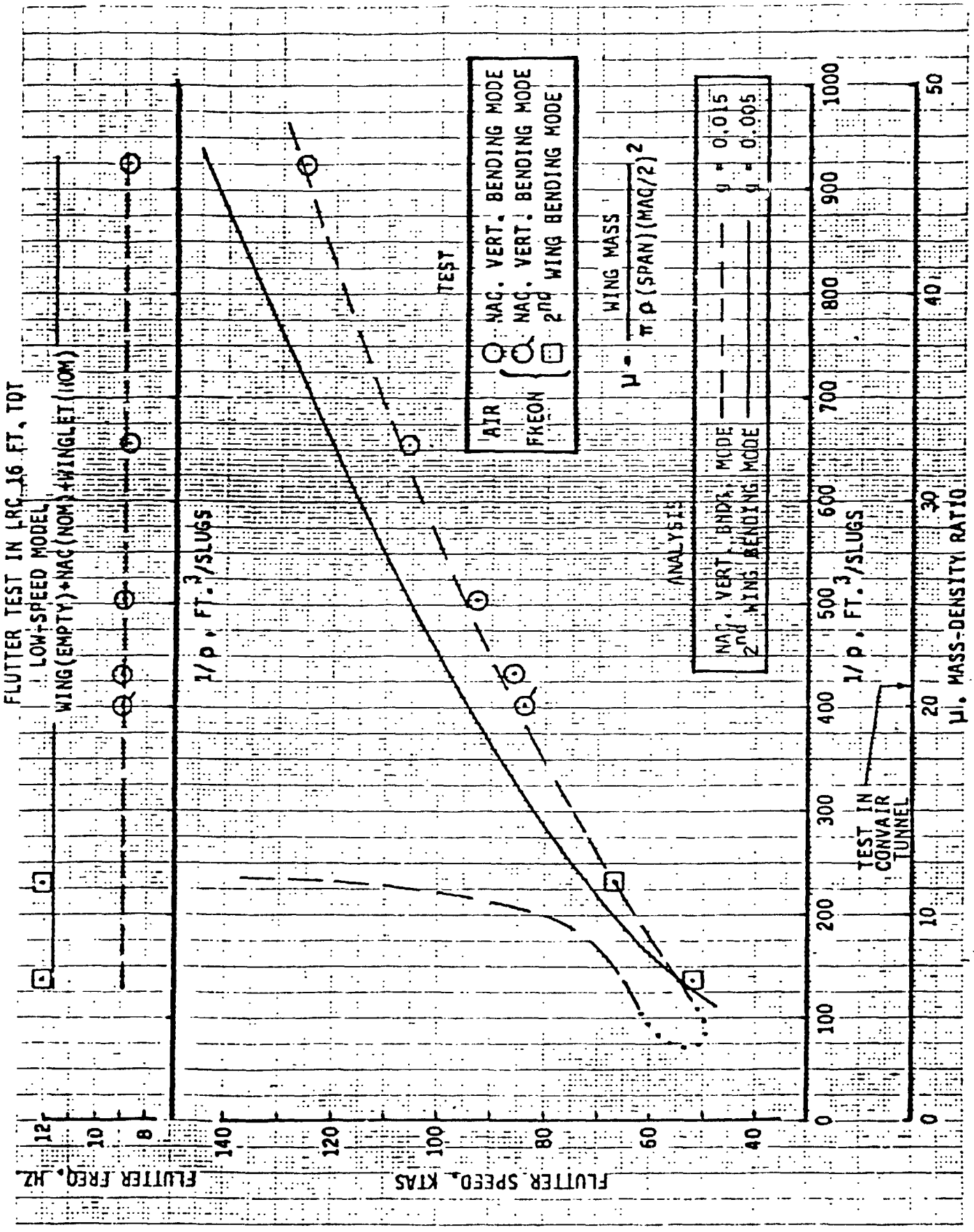

FIGURE 4b MASS-DENSITY RATIO EFFECTS ON FLUTTER - EXPANDED SCALE

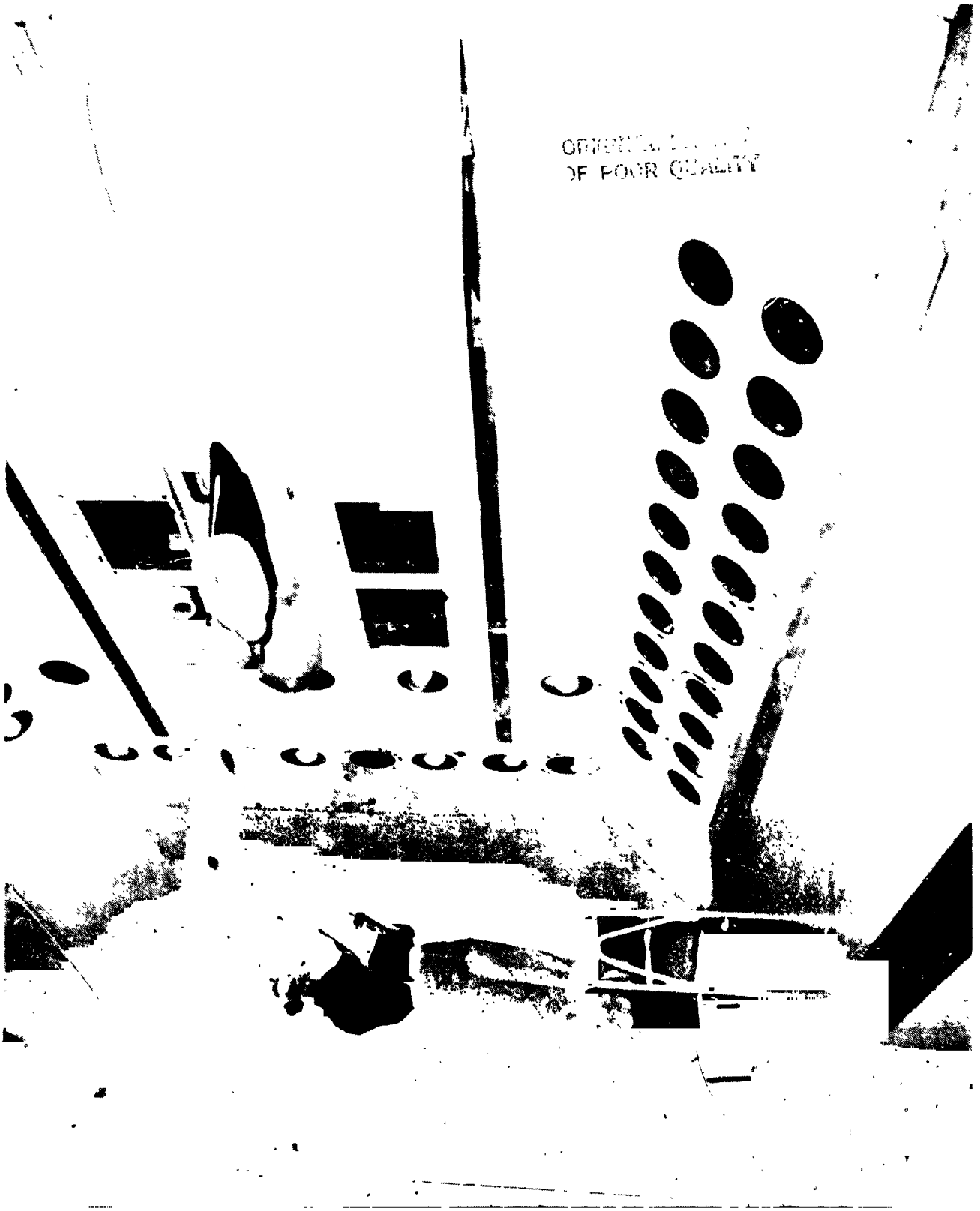

FIGURE 5 HIGH-SPEED MODEL SET-UP IN LANGLEY TUNNEL

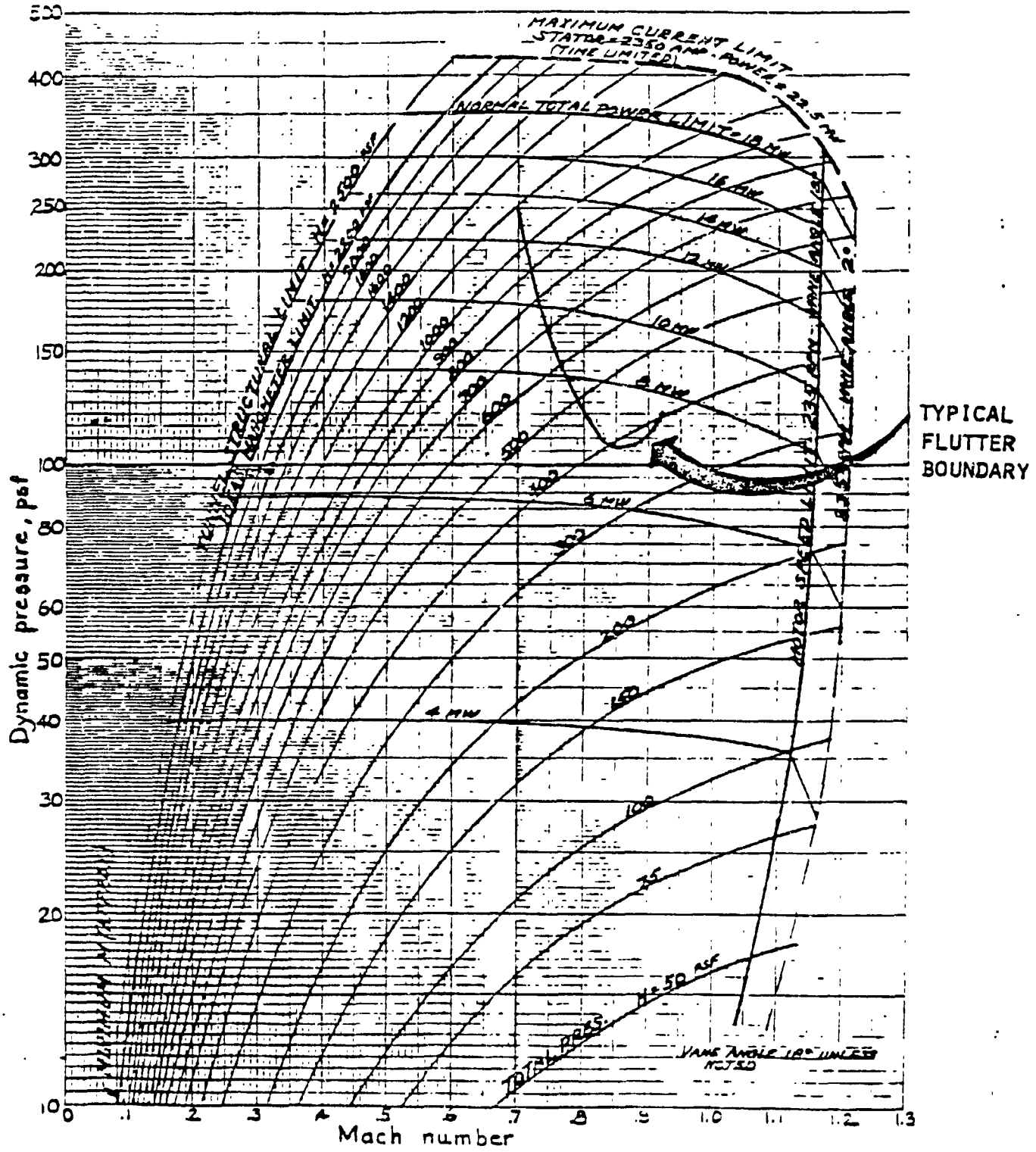

FIGURE 6 NASA LANGLEY TDT CHARACTERISTICS FOR FREON OPERATION

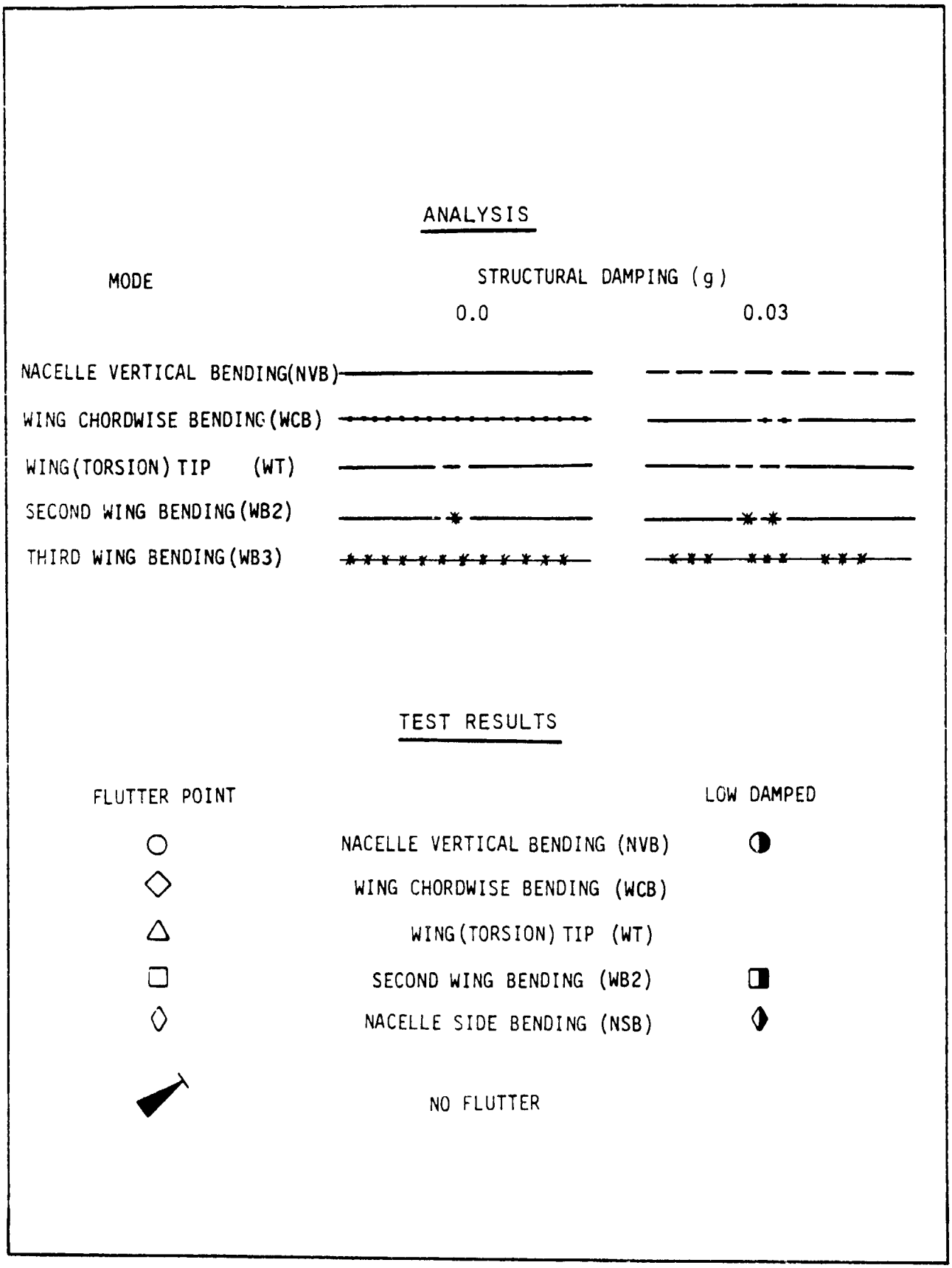

FIGURE 7a LEGEND FOR FLUTTER TEST AND CORRELATION FIGURES

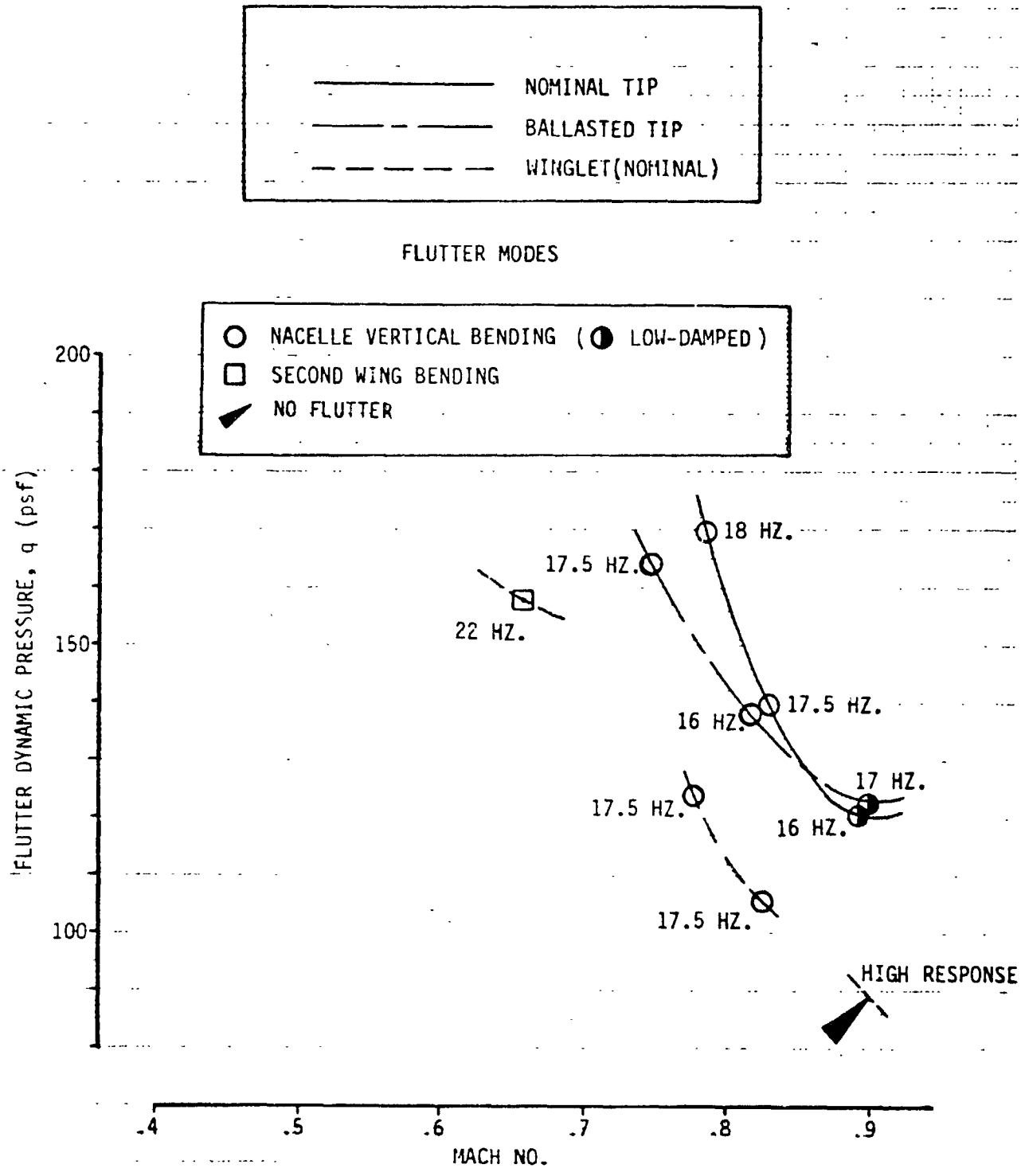

FIGURE 7b EFFECT OF WINGTIP CONFIGURATION ON TEST FLUTTER BOUNDARY, WING (EMPTY)- NACELLE (NOMINAL)

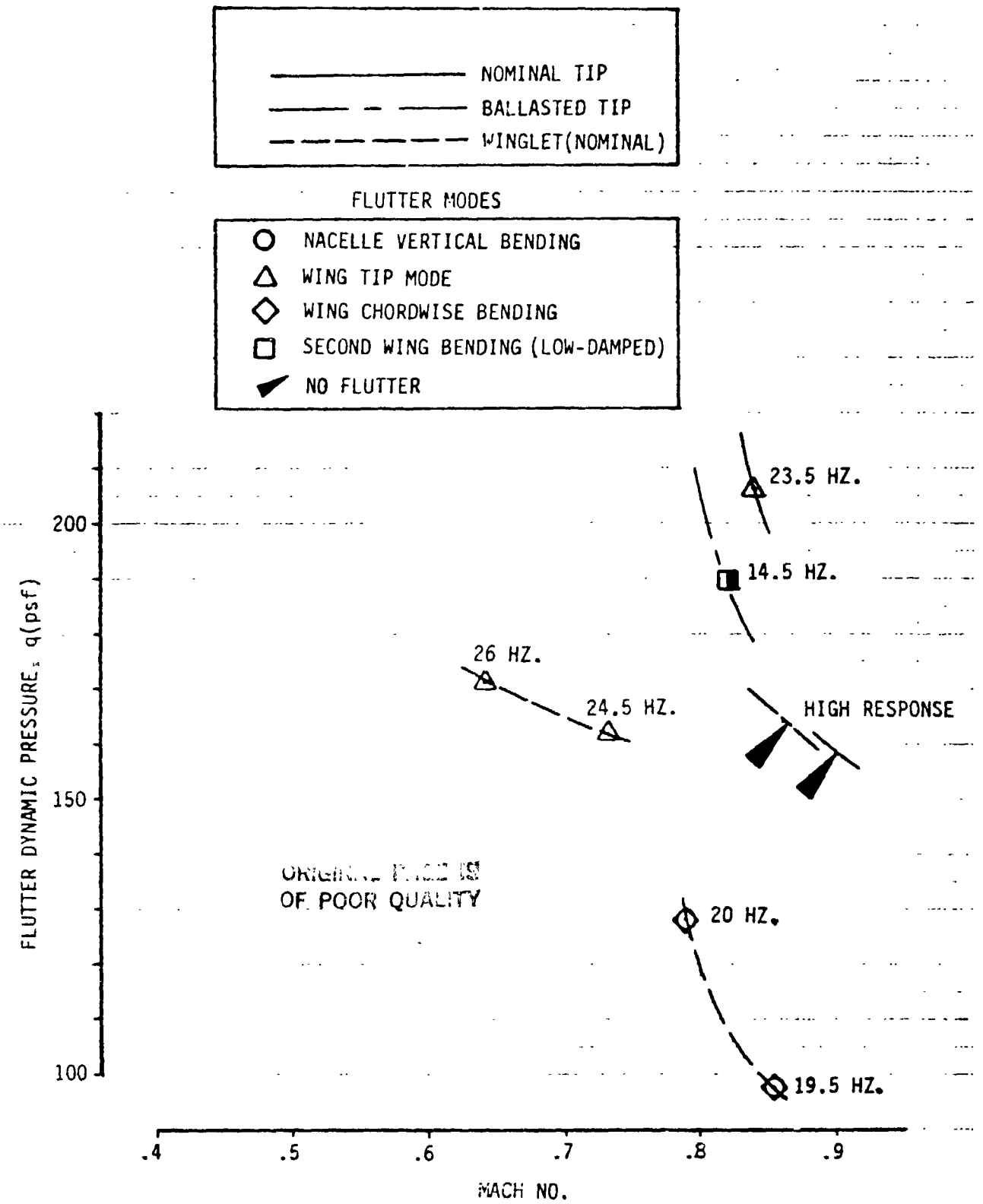

FIGURE 7c EFFECT OF WINGTIP CONFIGURATION ON TEST FLUTTER BOUNDARY, WING (FULL) - NACELLE (NOMINAL)

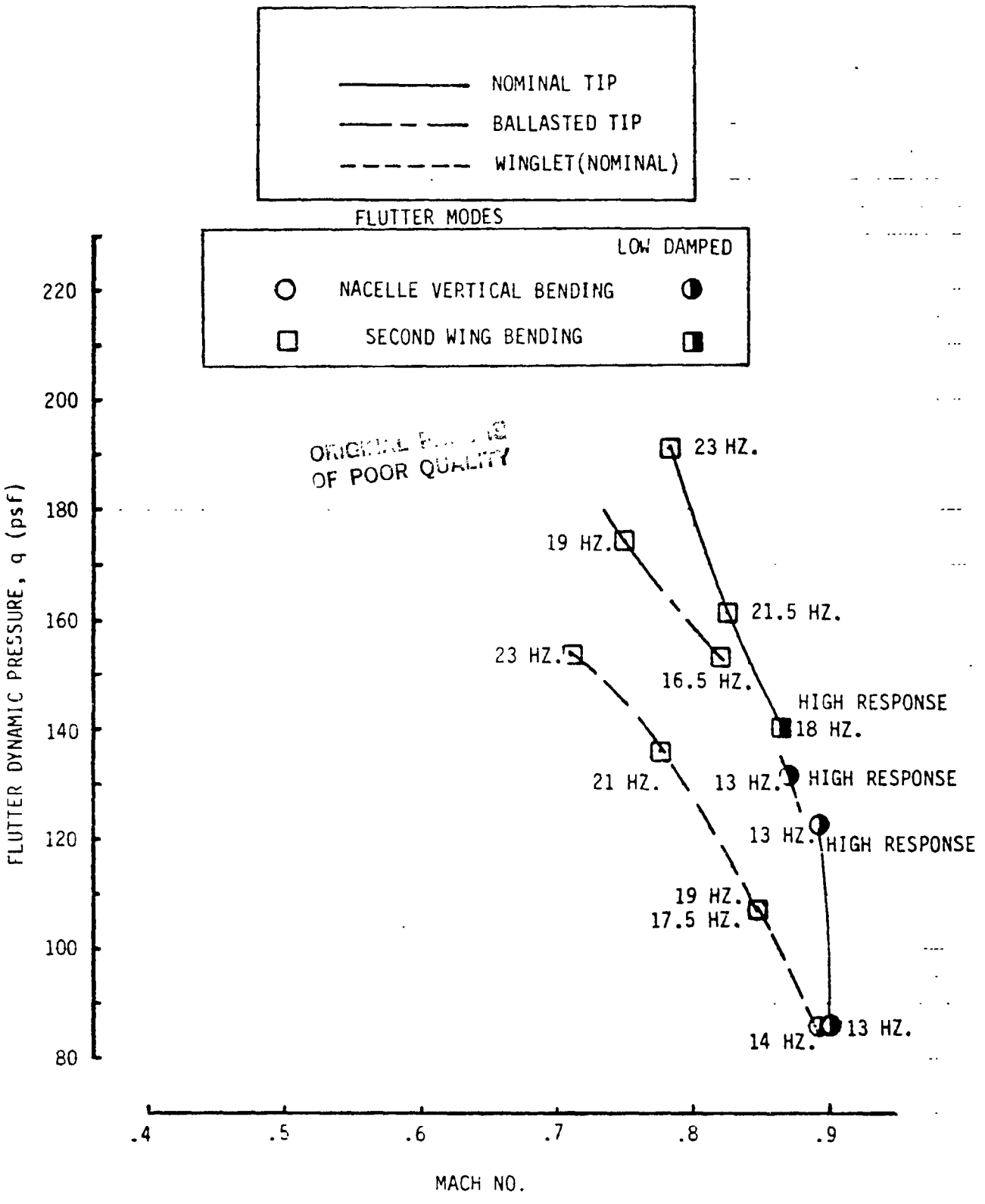

FIGURE 7d EFFECT OF WINGTIP CONFIGUPATION ON TEST FLUTTER BOUNDARY, WING (EMPTY) - NACELLE (SOFT)

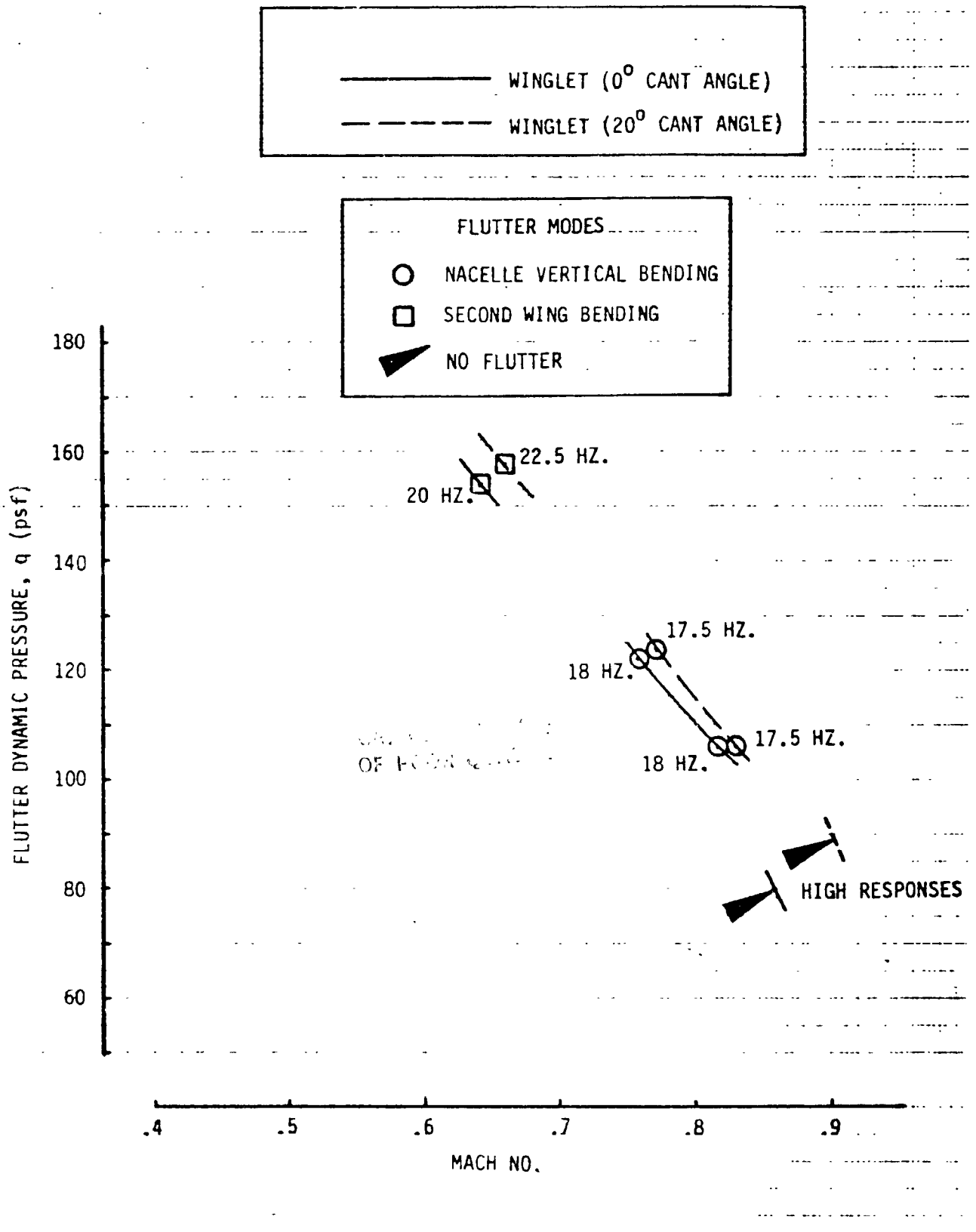

FIGURE 7e EFFECT OF WINGLET CANT ANGLE ON TEST FLUTTER BOUNDARY, WING (EMPTY) - NACELLE (NOMINAL) - WINGLET

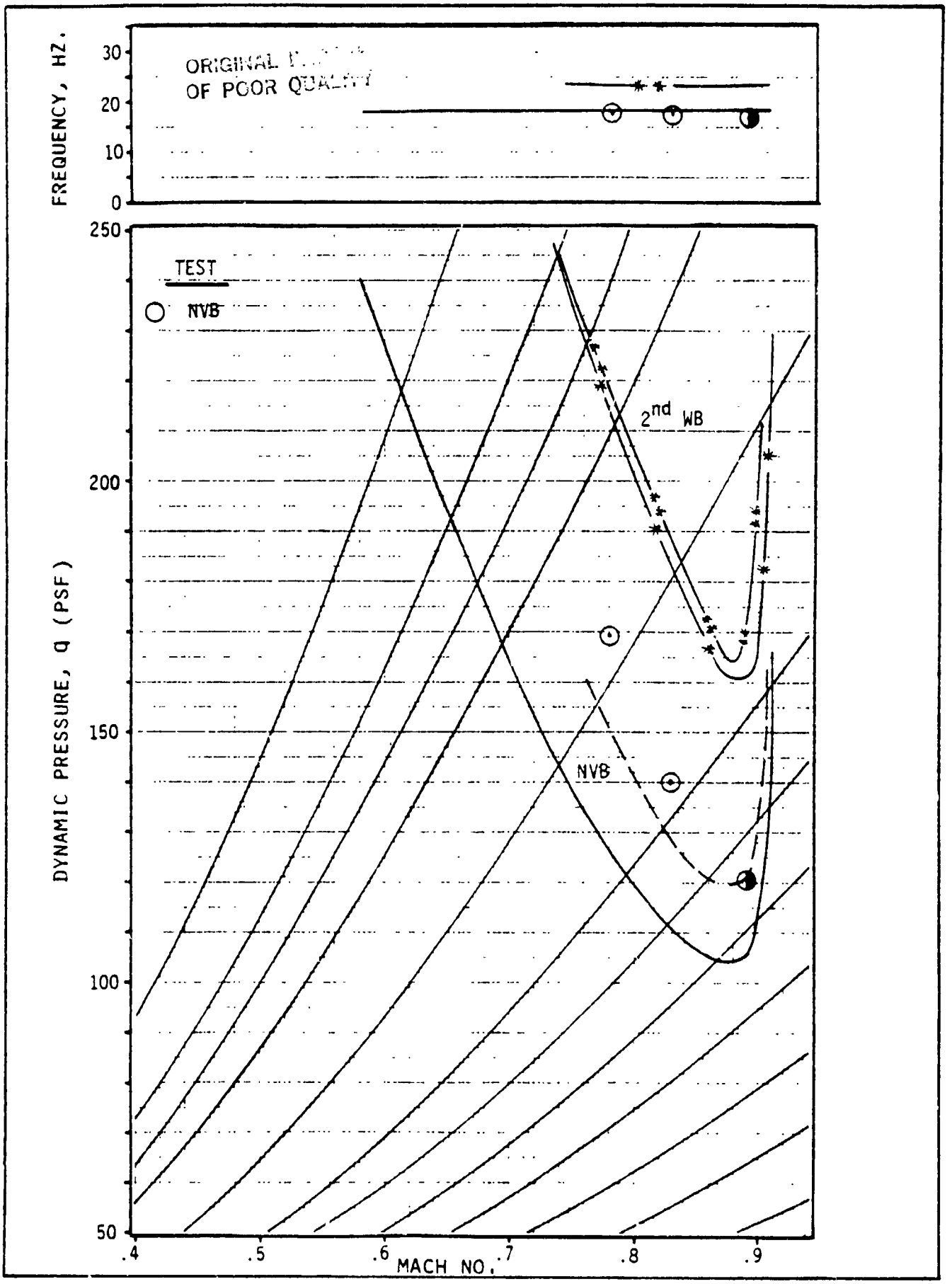

FIGURE 8a FLUTTER CORRELATION FOR WING (EMPTY) - NACELLE (NOMINAL) - NOMINAL TIP

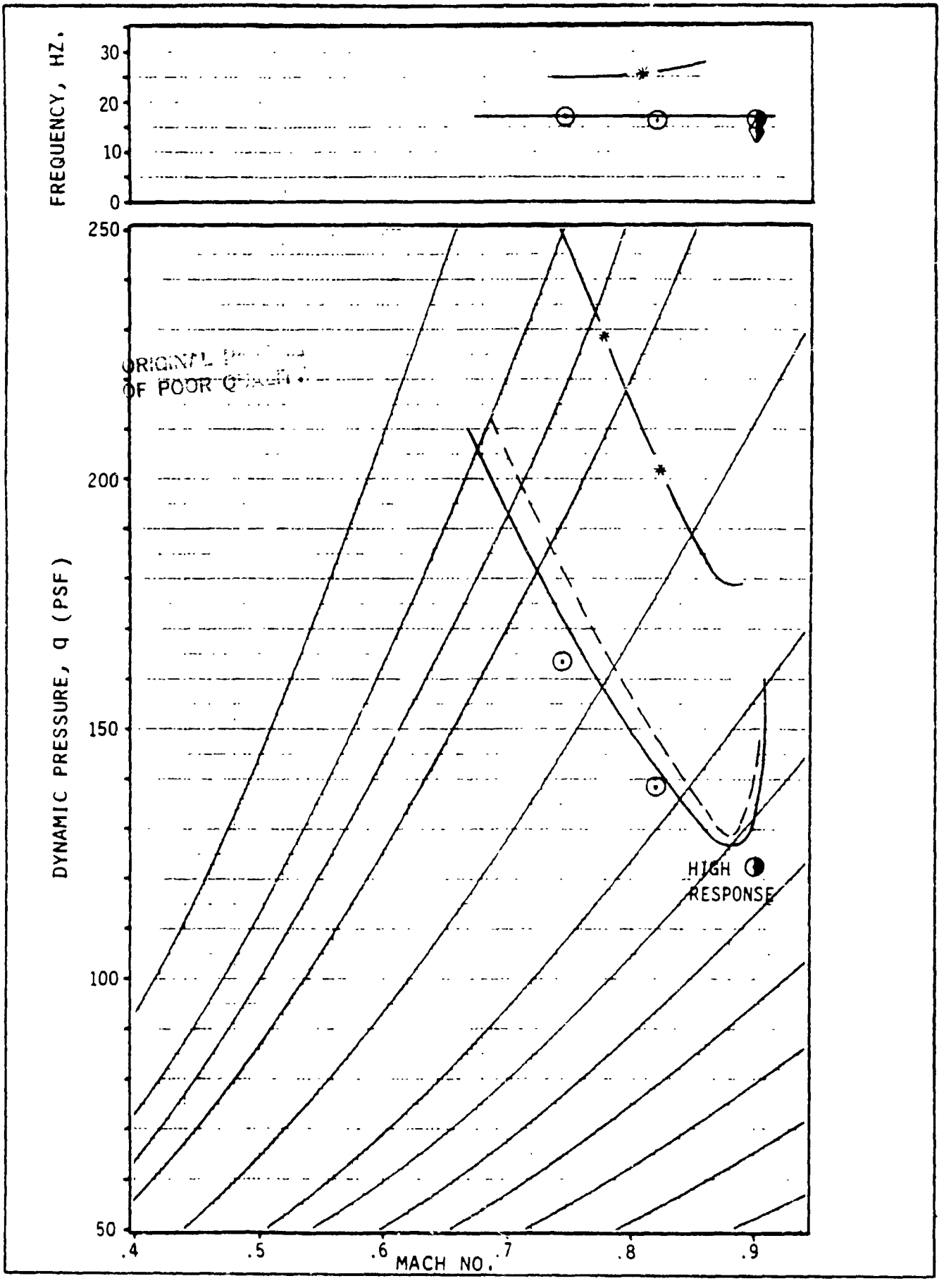

FIGURE 8b FLUTTEP CORRELATION FOP WING (EMPTY) - NACELLE (NOMINAL) - BALLASTED TIP

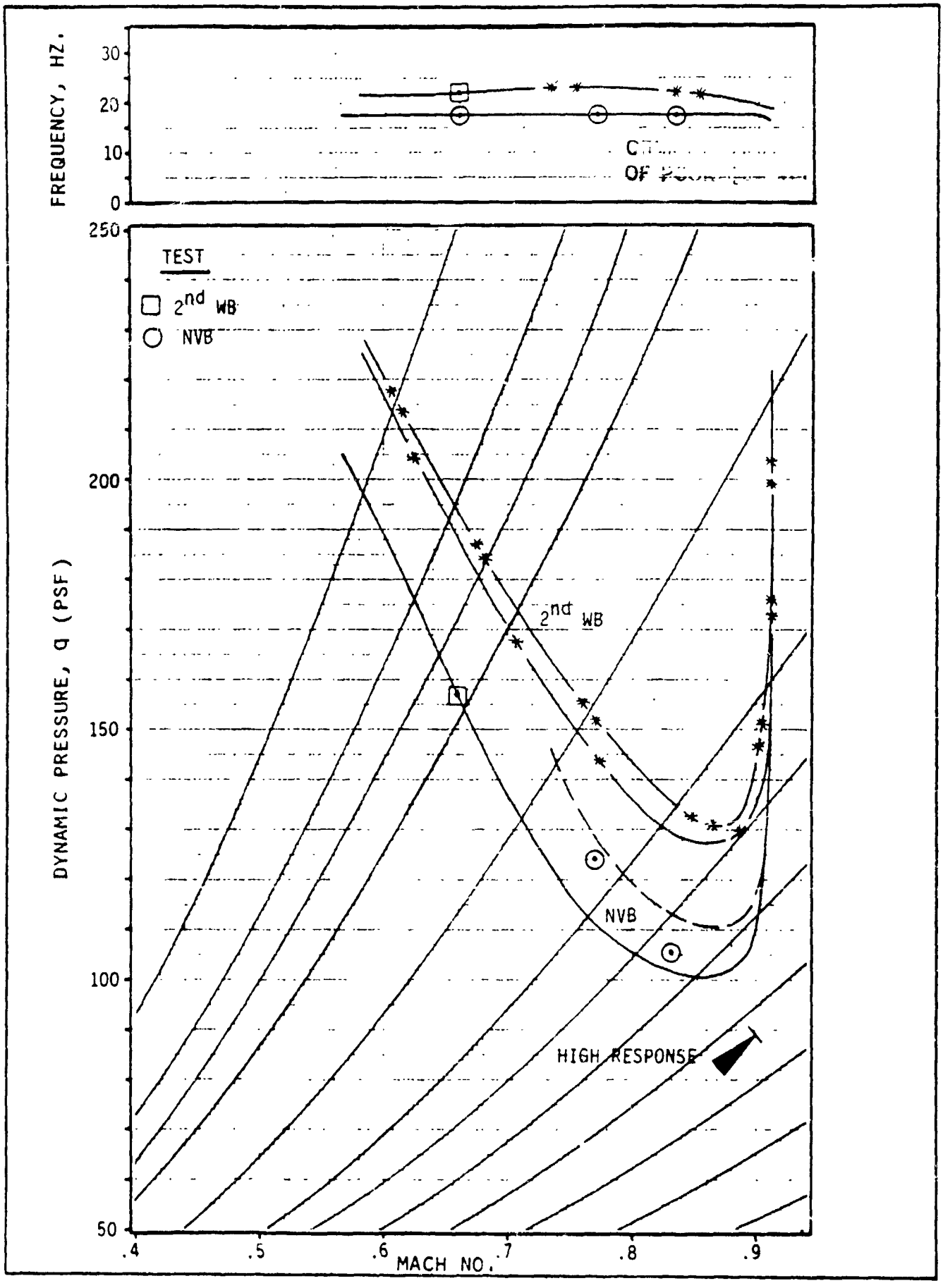

FIGURE 8c FLUTTER CORRELATION FOR WING (EMPTY) - NACELLE (NOMINAL) - WINGLET (20 DEG)

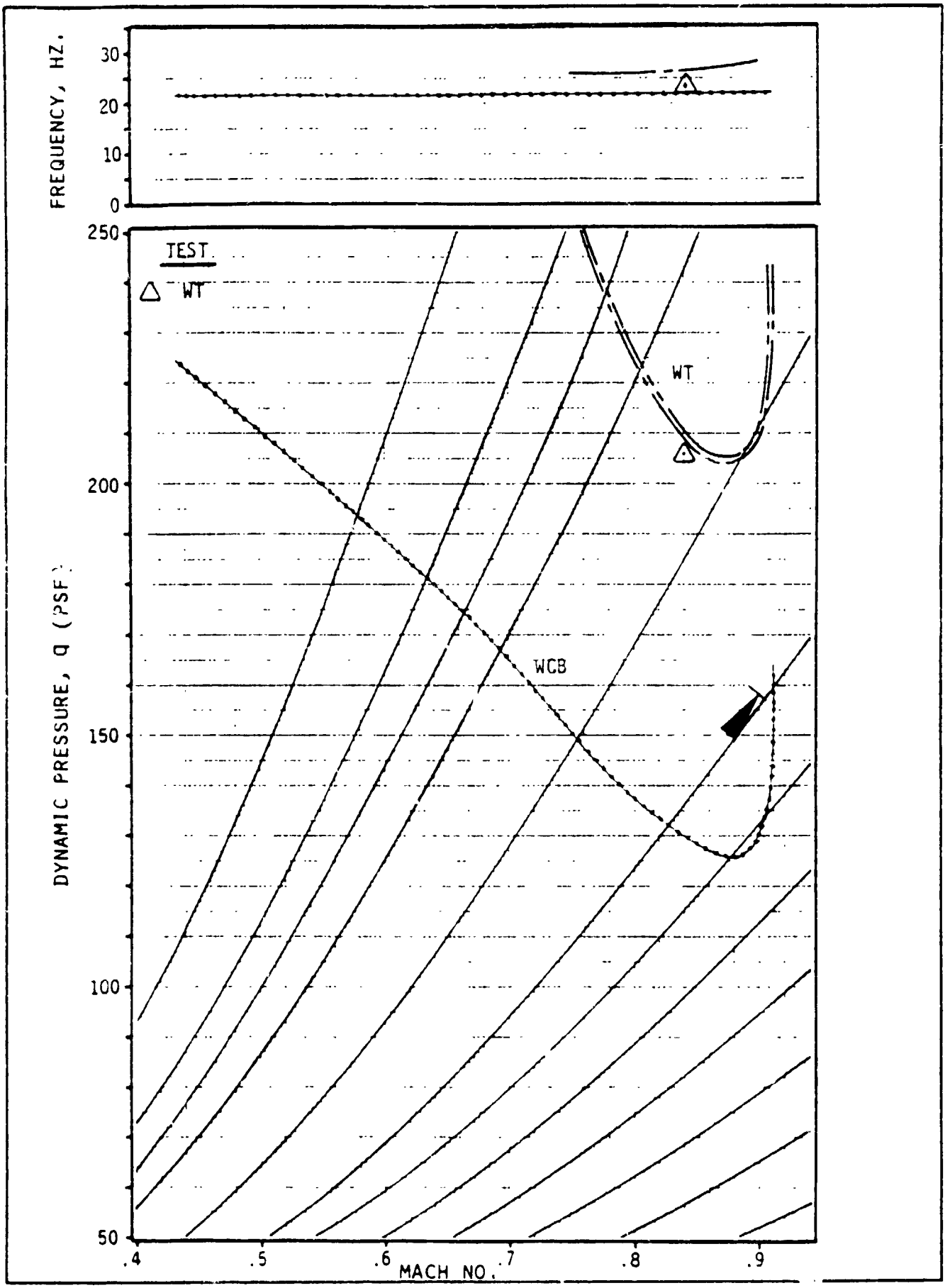

FIGURE 9a FLUTTER CORRELATION FOR WING (FULL) - NACELLE (NOMINAL) - NOMINAL TIP

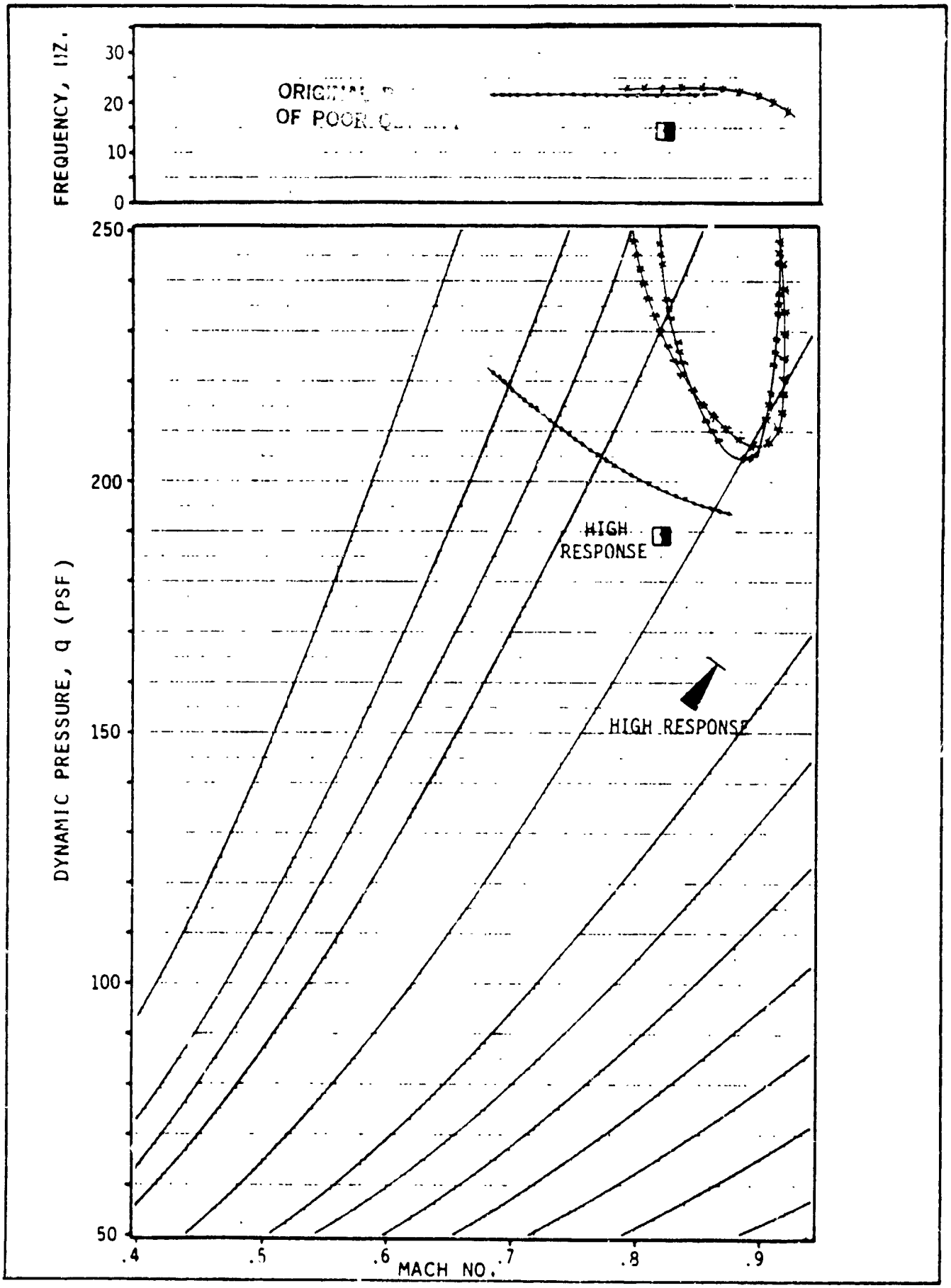

FIGURE 9b FLUTTER CORRELATION FOR WING (FULL) - NACELLE (NOMINAL) - BALLASTED TIP

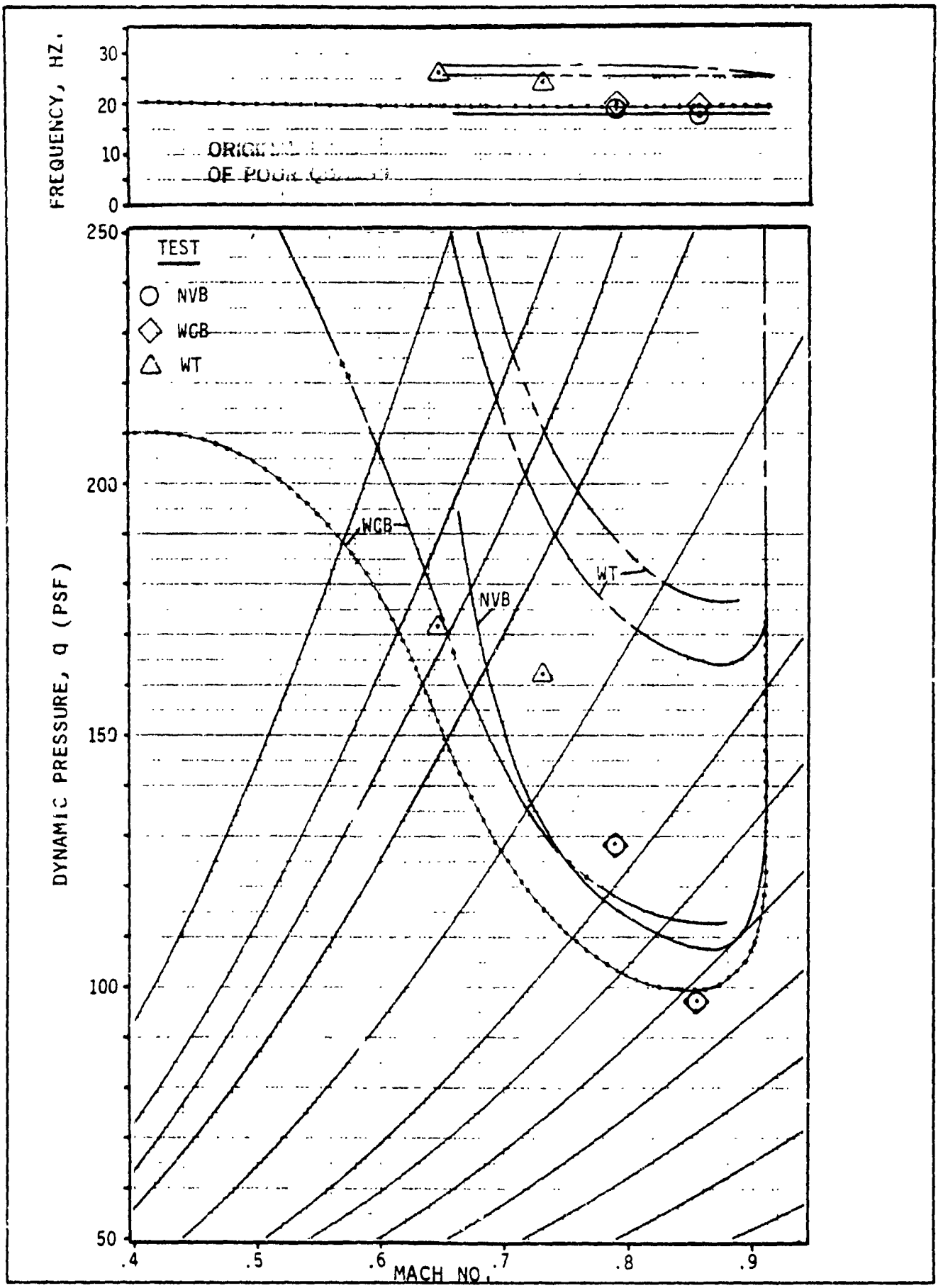

FIGURE 9c FLUTTER CORRELATION FOR WING (FULL) - NACELLE (NOMINAL) - WINGLET (20 DEG)

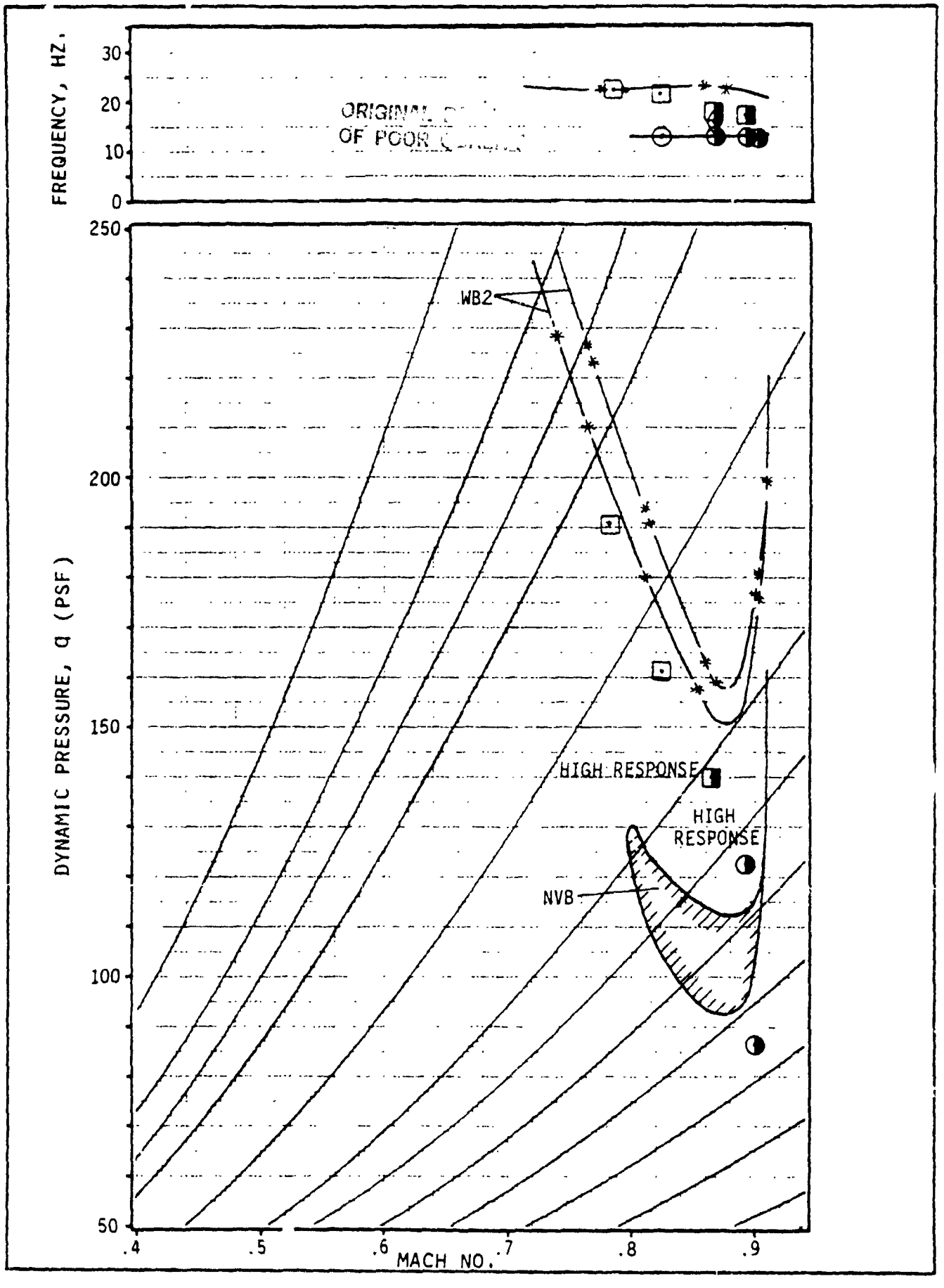

FIGURE 10a FLUTTER CORRELATION FOR WING (EMPTY) - NACELLE (SOFT) - NOMINAL TIP

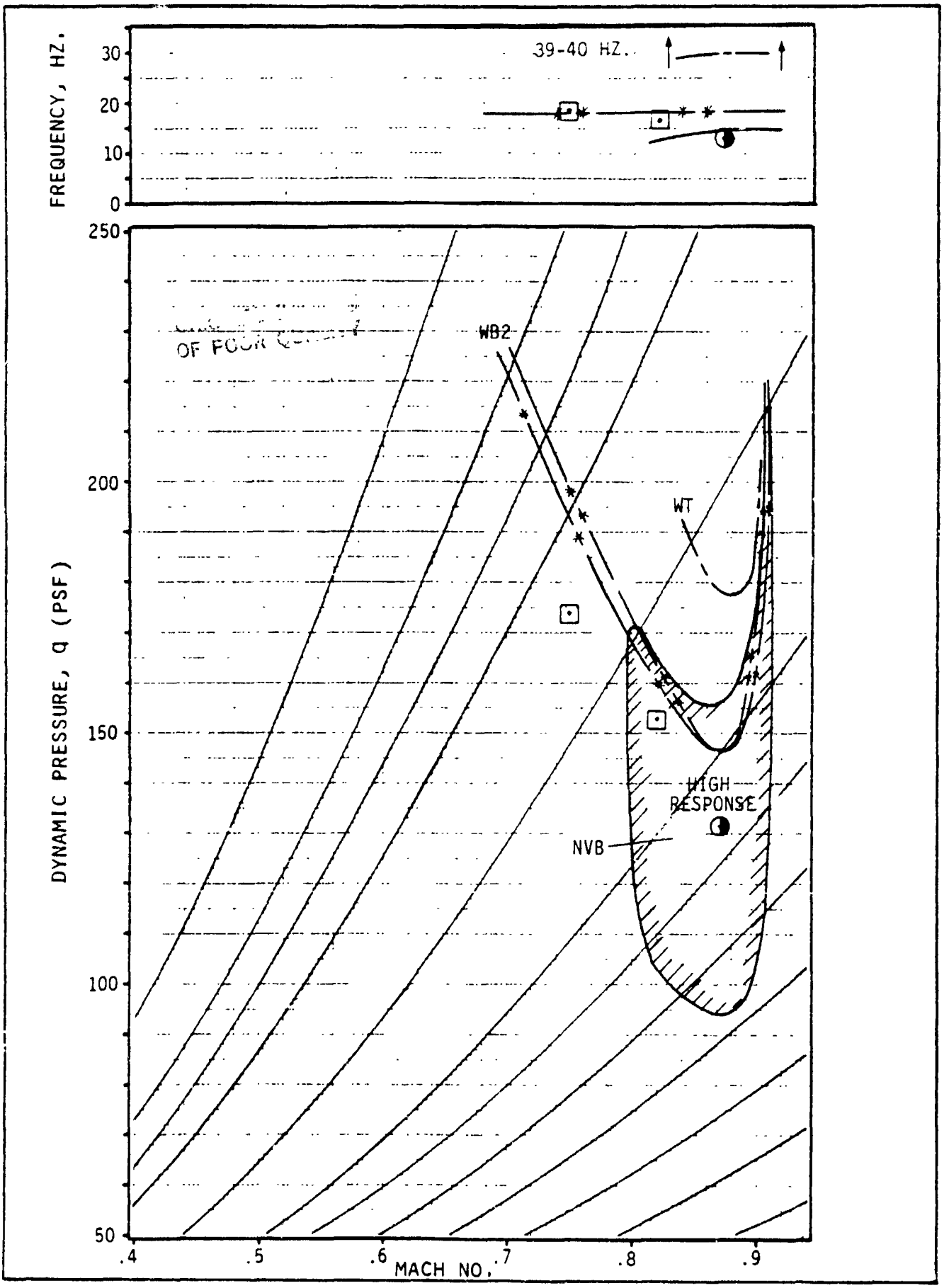

FIGURE 10b FLUTTER CORRELATION FOR WING (EMPTY) - NACELLE (SOFT) - BALLASTED TIP

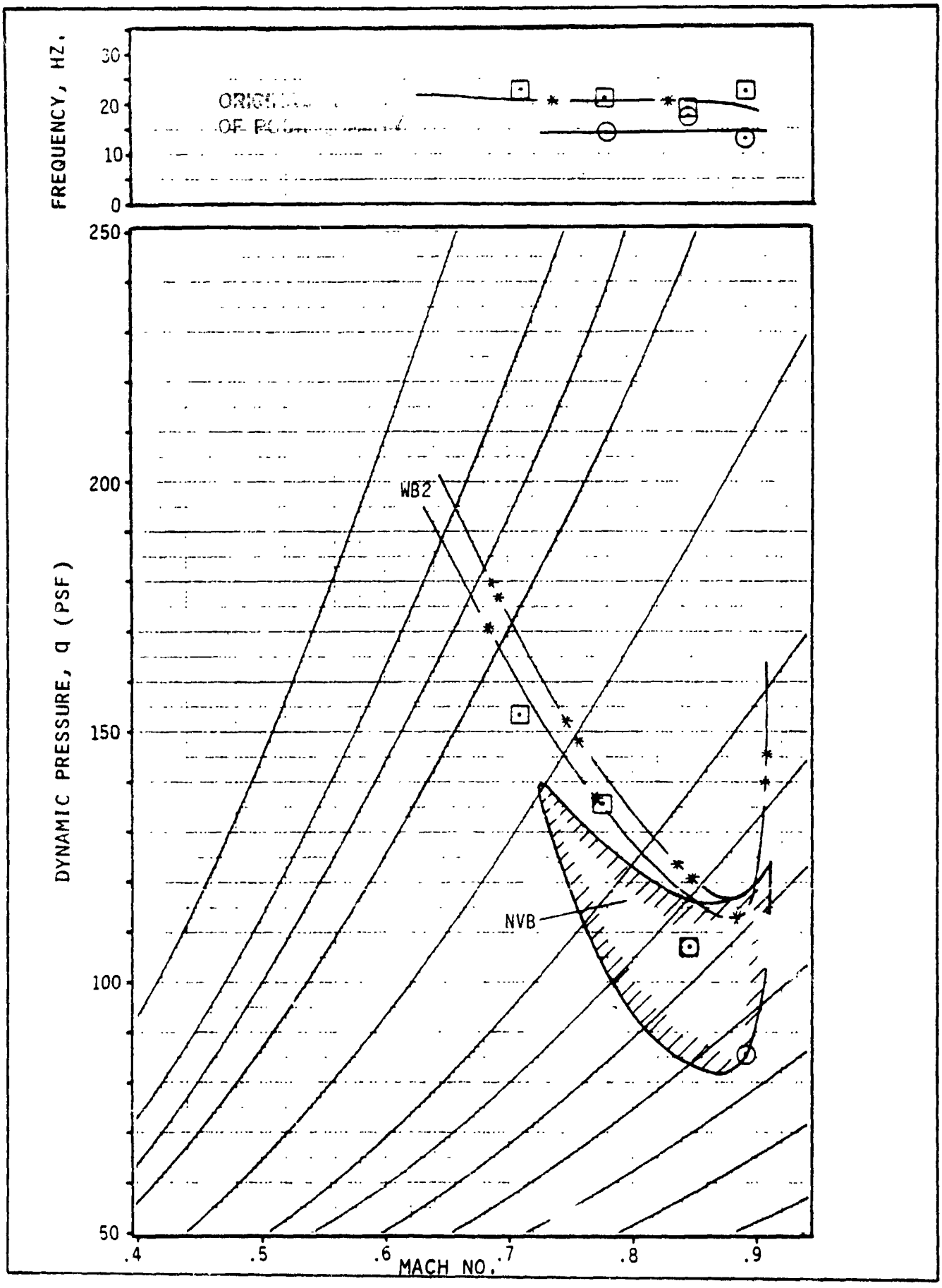

FIGURE 10c FLUTTER CORRELATION FOR WING (EMPTY) - NACELLE (SOFT) - WINGLET (20 DEG)

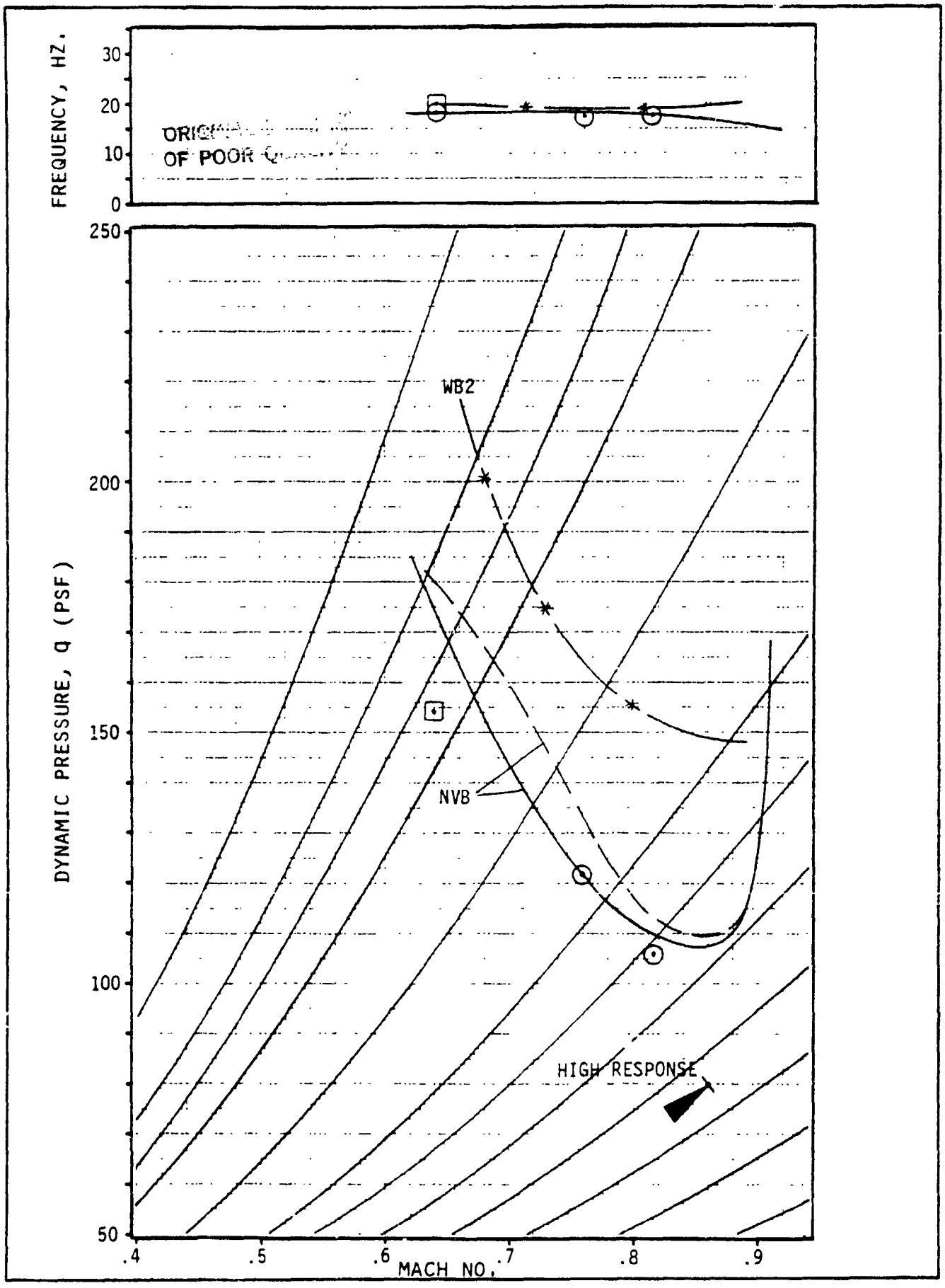

FIGURE 11 FLUTTER CORRELATION FOR WING (EMPTY) - NACELLE (NOMINAL) - WINGLET (0 DEG)

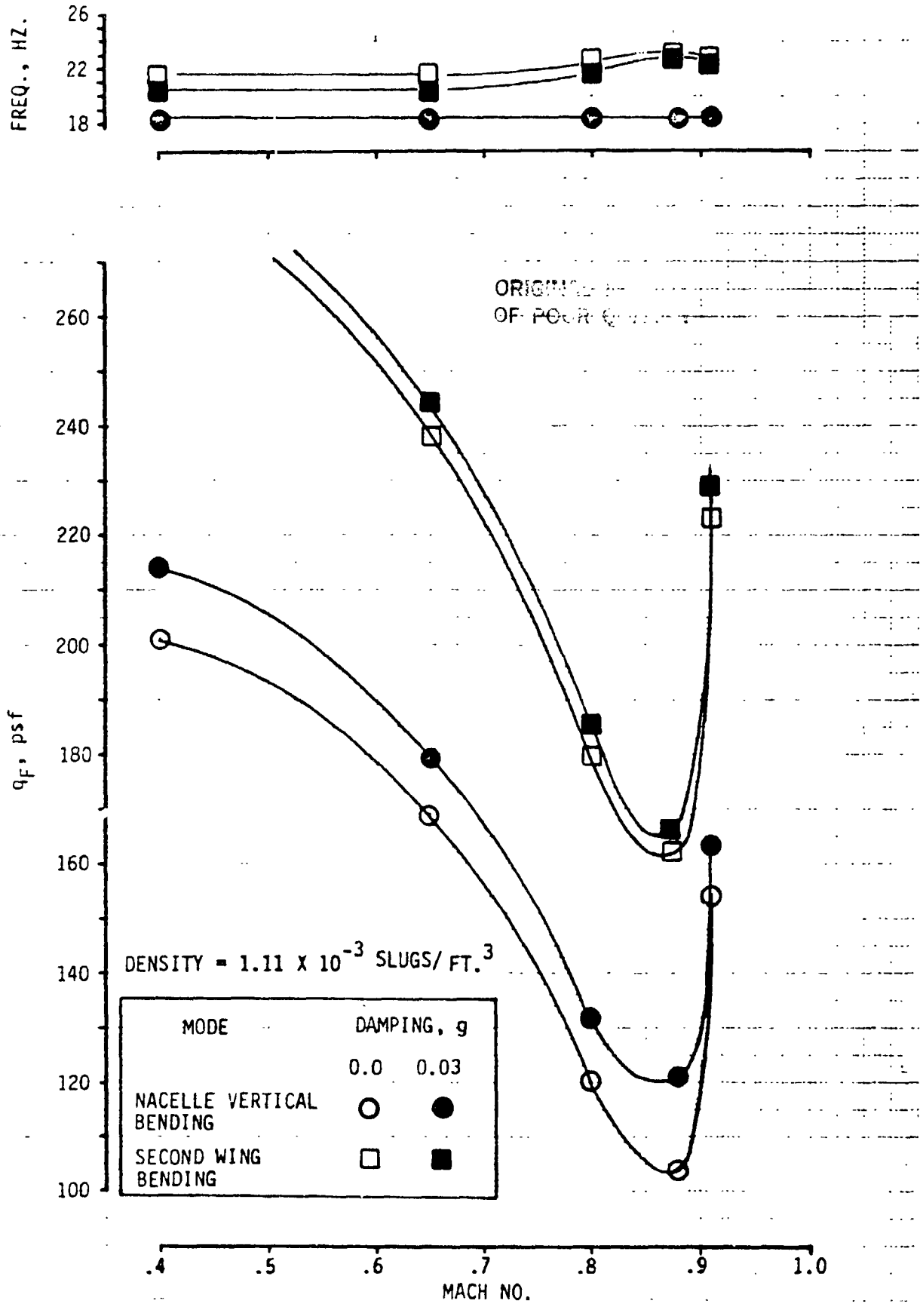

FIGURE 12a ANALYTICAL FLUTTER BOUNDARIES FOR WING (EMPTY) - NACELLE (NOMINAL) - NOMINAL TIP, MACH NUMBER EFFECT

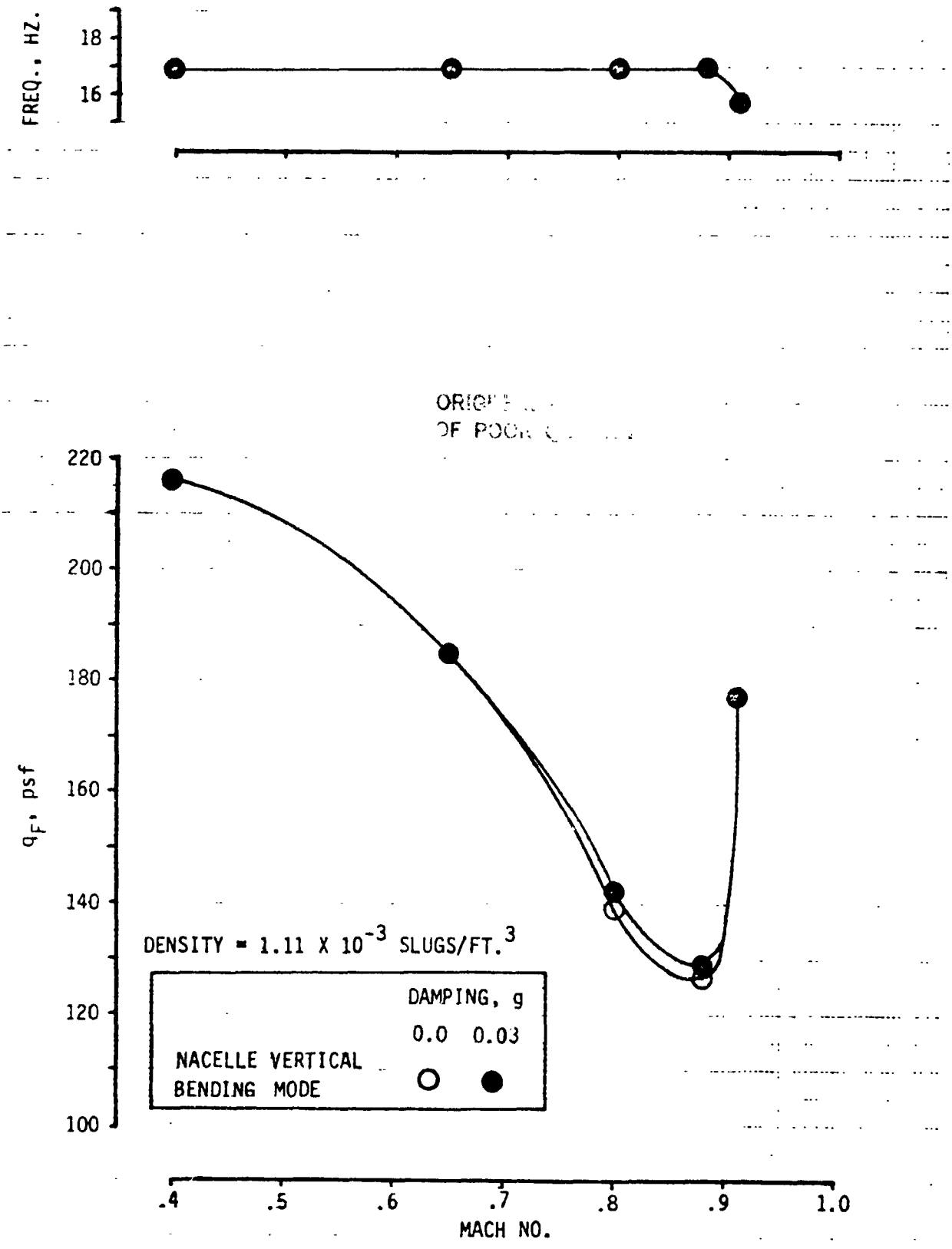

FIGURE 12b ANALYTICAL FLUTTER BOUNDARIES FOR WING (EMPTY) - NACELLE (NOMINAL)-BALLASTED TIP, MACH NUMBER EFFECT

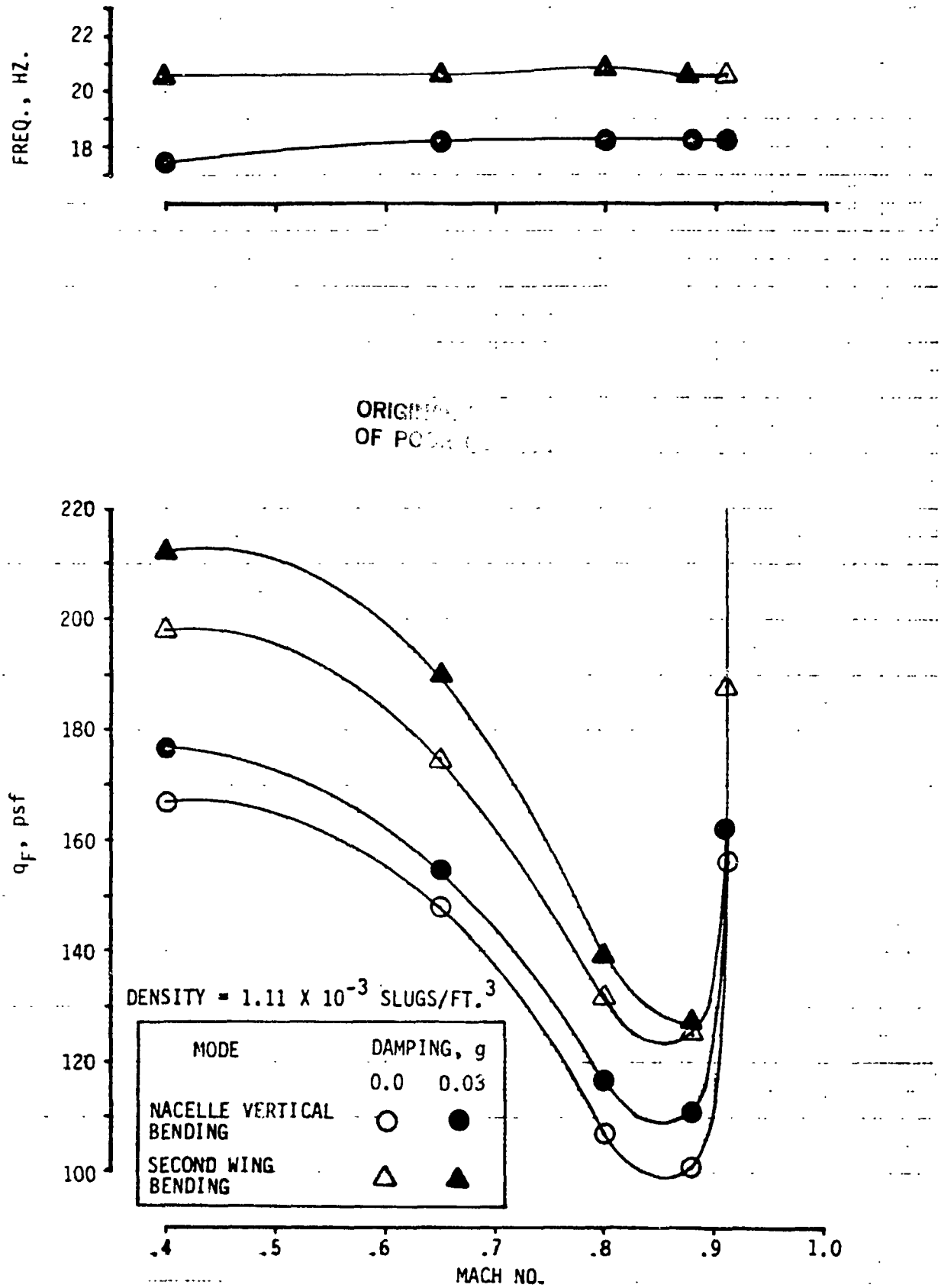

FIGURE 12c ANALYTICAL FLUTTER BOUNDARIES FOR WING (EMPTY) - NACELLE(NOMINAL)-WINGLET (20 DEG), MACH NUMBER EFFECT

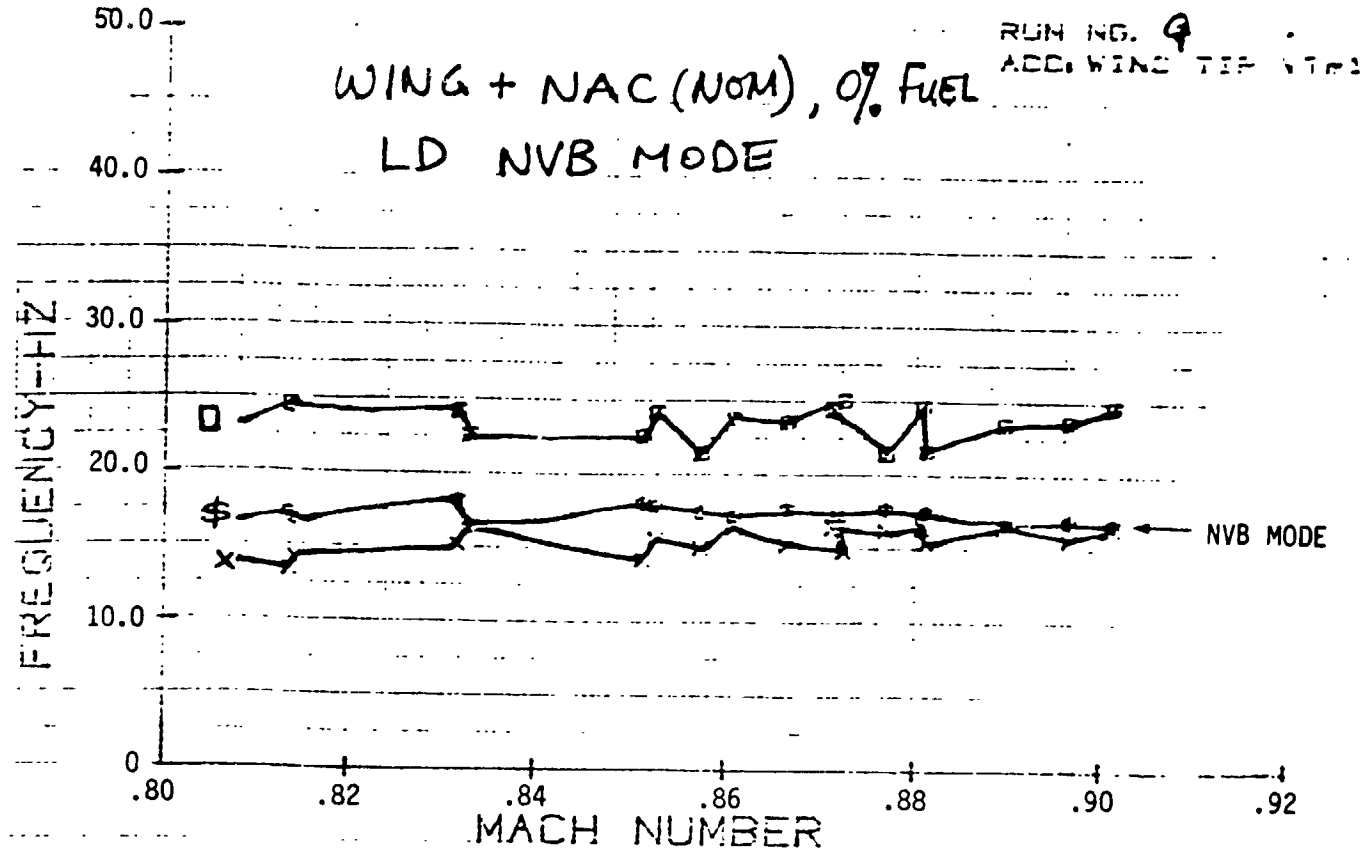

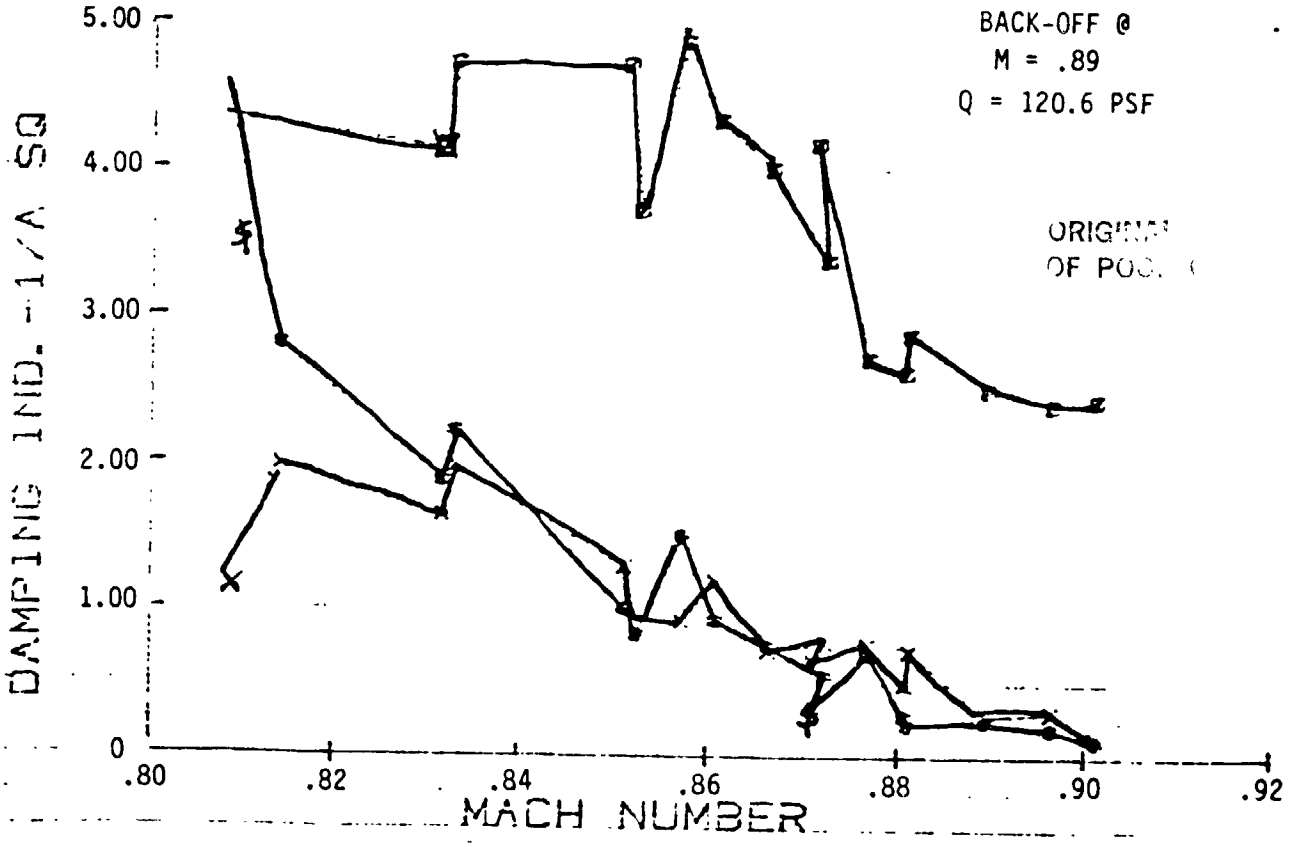

FIGURE 13a ON-LINE PLOT OF $1/(\text{AMPLITUDE})^2$ Vs MACH NUMBER, FLUTTER APPROACH, WING(EMPTY)-NACELLE (NOMINAL)

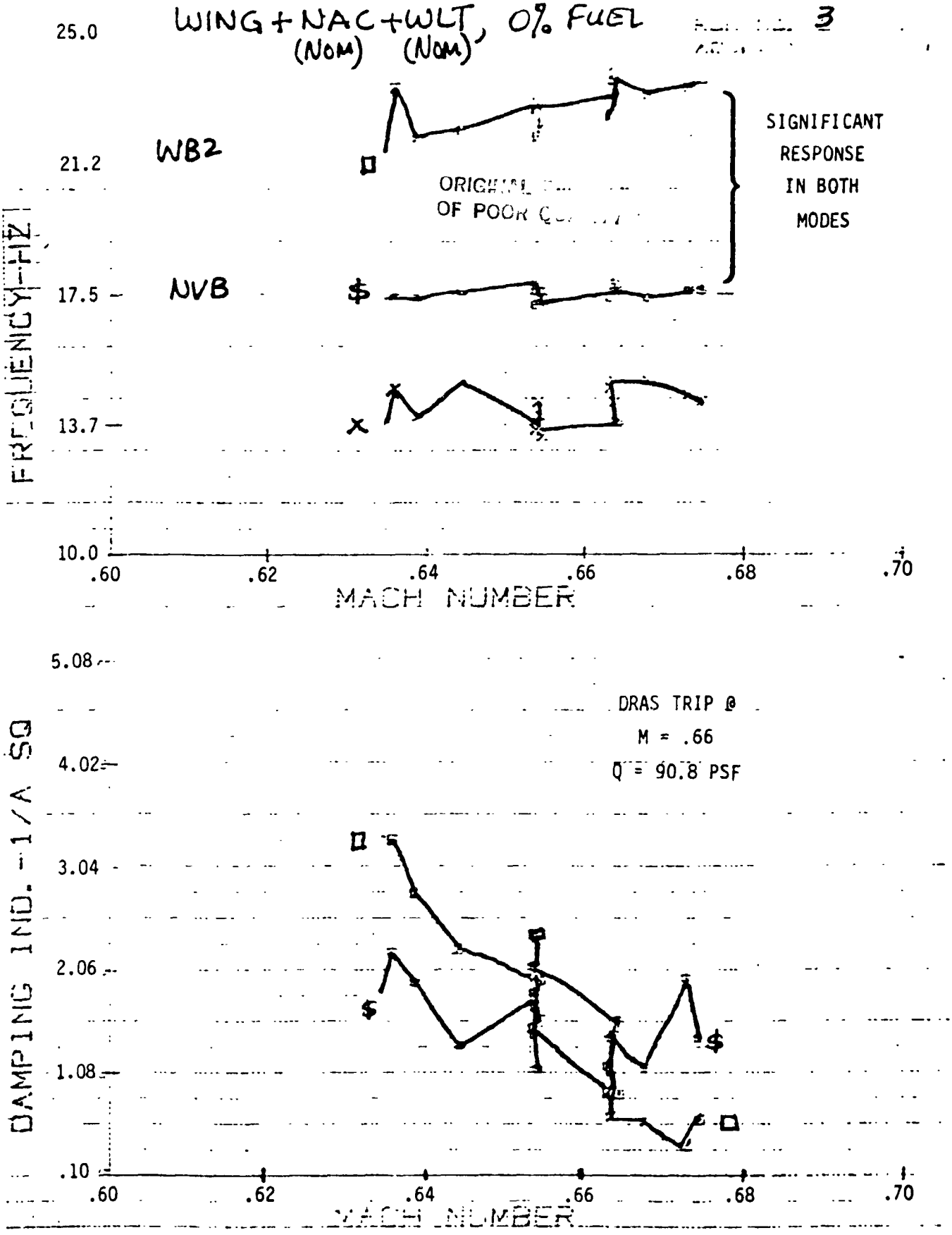

FIGUPE 13b ON-LINE PLOT OF $1/(\text{AMPLITUDE})^2$ Vs MACH NUMBER, FLUTTER APPROACH, WING(EMPTY)-NACELLE (NOMINAL)- WINGLET (20 DEG)

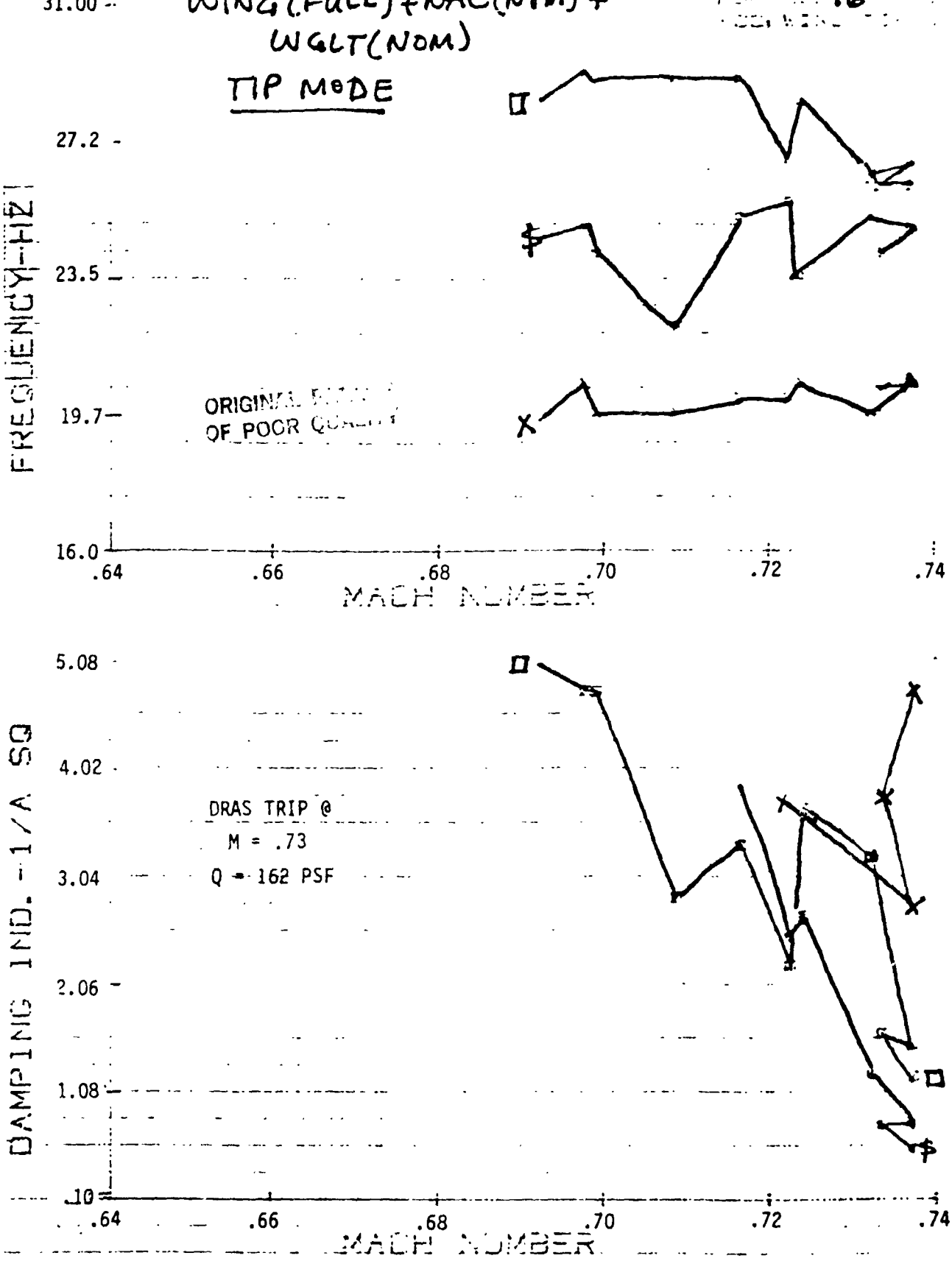

FIGURE 13c ON-LINE PLOT OF 1/(AMPLITUDE)^2 Vs MACH NUMBER, FLUTTER APPROACH, WING(FULL)-NACELLE (NOMINAL)- WINGLET (20 DEG)

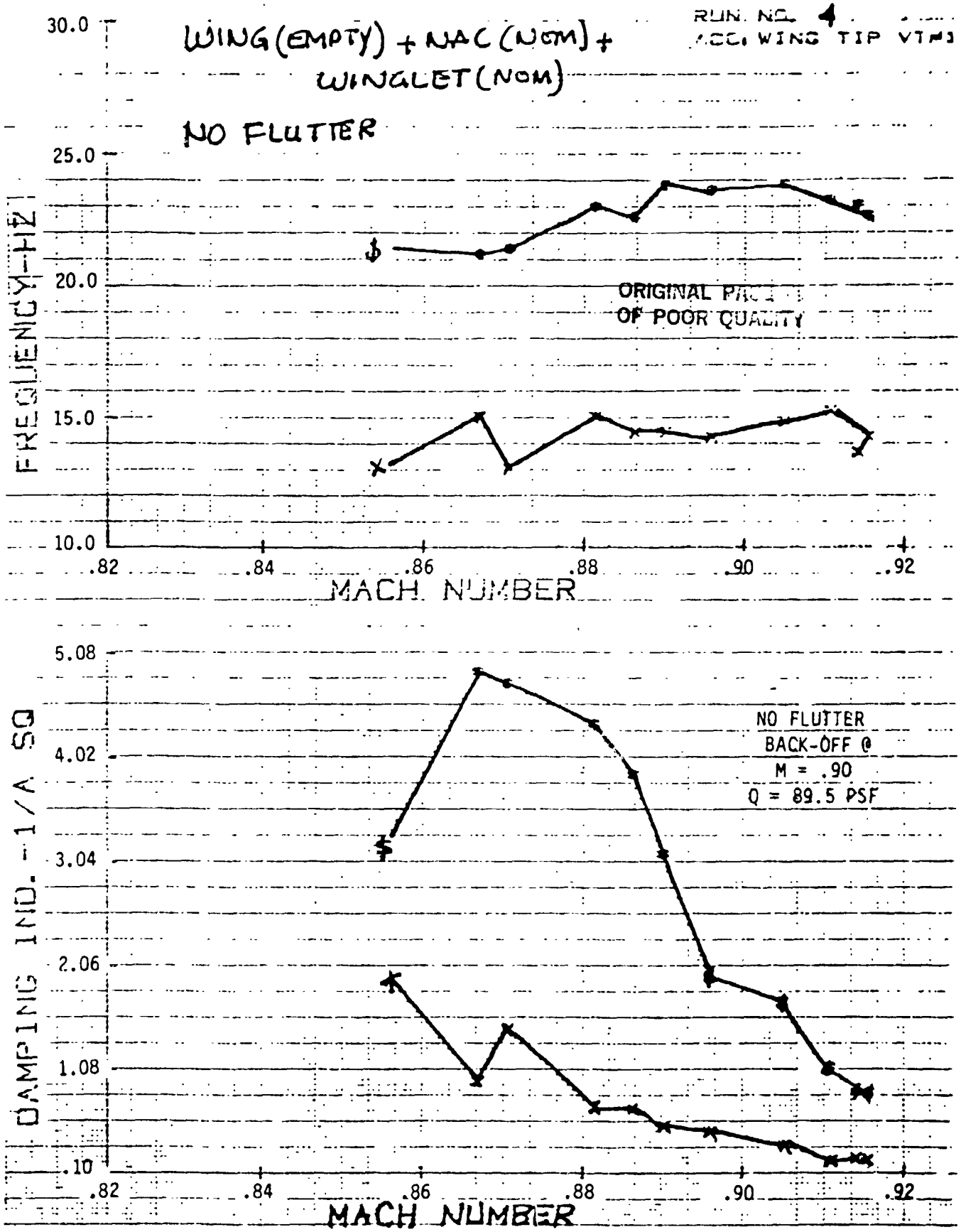

FIGURE 13d ON-LINE PLOT OF 1/(AMPLITUDE)^2 Vs MACH NUMBER, NO FLUTTER, WING(EMPTY)-NACELLE (NOMINAL)- WINGLET (20 DEG)

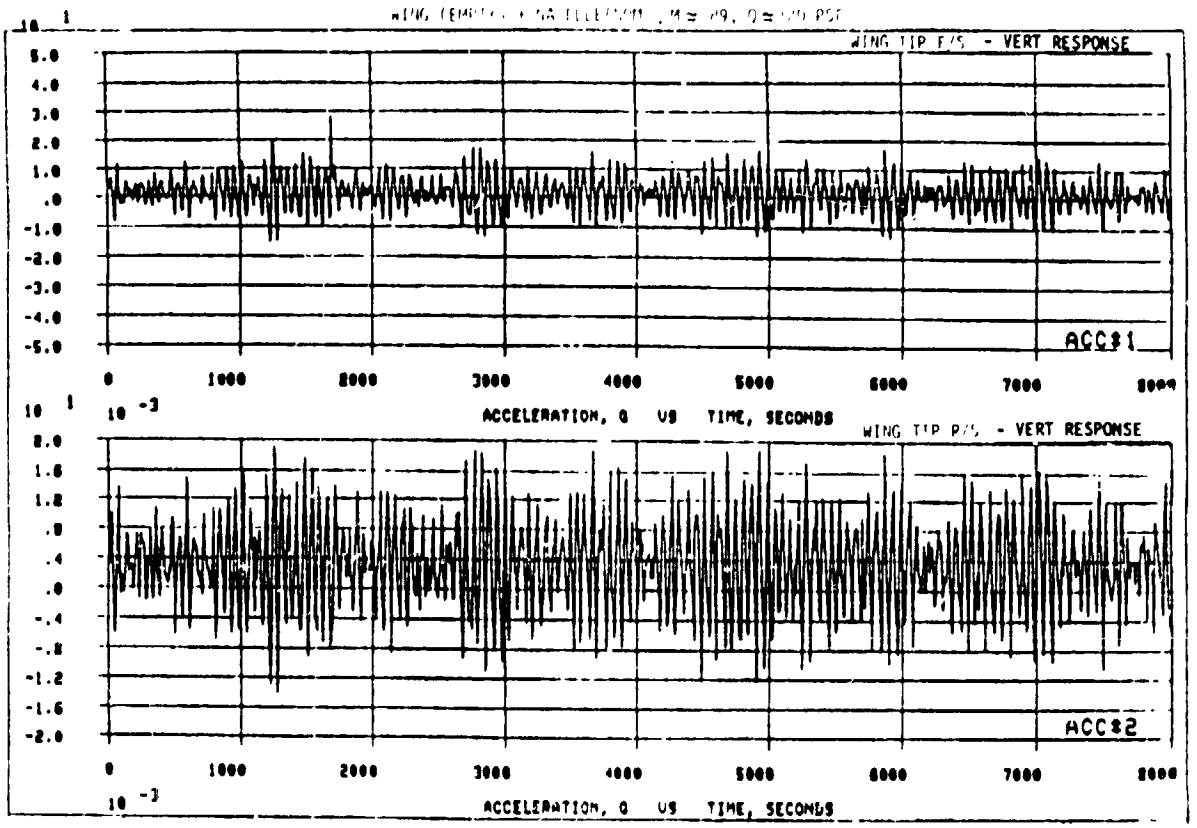

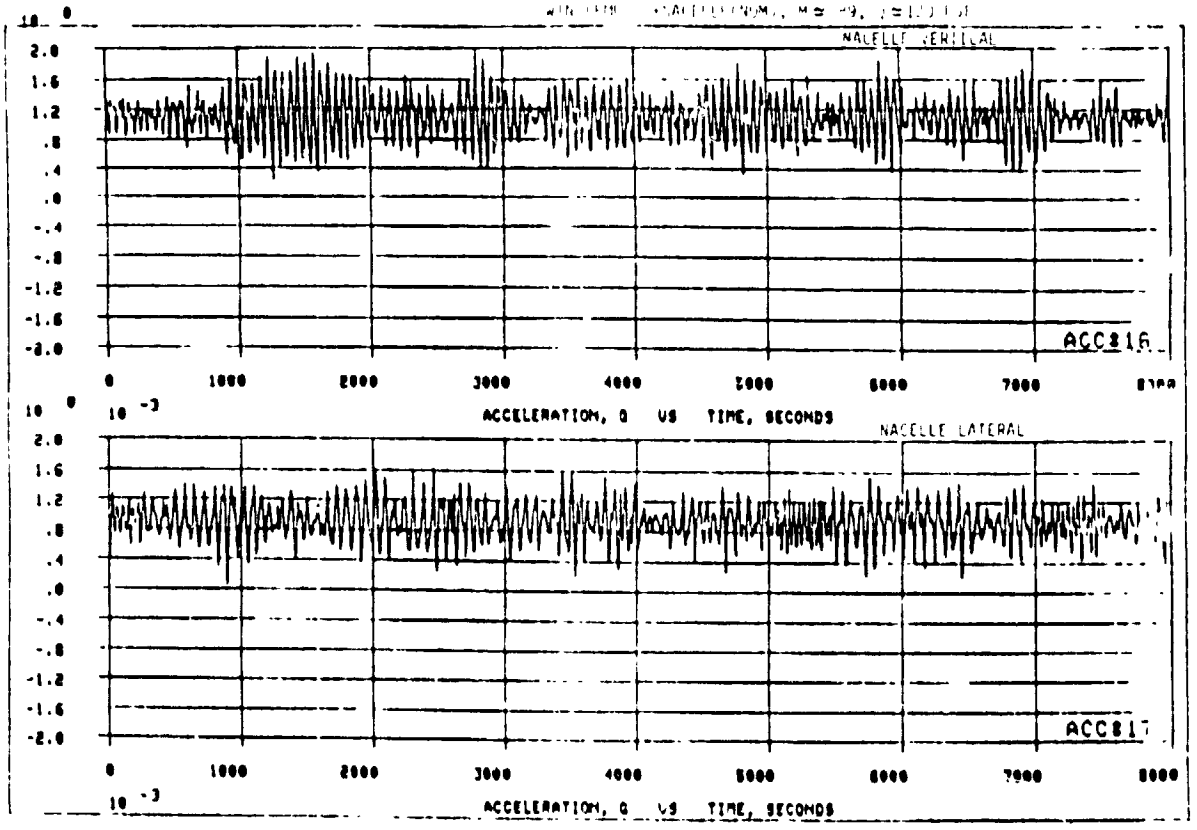

FIGURE 14a EXAMPLE OF RESPONSE TIME HISTORIES,
WING (EMPTY) -NACELLE(NOMINAL)

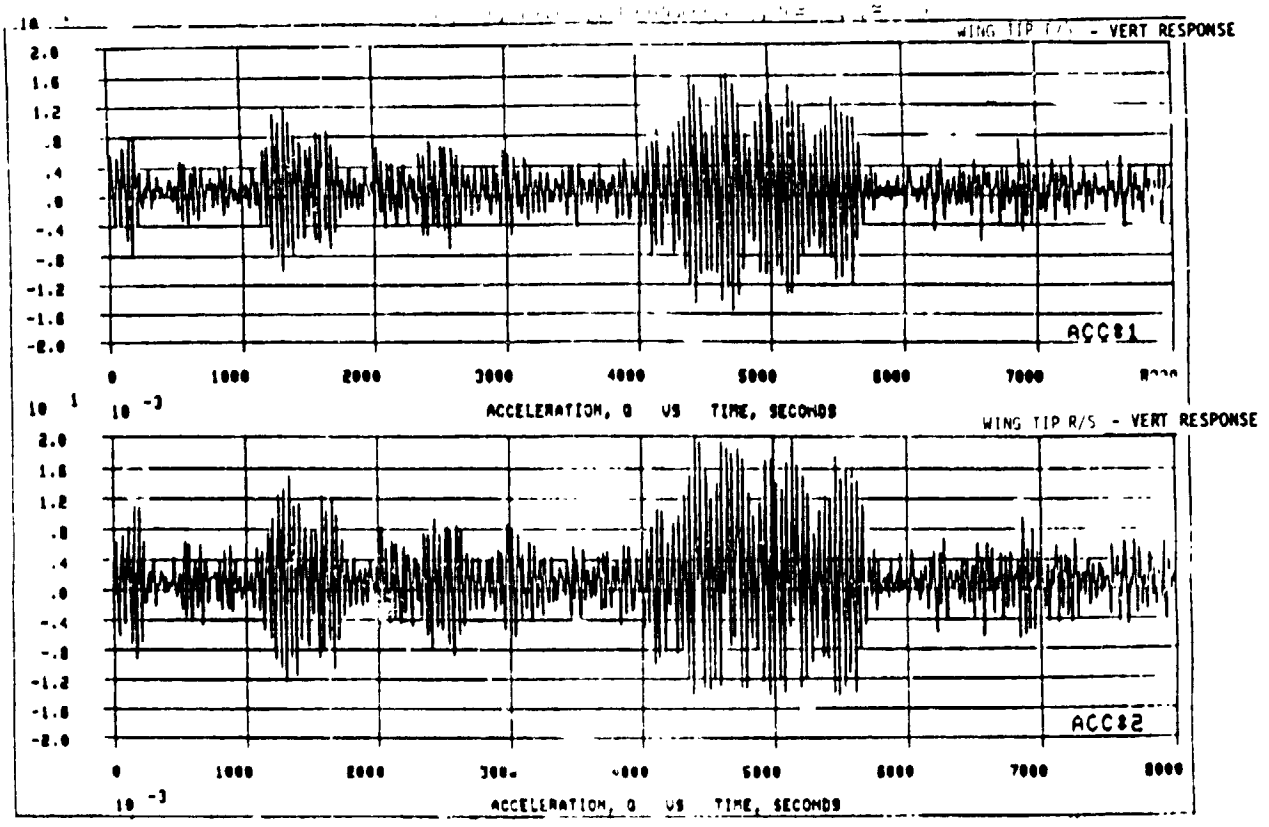

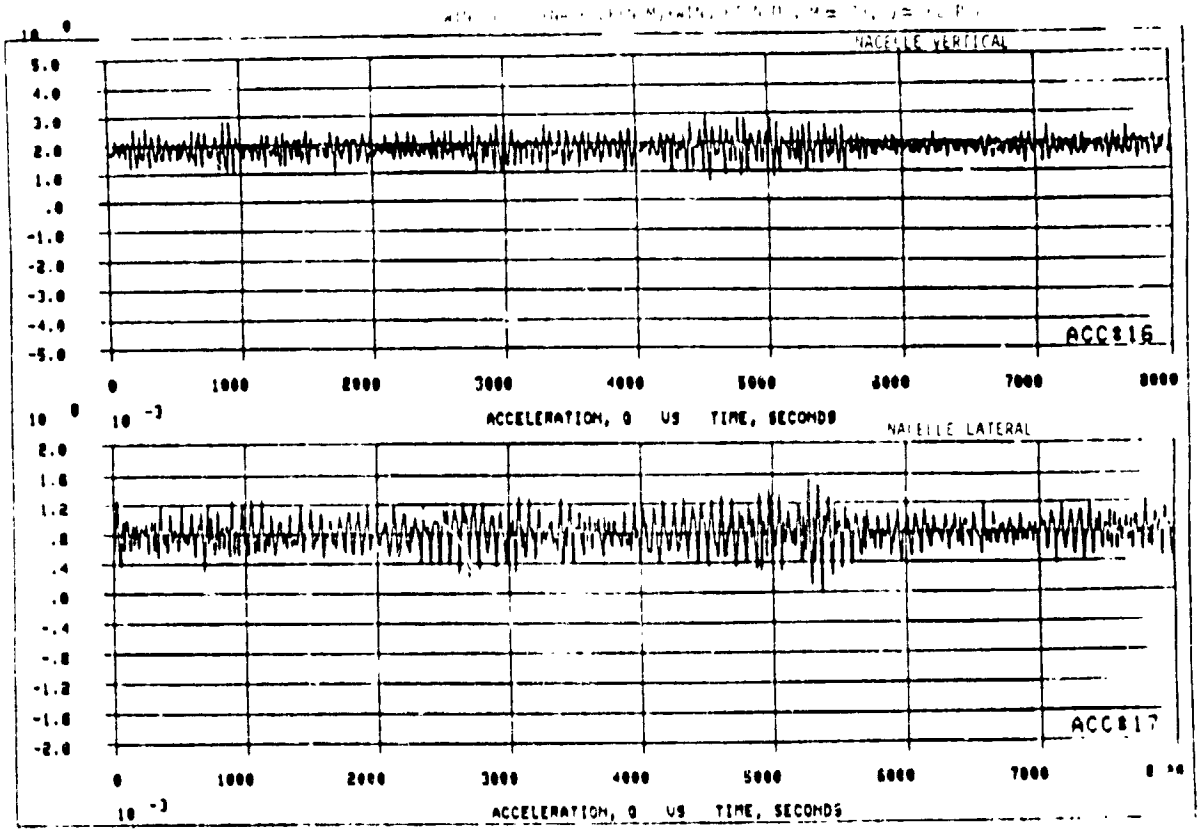

FIGURE 14b EXAMPLE OF RESPONSE TIME HISTORIES,
WING(FULL) -NACELLE(NOMINAL)-WINGLET (20 DEG)

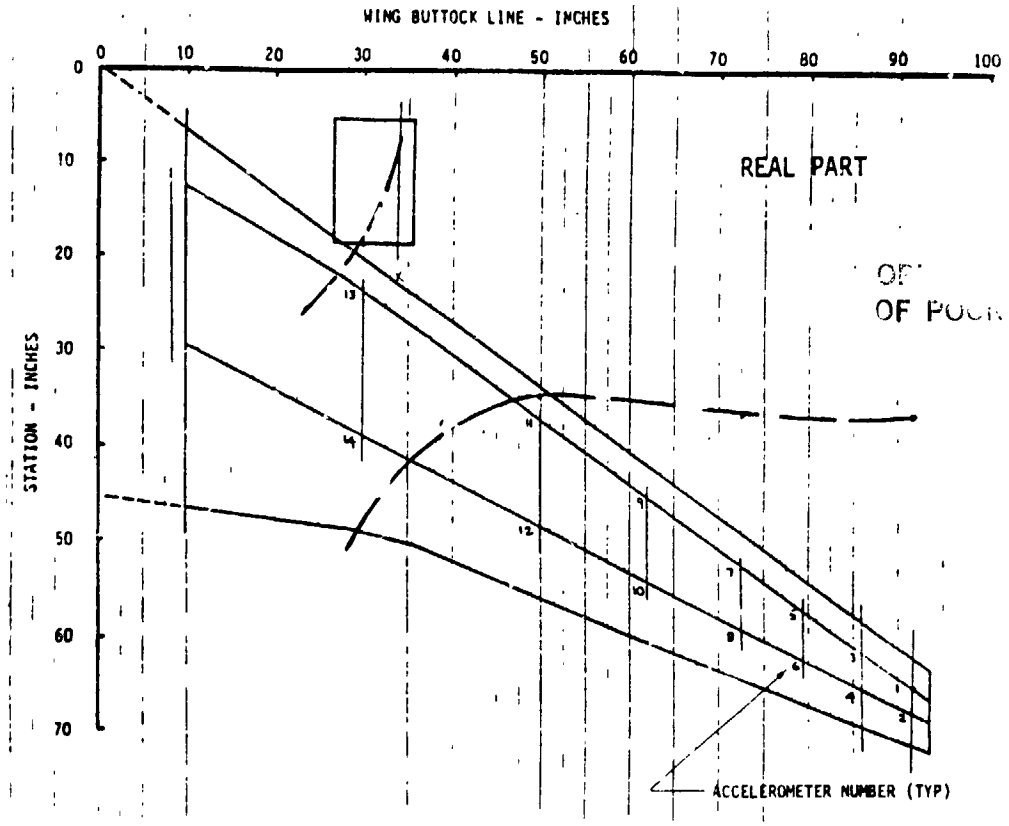

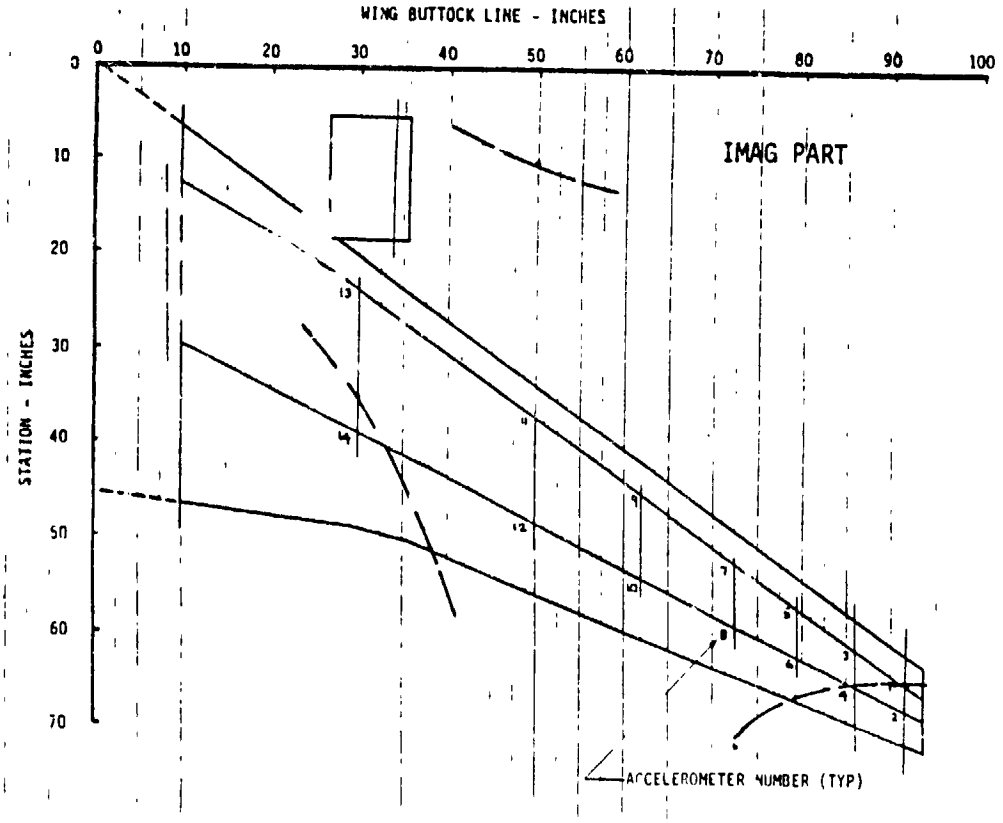

FIGURE 15a NODE LINE AT APPROACH TO FLUTTER, 17.5Hz MODE, M=0.66, WING(EMPTY)-NACELLE(NOMINAL)- WINGLET(20 DEG)

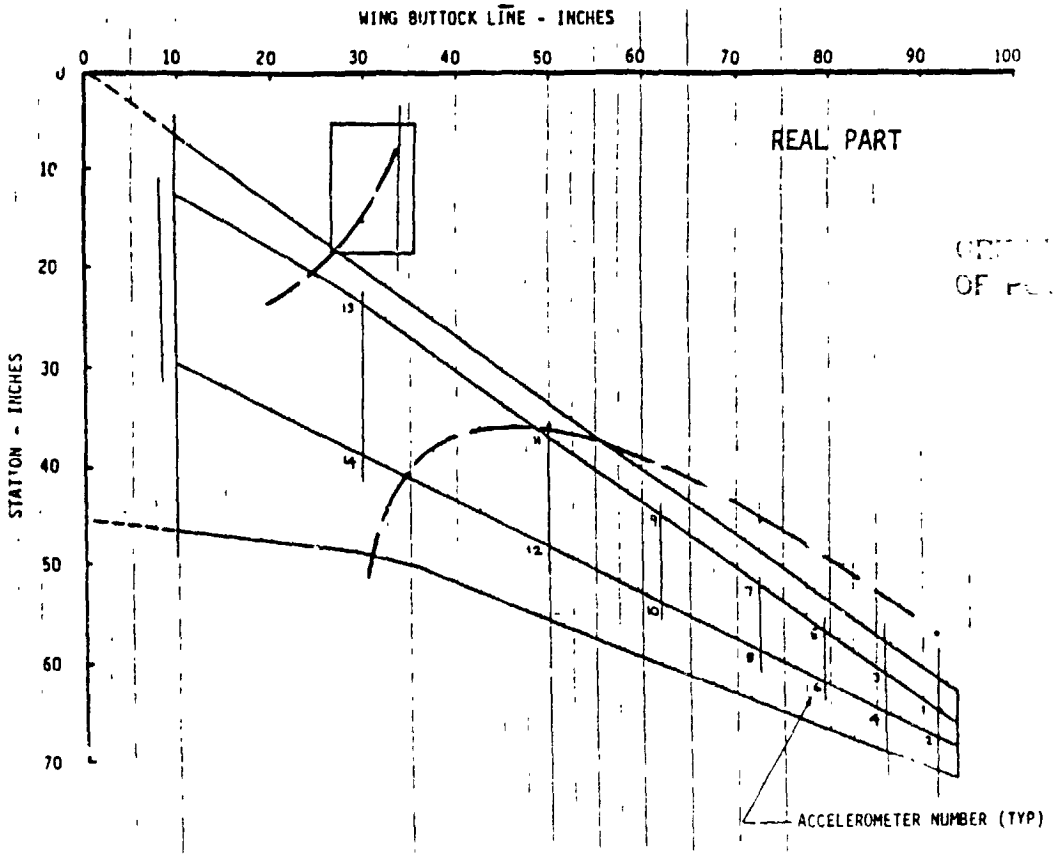

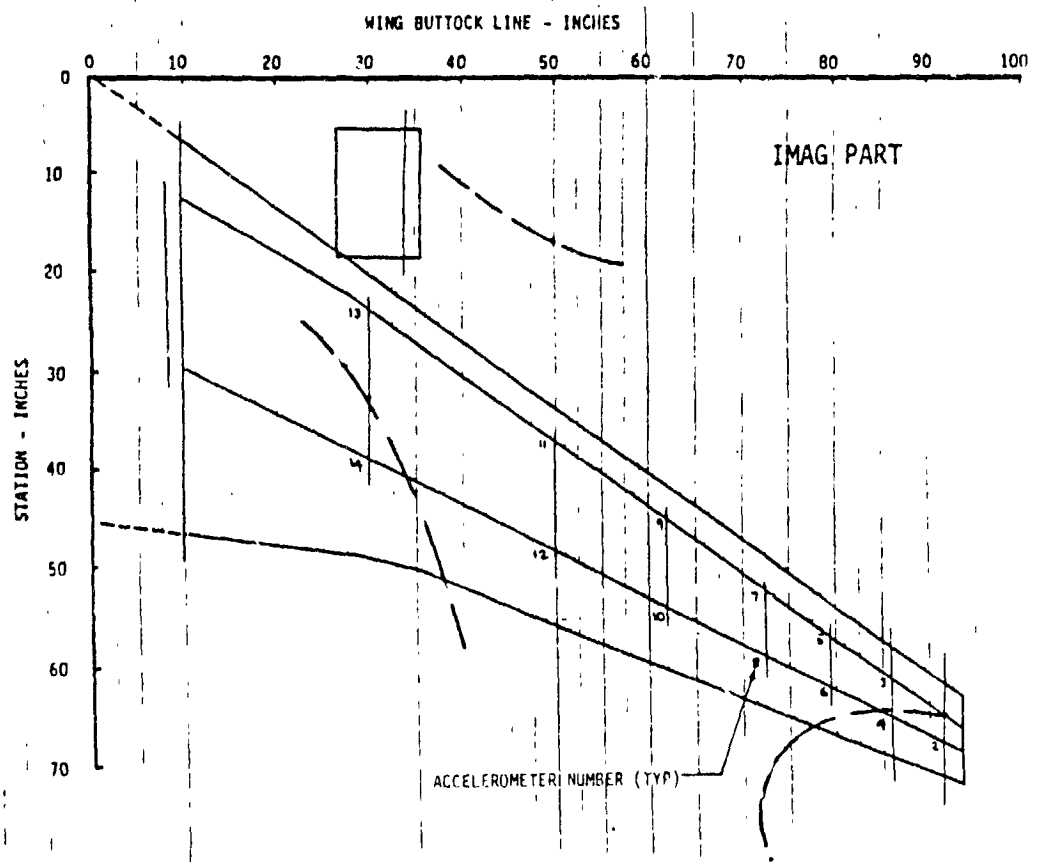

FIGURE 15b NODE LINE AT APPROACH TO FLUTTER, 22Hz MODE, M=0.66,
WING(EMPTY)-NACELLE(NOMINAL)-WINGLET (20 DEG)

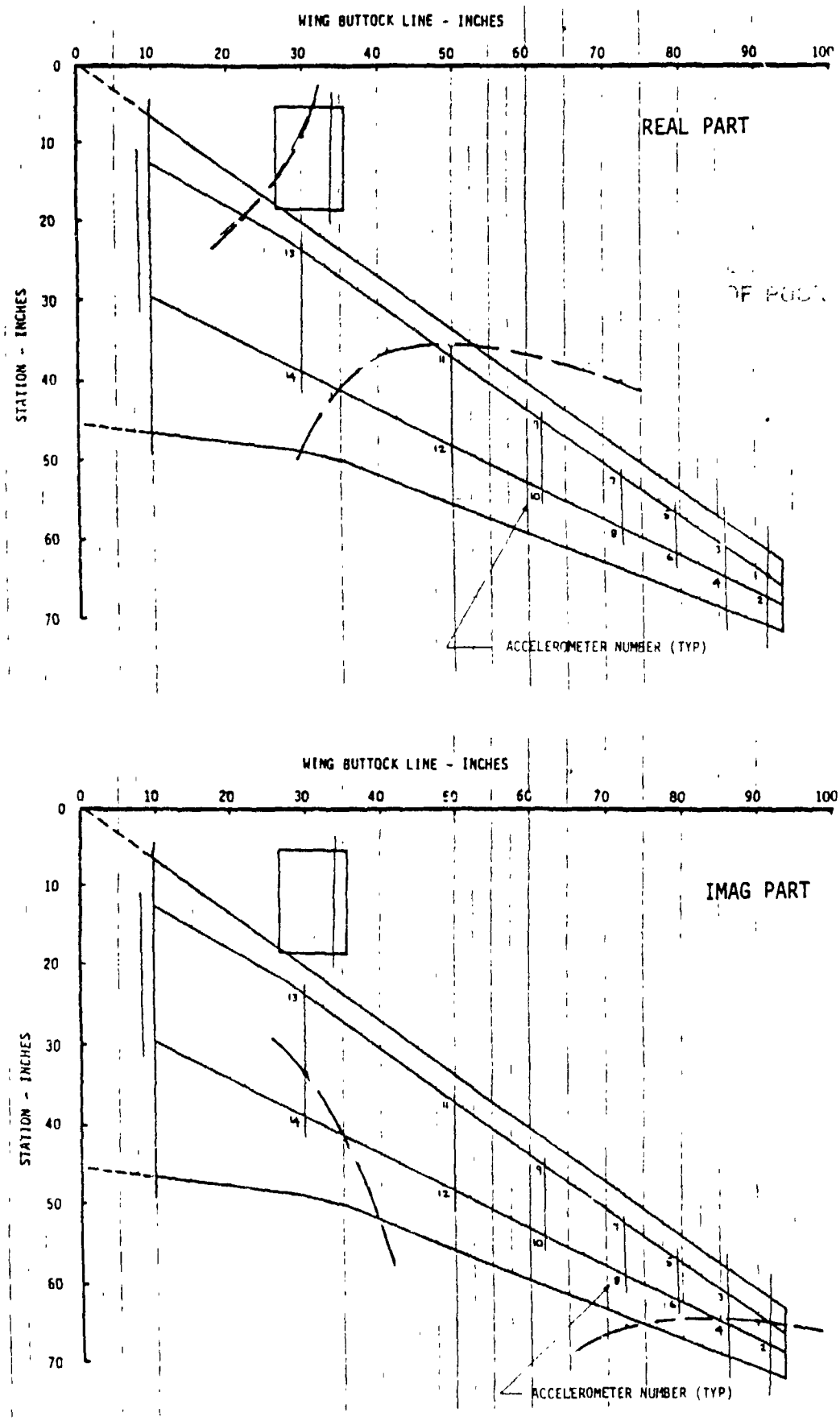

FIGURE 15c NODE LINE AT APPROACH TO FLUTTER, 17.5Hz MODE, M=0.828, WING(EMPTY)-NACELLE(NOMINAL) -WINGLET (20 DEG)

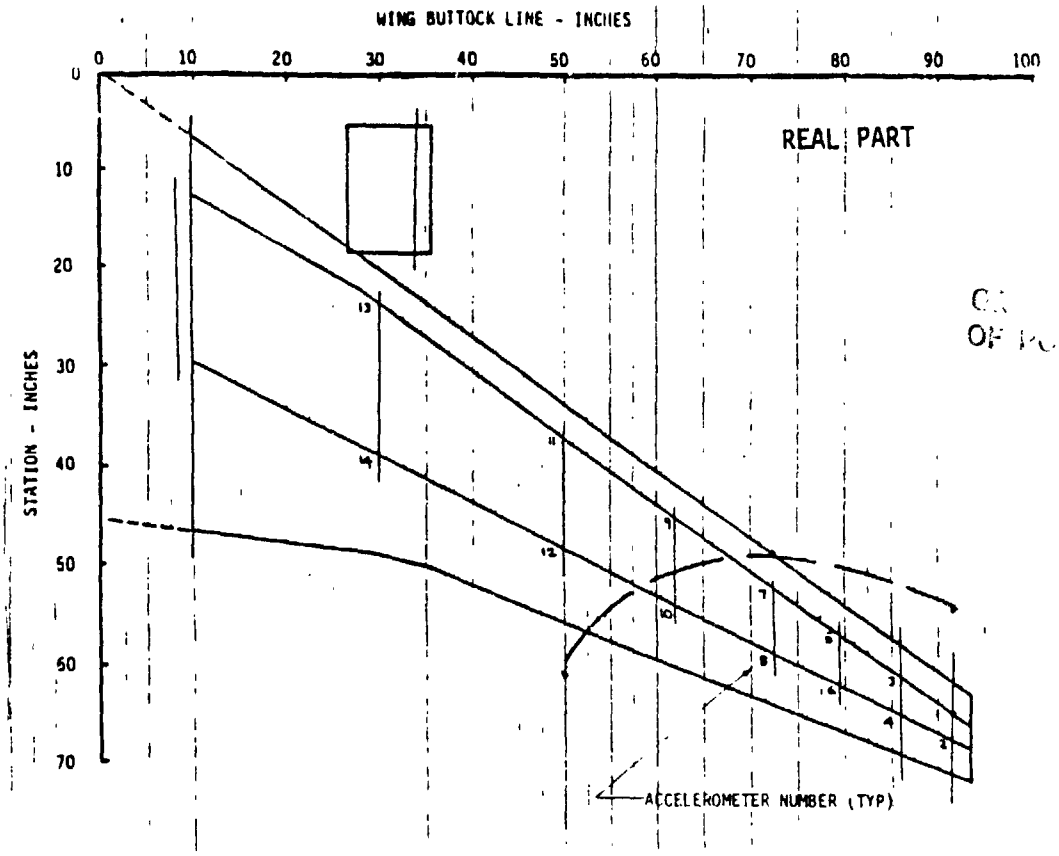

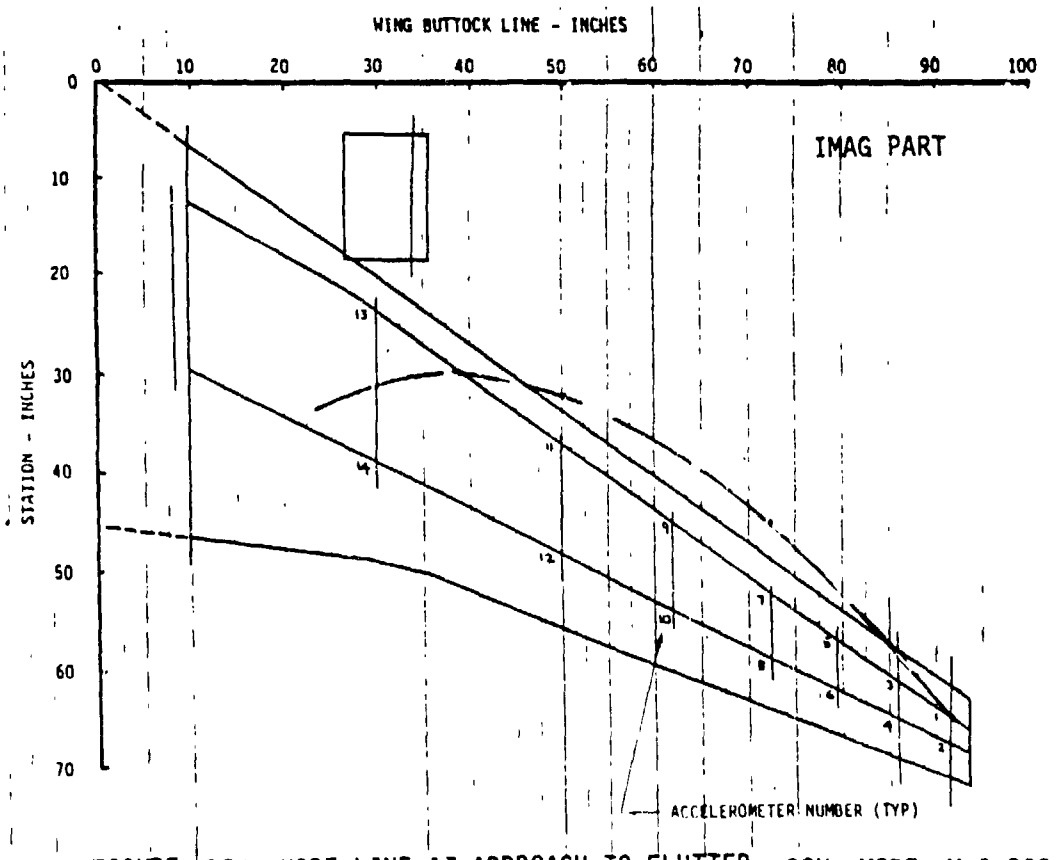

FIGURE 15d NODE LINE AT APPROACH TO FLUTTER, 22Hz MODE, M=0.828, WING(EMPTY)-NACELLE(NOMINAL)-WINGLET (20 DEG)

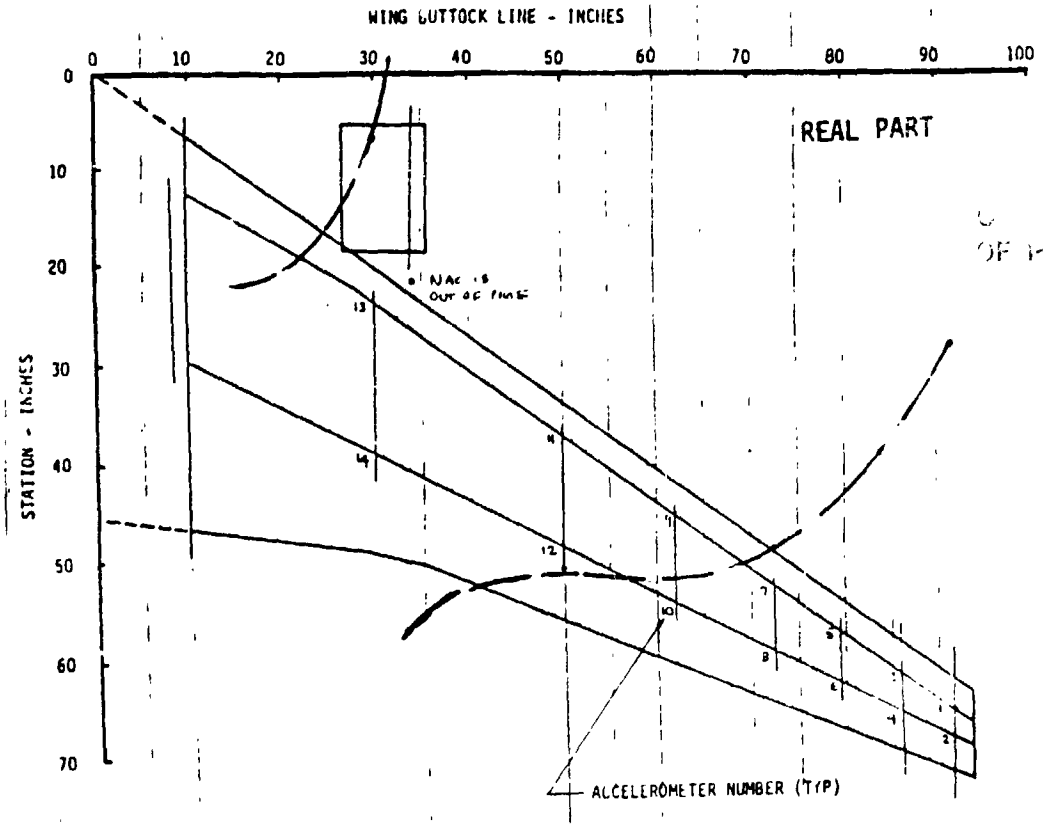

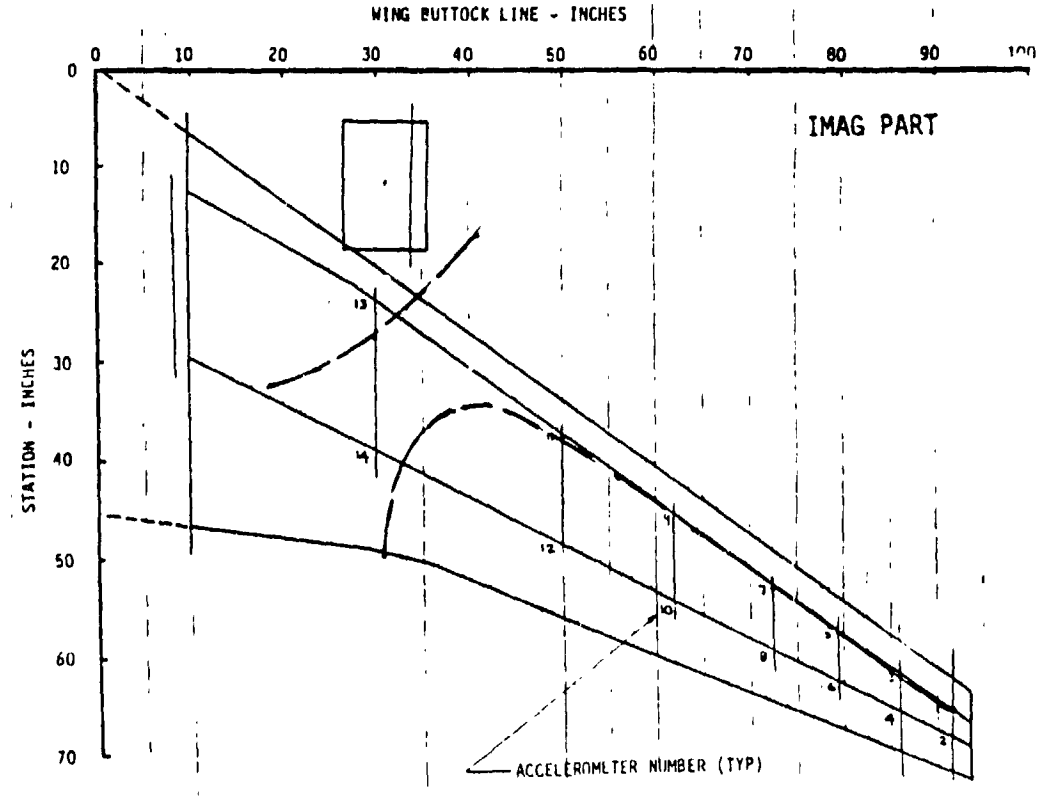

FIGURE 15e NODE LINE AT APPROACH TO FLUTTER, 24.5Hz MODE, M=.73, WING(FULL)-NACELLE(NOMINAL)-WINGLET (20 DEG)

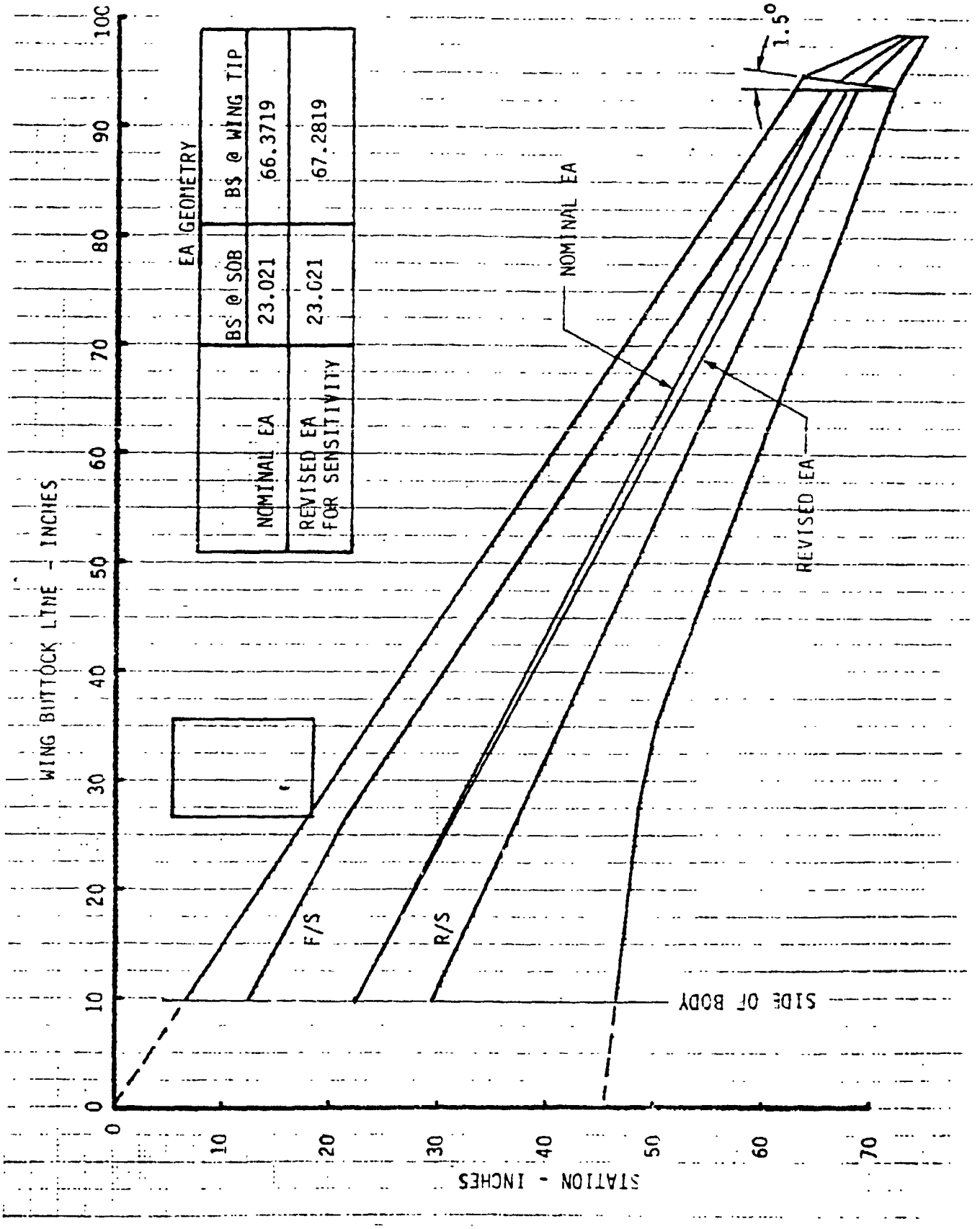

FIGURE 16 VARIATION OF ELASTIC AXIS LOCATION FOR ANALYSIS

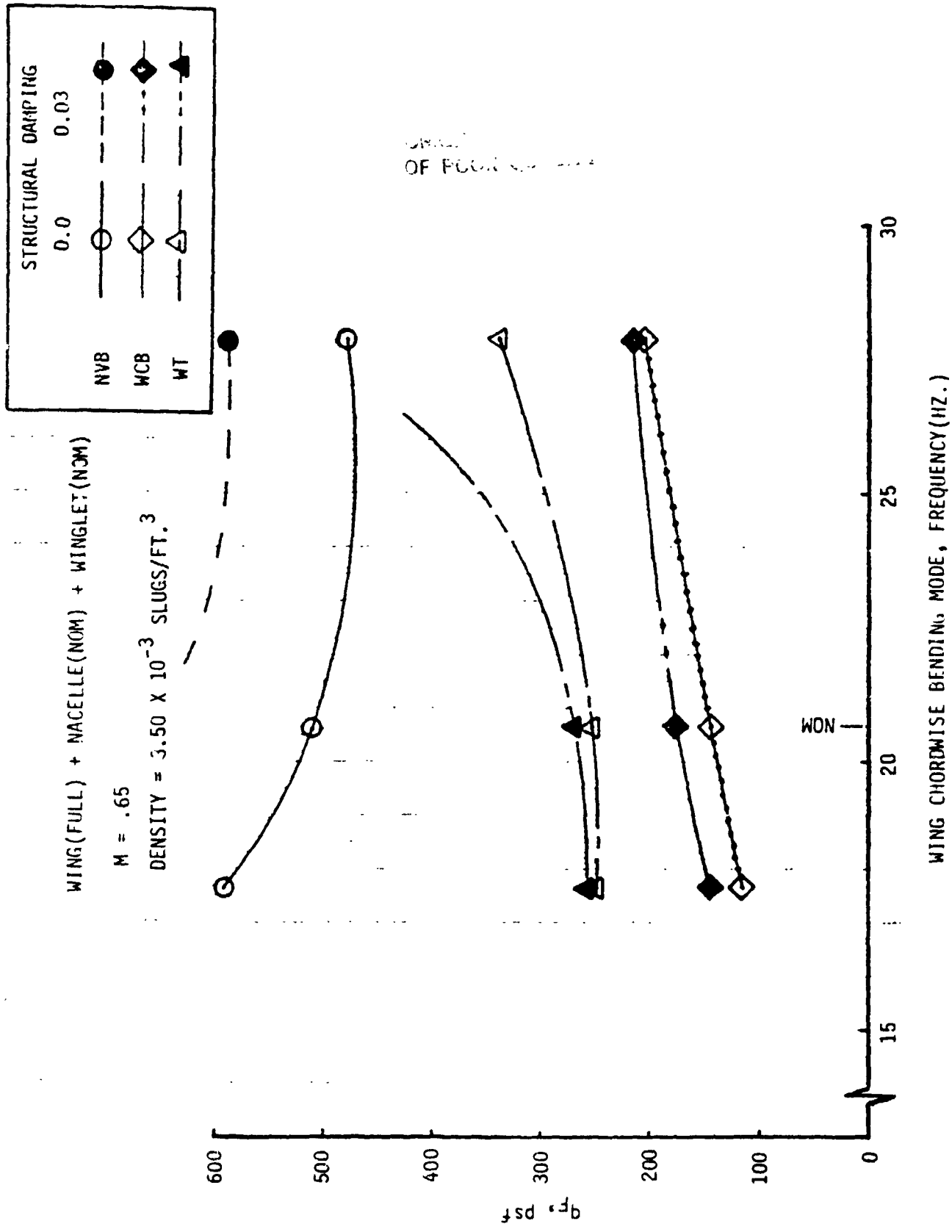

FIGURE 17a EFFECT OF WING CHORDWISE BENDING MODE FREQUENCY, M=0.65, WING(FULL)-NACELLE(NOMINAL)-WINGLET (20 DEG)

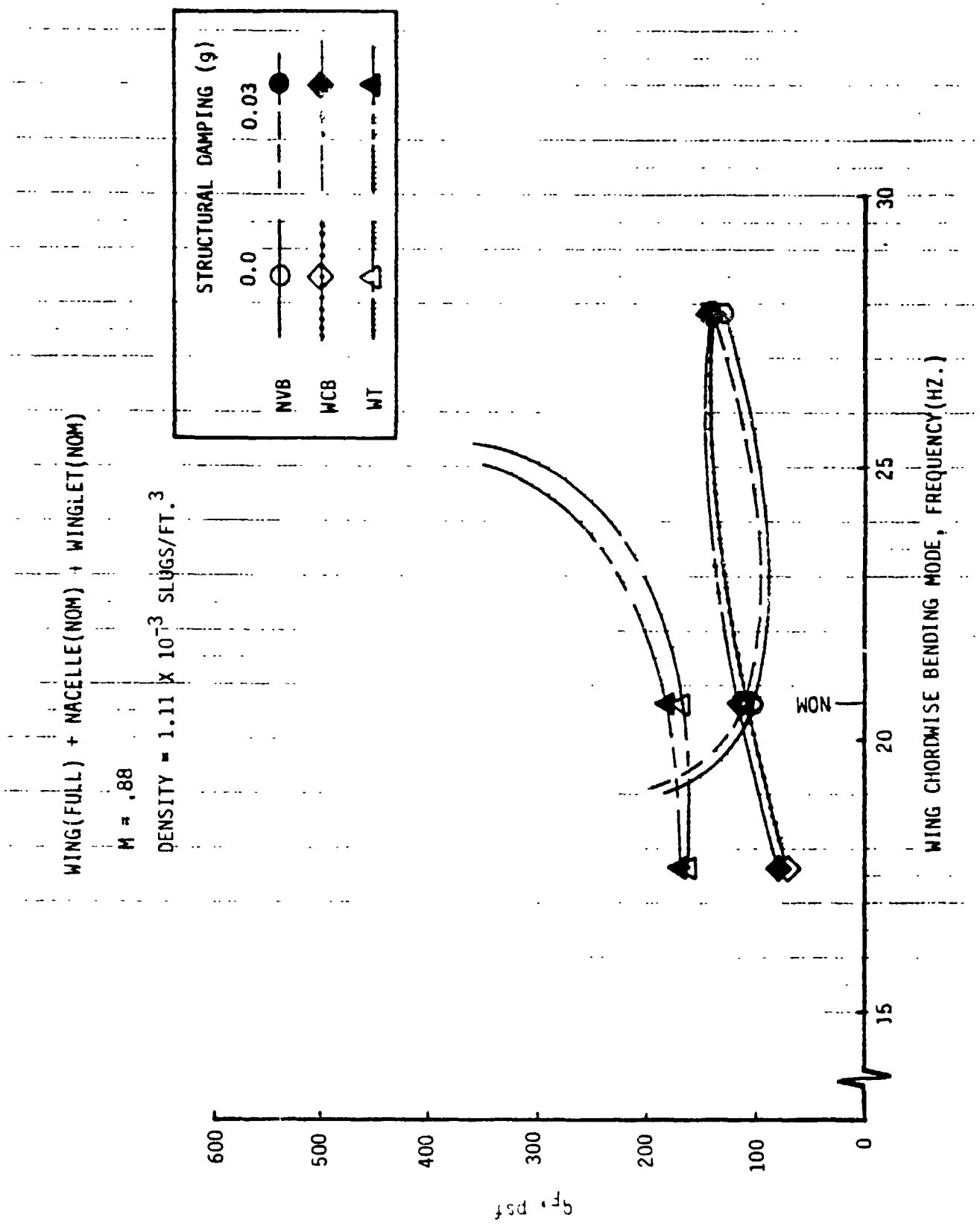

FIGURE 17b EFFECT OF WING CHORDWISE BENDING MODE FREQUENCY, M=0.88, WING(FULL)-NACELLE(NOMINAL)-WINGLET (20 DEG)

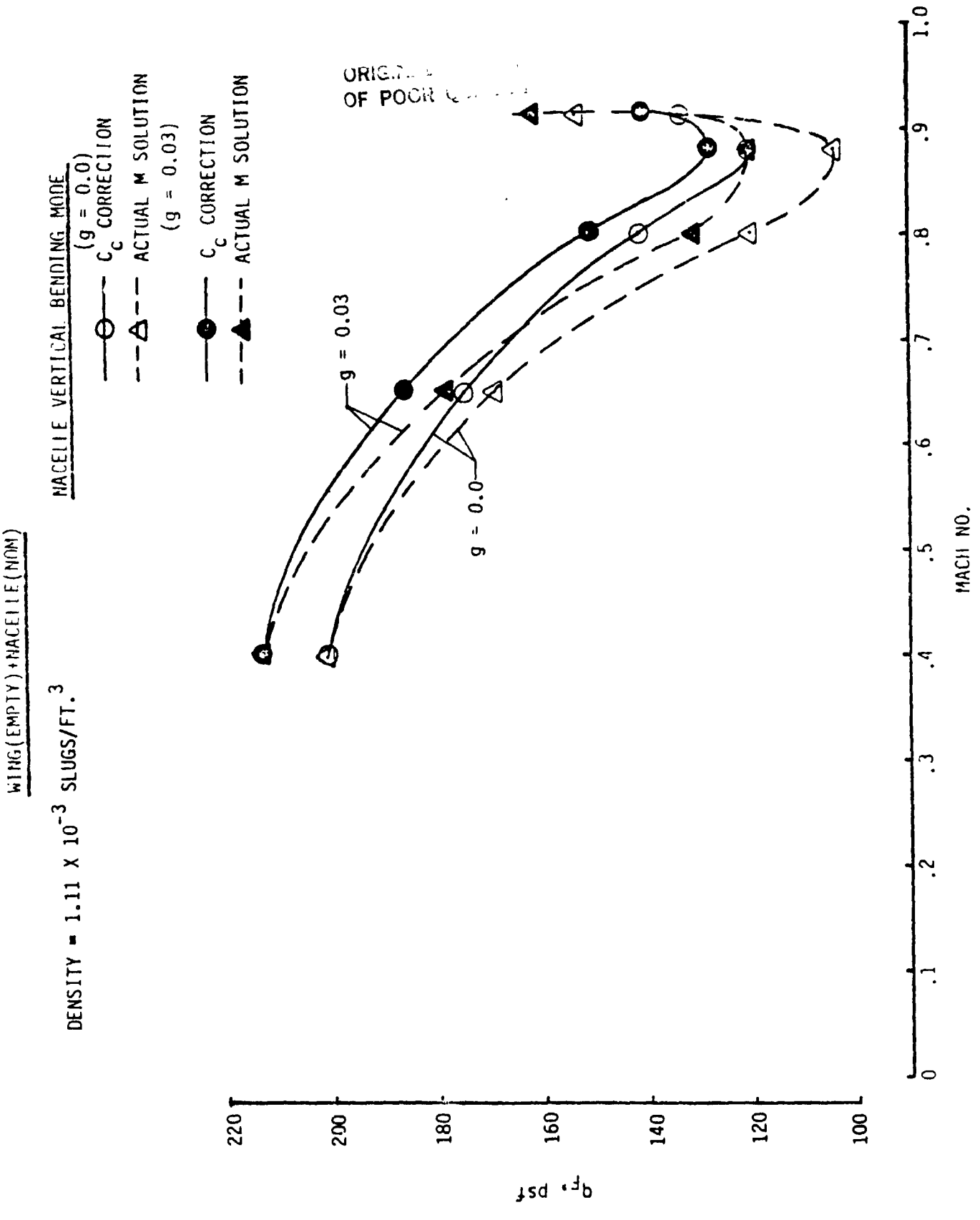

FIGURE 18a COMPRESSIBILITY CORRECTION AND FLUTTER DYNAMIC PRESSURE, NACELLE VERTICAL BENDING MODE, WING(EMPTY)-NACELLE(NOMINAL)

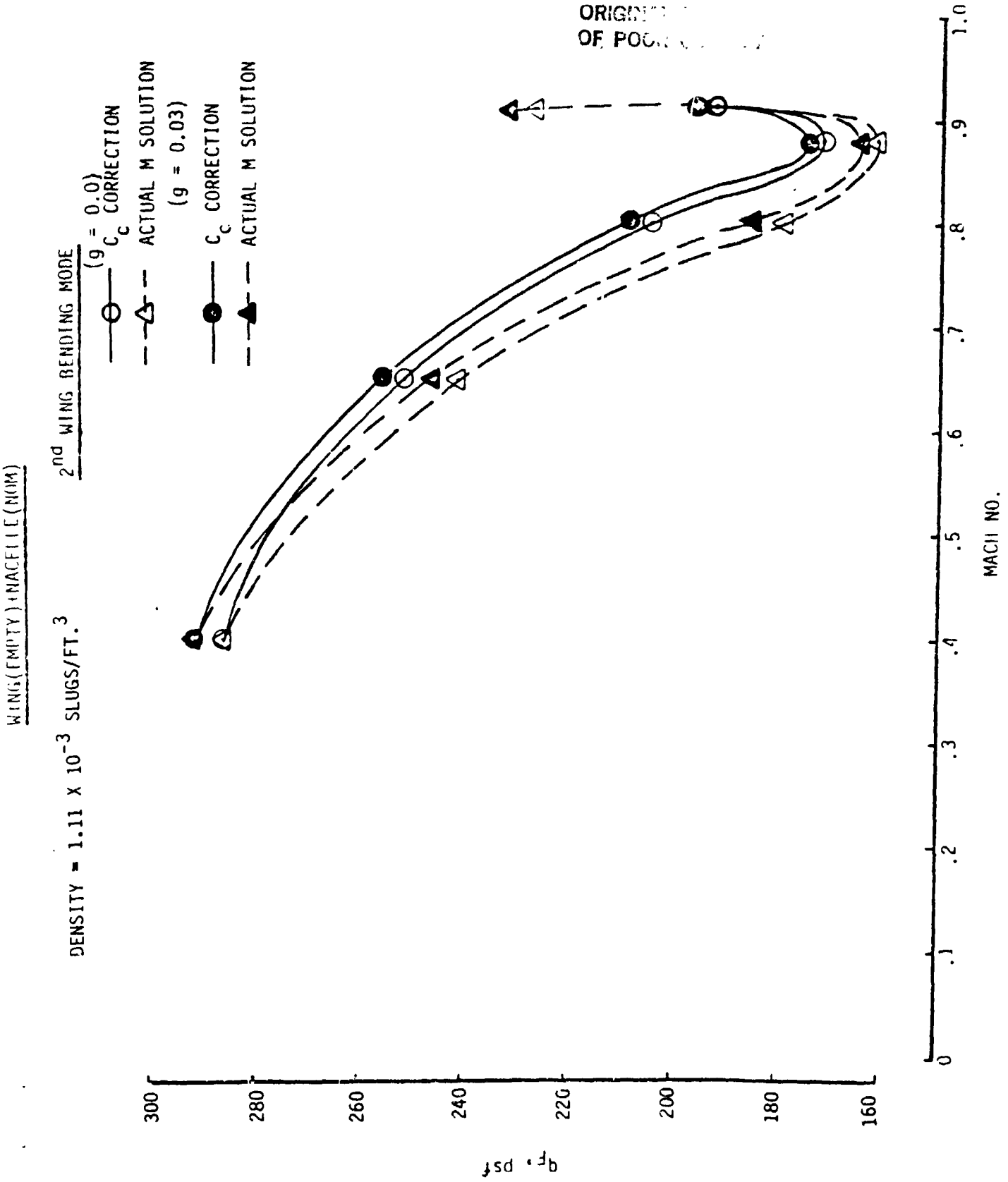

FIGURE 18b COMPRESIBILITY CORRECTION AND FLUTTER DYNAMIC PRESSURE SECOND WING BENDING MODE, WING(EMPTY)-NACELLE(NOMINAL)

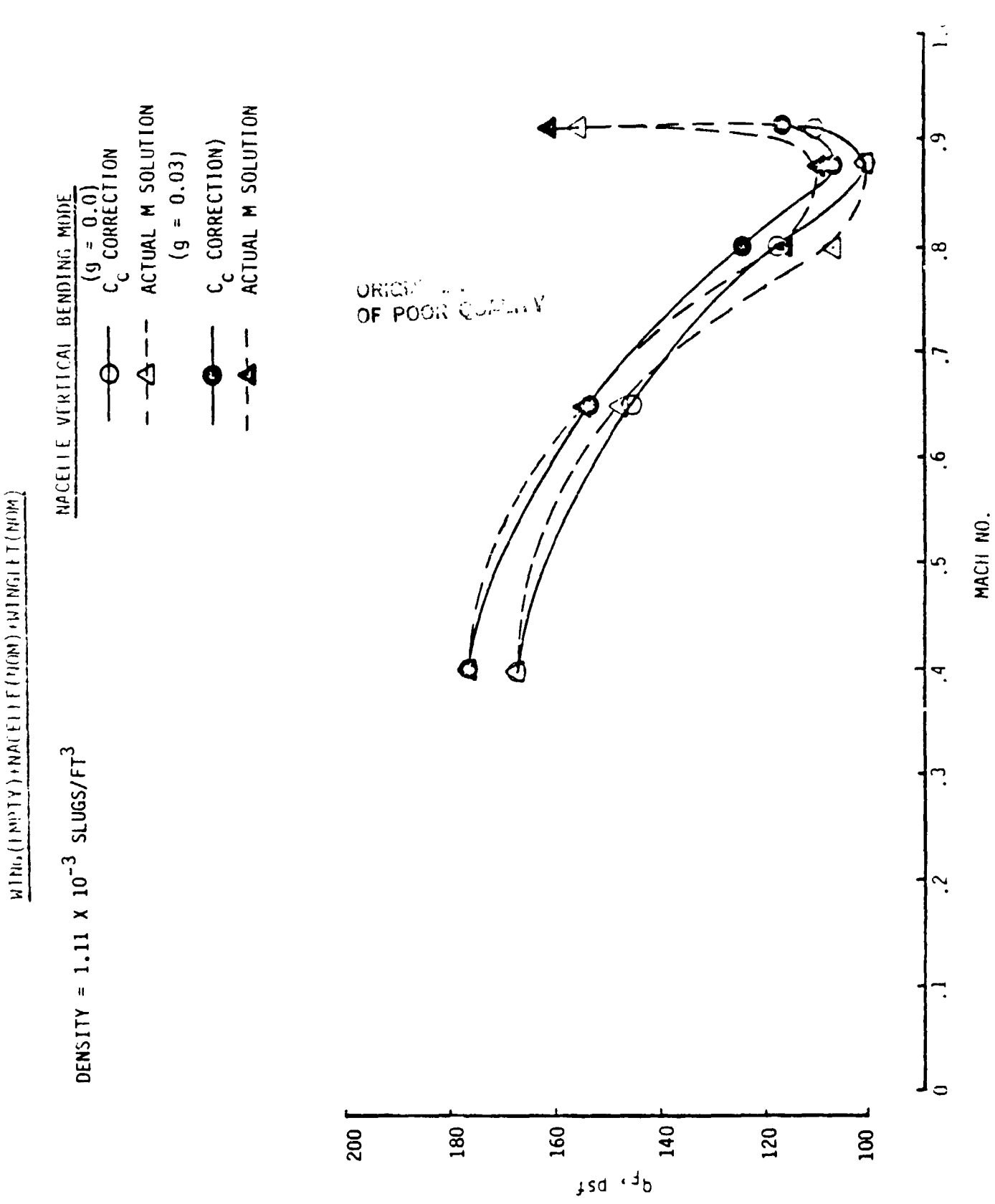

FIGURE 18c COMPRESSIBIITY CORRECTION AND FLUTTER DYNAMIC PRESSURE NACELLE VERTICAL BENDING MODE, WING(EMPTY)-NACELLE(NOMINAL)-WINGLET (20 DEG)

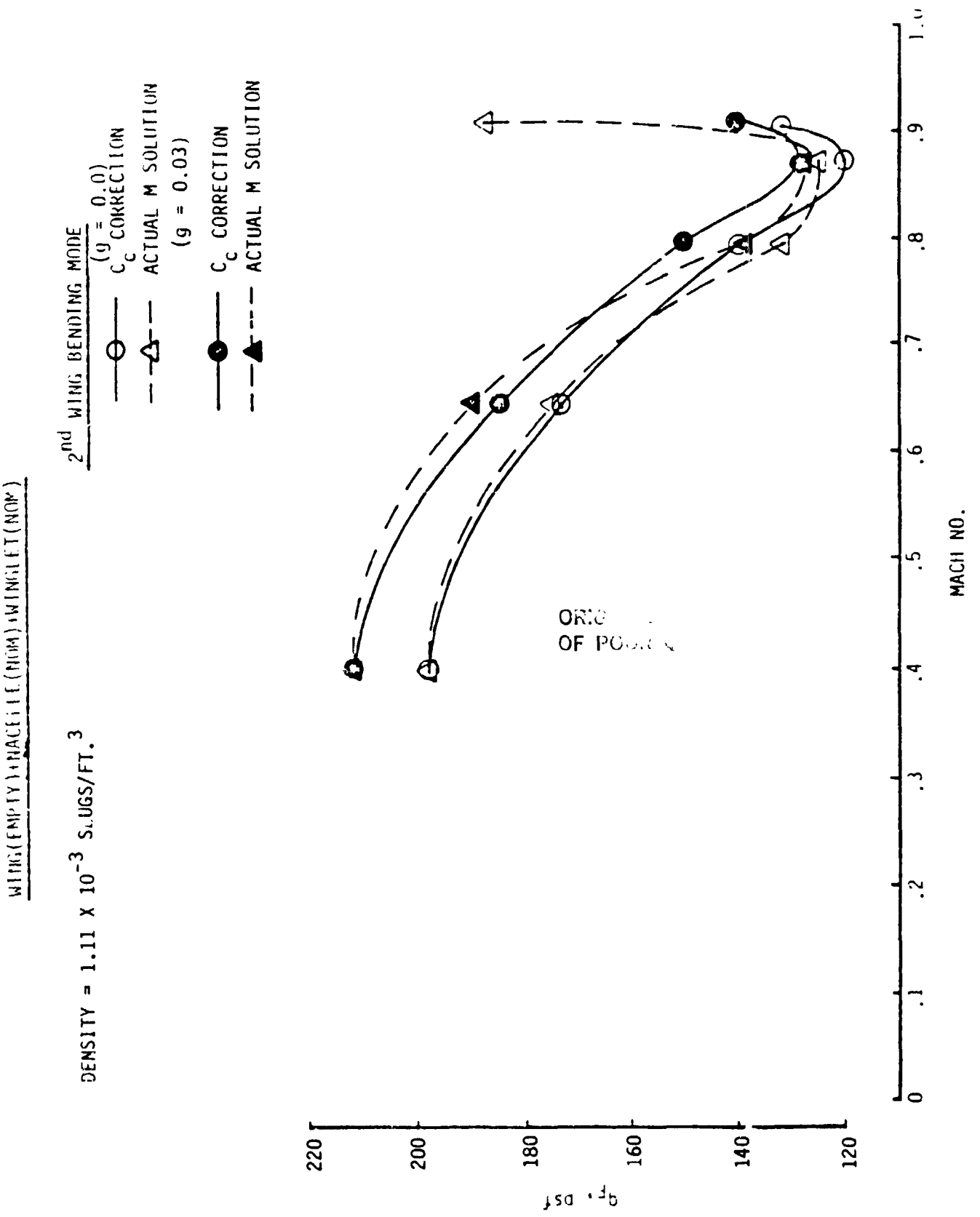

FIGURE 18d COMPRESSIBILITY CORRECTION AND FLUTTER DYNAMIC PRESSURE, SECOND WING BENDING MODE, WING(EMPTY)-NACELLE(NOMINAL)- WINGLET (20 DEG)

APPENDIX A

MODEL GEOMETRY, MASS AND STIFFNESS DATA

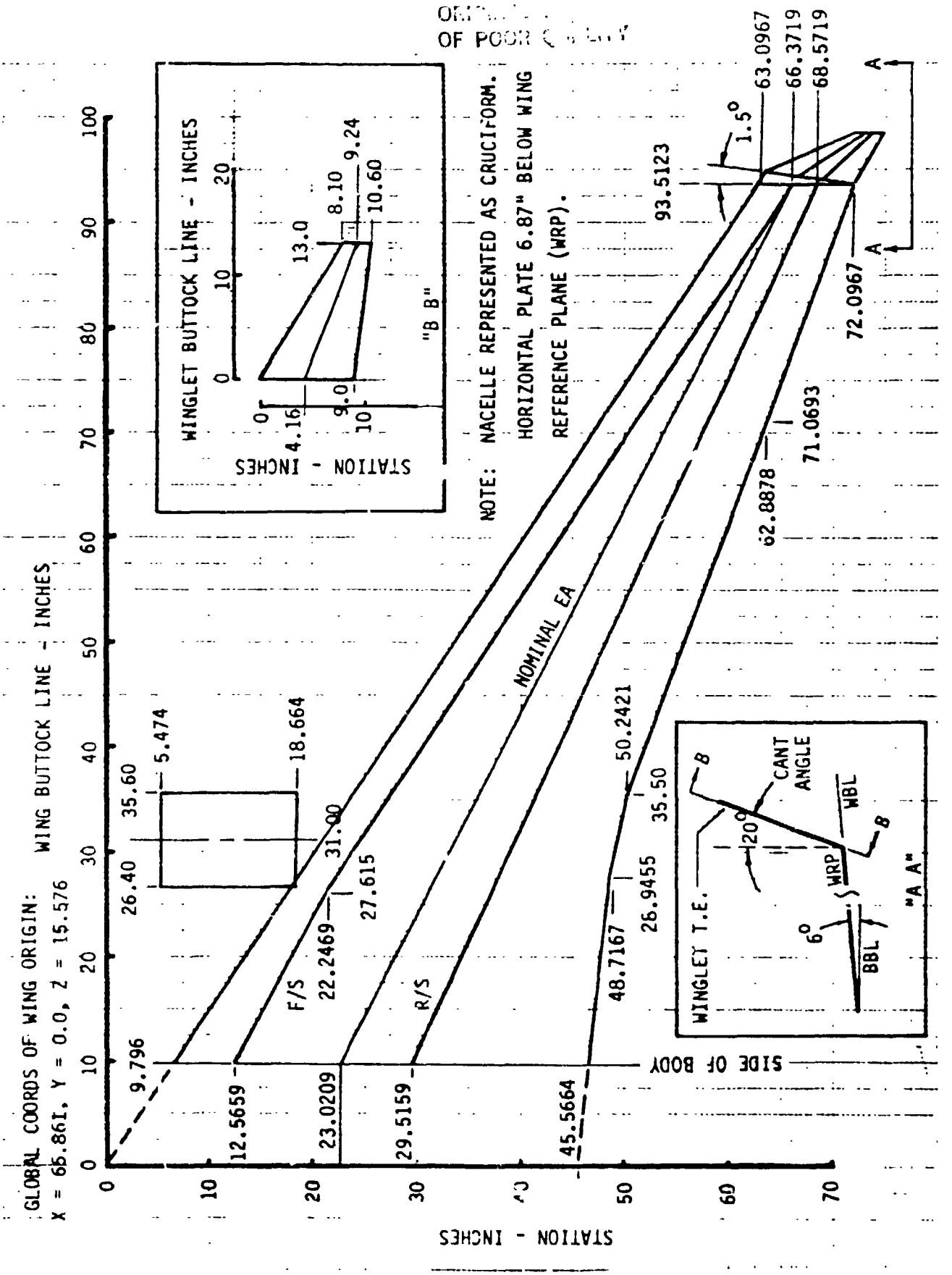

FIGURE A1 GEOMETPY OF WING, WINGLET AND NACELLE

η	$EI_{XX} \times 10^{-6}$ LBS-IN^2	GJ $\times 10^{-6}$ LBS-IN^2
0.0	22,400	43.30
0.041	22,400	43.30
[illegible]	21,500	38.60
0.239	11,900	15.60
0.321	6,000	10.20
0.411	3,860	3.14
0.503	2.13	1.61
0.607	1.33	1.03
0.698	0.810	0.586
0.774	0.430	0.298
0.836	0.268	0.167
0.889	0.187	0.101
0.933	0.116	0.048
0.975	0.076	0.041
1.000	0.040	0.051
	0.040	0.051

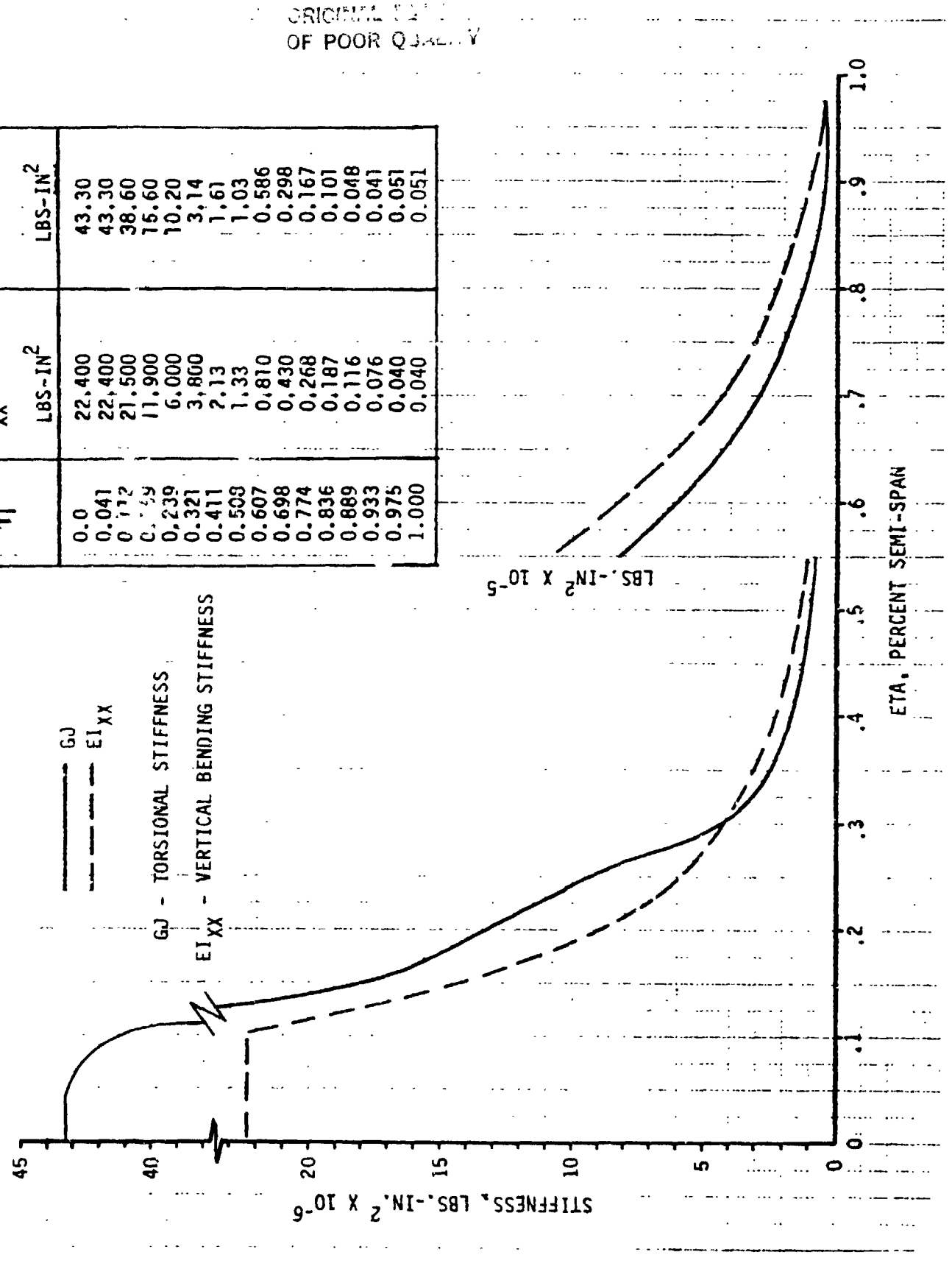

FIGURE A2 WING SPANWISE STIFFNESS DISTRIBUTION ALONG ELASTIC AXIS

C-2

η	$EI_{ZZ} \times 10^{-6}$ LBS-IN^2	FACTOR FOR SENSITIVITY STUDY
0.0	576.00	4.77
0.041	576.00	4.77
0.112	652.00	2.34
0.169	306.00	0.28
0.239	154.00	0.46
0.321	73.40	0.65
0.411	41.20	0.86
0.508	25.80	0.84
0.607	15.70	0.75
0.698	8.30	0.62
0.774	5.20	0.59
0.836	3.60	0.50
0.889	2.24	0.39
0.933	1.47	0.37
0.975	0.772	0.33
1.000	0.772	0.33

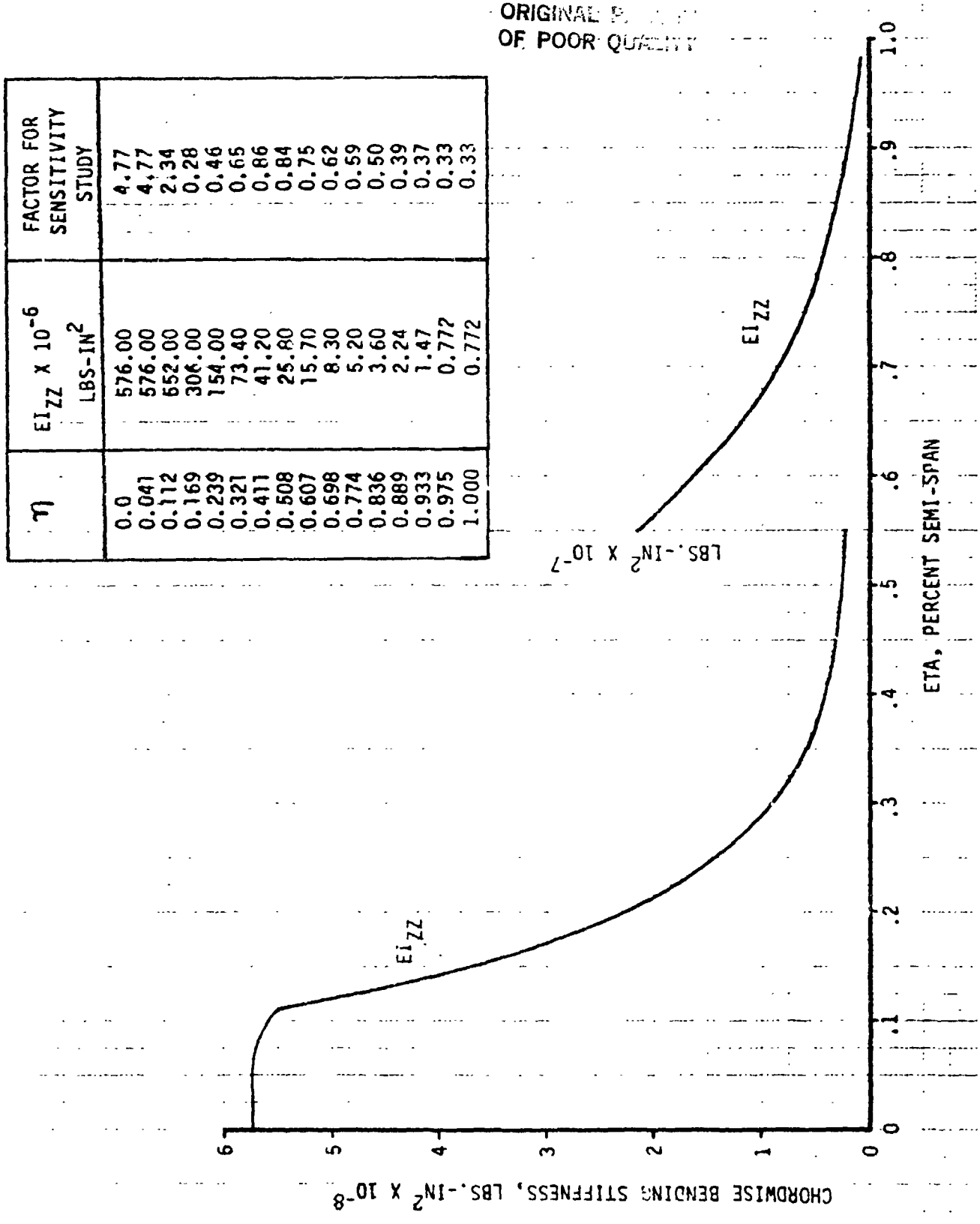

FIGURE A2 CONT.

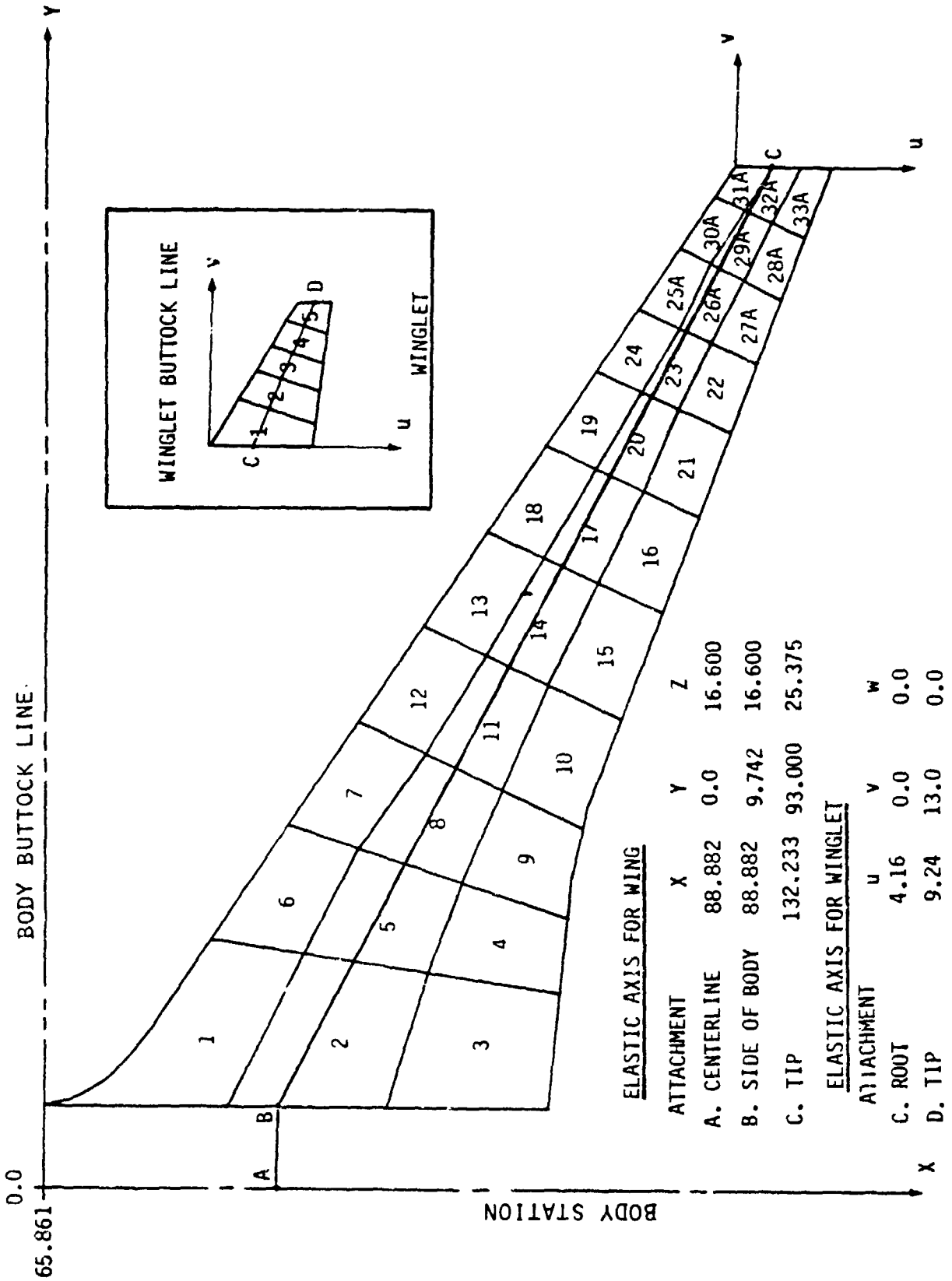

FIGURE A3 MASS PANELS FOR TEST MODEL

a)

PANEL	WEIGHT (LBS)	X (inches)	Y (inches)	Z (inches)	I_{XX} (lb-in^2)	I_{YY} (lb-in^2)	I_{ZZ} (lb-in^2)
1	1.5152	81.79	15.16	17.26	26.1799	25.8358	43.0908
2	2.0257	93.19	15.28	16.73	31.1621	38.8700	58.1186
3	.9644	104.23	15.28	15.64	10.3202	9.2511	18.1377
4	.7504	105.96	22.82	16.72	2.7575	7.1399	9.2932
5	1.2184	97.60	24.84	17.96	11.4647	15.5340	22.9020
6	.8932	89.03	27.16	18.60	9.0077	6.3928	13.5800
7	.7426	95.41	36.15	19.60	6.5759	5.3166	10.9228
8	1.0410	102.08	33.45	19.07	9.1526	8.2932	15.5698
9	.3643	109.12	31.86	18.54	3.2248	2.0907	5.0689
10	.3794	112.49	40.68	19.56	3.6570	2.4819	5.8711
11	.7713	106.67	42.93	20.17	6.2762	4.4731	9.8104
12	.5539	100.99	45.70	20.61	3.9633	2.9072	6.4476
13	.4422	106.41	54.25	21.43	2.8395	2.0584	4.6470
14	.5976	111.48	51.96	21.05	5.2324	3.2884	8.4956
15	.6066	115.56	47.95	20.51	5.2781	2.5627	7.3311
16	.5040	120.94	60.52	21.53	3.7356	1.3057	4.8433
17	.3710	116.27	60.62	21.80	2.9533	2.1636	3.4038
18	.3534	111.70	62.62	22.22	2.1519	1.1392	3.1105
19	.2660	116.54	70.08	22.95	1.1069	.6799	1.7108
20	.2426	120.22	68.15	23.63	1.1095	.7099	1.6593
21	.1601	123.49	66.53	22.31	.8287	.4322	1.1871
22	.1821	126.13	73.49	23.03	.8369	.3516	1.1446
23	.1690	123.99	74.77	23.27	.8000	.4781	1.1860
24	.2055	120.44	76.42	23.61	.6768	.4211	1.0262
25A	.1514	124.00	82.04	24.89	.5119	.2698	.7391
26A	.1061	127.14	80.57	24.61	.3222	.1862	.4667
27A	.1743	129.11	79.24	24.37	.5621	.3085	.8749
28A	.0799	131.88	84.62	24.94	.2009	.1160	.3058
29A	.0910	130.08	85.84	25.10	.2054	.1207	.2880
30A	.1404	127.45	87.16	25.36	.3055	.2120	.4999
31A	.0706	130.54	91.35	25.81	.1338	.1341	.2493
32A	.2265	132.92	91.76	25.76	.2975	.1517	.4209
33A	.0756	134.70	90.23	25.55	.2659	.1241	.3733
TOTAL	16.4356	104.01	38.35	19.42	8065.	2952.	10983.

b)

	WEIGHT (LBS)	X (inches)	Y (inches)	Z (inches)	I_{xx} (lb-in^2)	I_{yy} (lb-in^2)	I_{zz} (lb-in^2)
NACELLE POD	10.7343	82.115	31.356	12.331	132.126	249.334	242.128
STRUT AS WGD	3.5650	91.678	30.997	16.961	3.934	79.351	77.863

NOTE: ALL INERTIAS ABOUT C.G.

FIGURE A4 MASS AND INERTIA PROPERTIES FOR

a) WING

b) NACELLE

c) WING TIPS

c)

WING TIP CONFIGURATION

WING TIP	PANEL	WEIGHT (LBS)	u (INCHES)	v (INCHES)	w (INCHES)	I_{uu} (Lb -In^2)	I_{vv} (Lb-In^2)	I_{ww} (Lb - In^2)
WINGLET*	1	.1217	4.657	1.435	.245	.0756	.1640	.1928
	2	.0519	5.863	4.053	.192	.0570	.1022	.1291
	3	.0326	6.808	6.771	.140	.0358	.0656	.0864
	4	.0359	7.738	8.981	.094	.0284	.0322	.0591
	5	.0166	8.873	11.864	.045	.0182	.0123	.0208
	TOTAL	.2586	5.869	4.350	.187	3.0748	.8550	3.9062
	WINGLET BRACKET -							
	20 DEG.	.1000	4.33	.50	.0	.0445	.1287	.0965
	0 DEG.	.0901	4.37	.54	.0	.0350	.1105	.0850
NOMINAL TIP**	BULL NOSE	.0198	3.96	.30	.60	.0008	.0792	.0790
BALLASTED TIP**	WEIGHTED BULL NOSE	.3503	5.00	.40	.60	.0265	.2858	.2848

*NOTE: (u, v, w) IS WITH RESPECT TO WINGLET REFERENCE FRAME (SEE FIGURE A3)
** (u, v, w) IS WITH RESPECT TO WING TIP FRAME (SEE FIGURE A3)

BULL NOSE REFERS TO WING TIP CLOSURE

FIGURE A4 CONT.

PANEL	WEIGHT (LBS)	X (inches)	Y (inches)	Z (inches)	I_{XX} (lb-in^2)	I_{YY} (lb-in^2)	I_{ZZ} (lb-in^2)
1	2.8653	86.25	19.16	17.45	12.011	8.294	10.556
2	4.1605	94.05	18.43	17.08	14.835	50.725	52.925
5	6.1572	98.04	24.63	17.94	50.234	56.291	93.755
6	1.1958	88.80	22.85	17.94	2.198	2.726	2.115
7	1.8406	97.47	36.59	19.61	12.638	4.164	14.811
8	4.3684	101.94	33.44	19.08	33.068	35.358	63.324
11	3.2216	106.84	42.39	20.07	25.452	16.478	39.142
12	1.8514	102.15	44.63	20.44	14.146	4.717	17.336
13	1.4225	107.71	53.50	21.31	10.421	3.222	12.694
14	2.3607	111.71	51.53	21.00	18.538	10.420	26.981
17	1.5488	116.31	60.15	21.85	9.113	4.776	13.054
18	.83[illegible]	112.92	61.73	22.11	4.870	1.452	5.876
19	.4552	117.26	68.61	22.77	1.334	.530	1.689
20	.8415	120.44	67.95	22.60	4.797	1.469	5.900
23	.4008	123.39	74.73	23.30	1.119	.631	1.634
TOTAL	33.5283	101.47	35.91	19.27	8118.27	2944.27	10810.31

NOTE: ALL INERTIAS ARE ABOUT C.G.

FIGURE A5 FULL FUEL MASS & INERTIA PROPERTIES

CANTILEVER NACELLE FREQUENCIES AND MODE SHAPES*			
No.	MODE	FREQ (HZ)	MODE SHAPE
1	NAC SIDE BNDG	15.74	TY 1.0 RX .152 RZ -.111
2	NAC VERT BNDG	24.70(NOM),15.99(SOFT)	TX 1.00 TZ -.968 RY -.179
3	NAC ROLL	28.97	TX .72336 TY 1.0 TZ -.89376 RX 6.591 RY -.181 RZ 2.509

CANTILEVER WINGLET MODE SHAPES** (93.00 HZ)			
WINGLET NODE AT WBL	TZ	RX	RY
1.351	.003174	.00061688	-.0003185
4.197	.055950	.0029368	-.0015398
6.760	.20376	.006447	-.0034839
9.051	.45002	.01098	-.0063343
11.939	1.0000	.018689	-.011197

*IN GLOBAL FRAME

**IN WINGLET REF FRAME

FIGURE A6 CANTILEVERED NACELLE AND WINGLET FREQUENCIES AND MODE SHAPES

APPENDIX B

AERODYNAMIC DATA

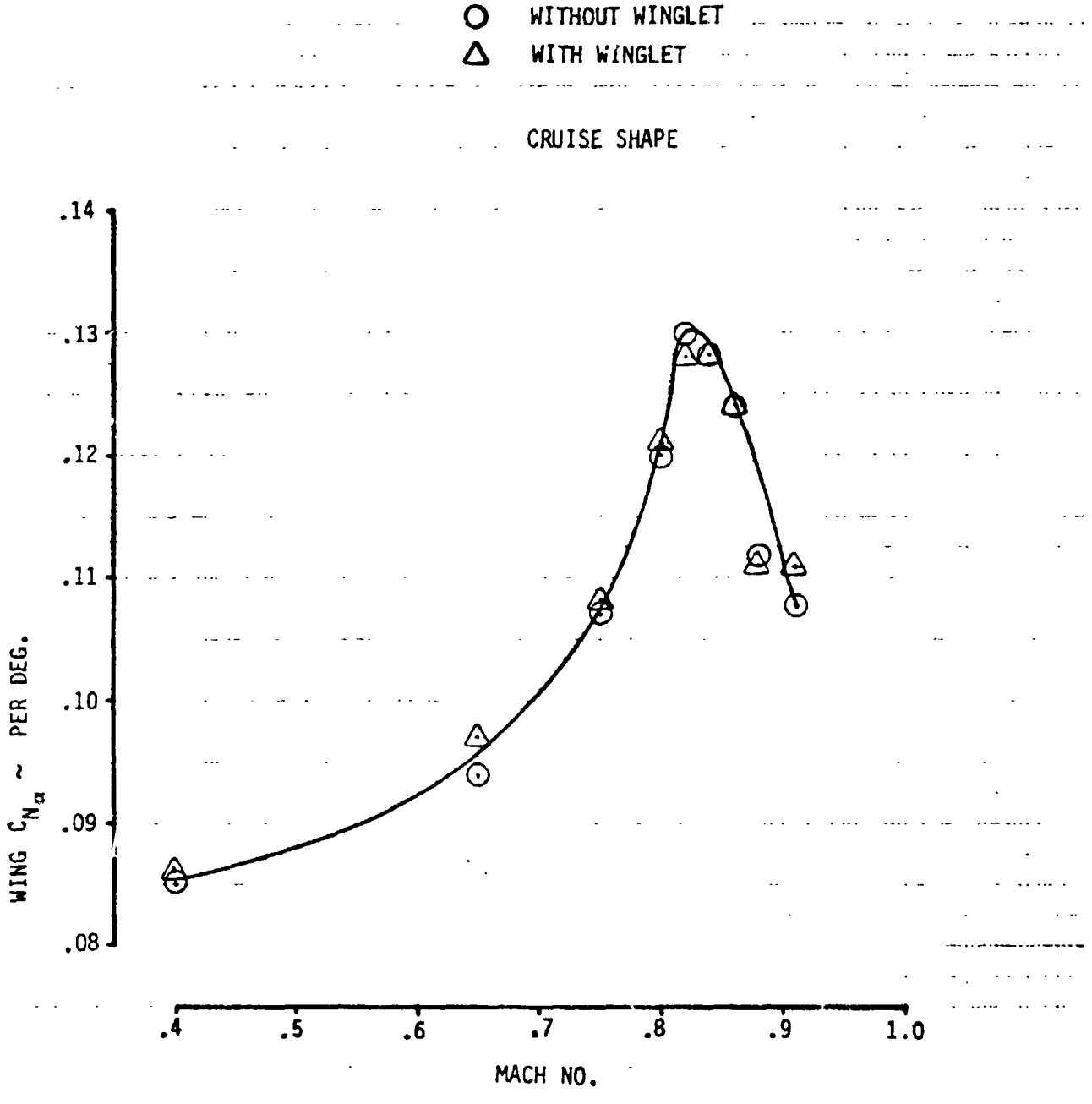

FIGURE B1 WING C_{N_α} Vs. MACH NUMBER

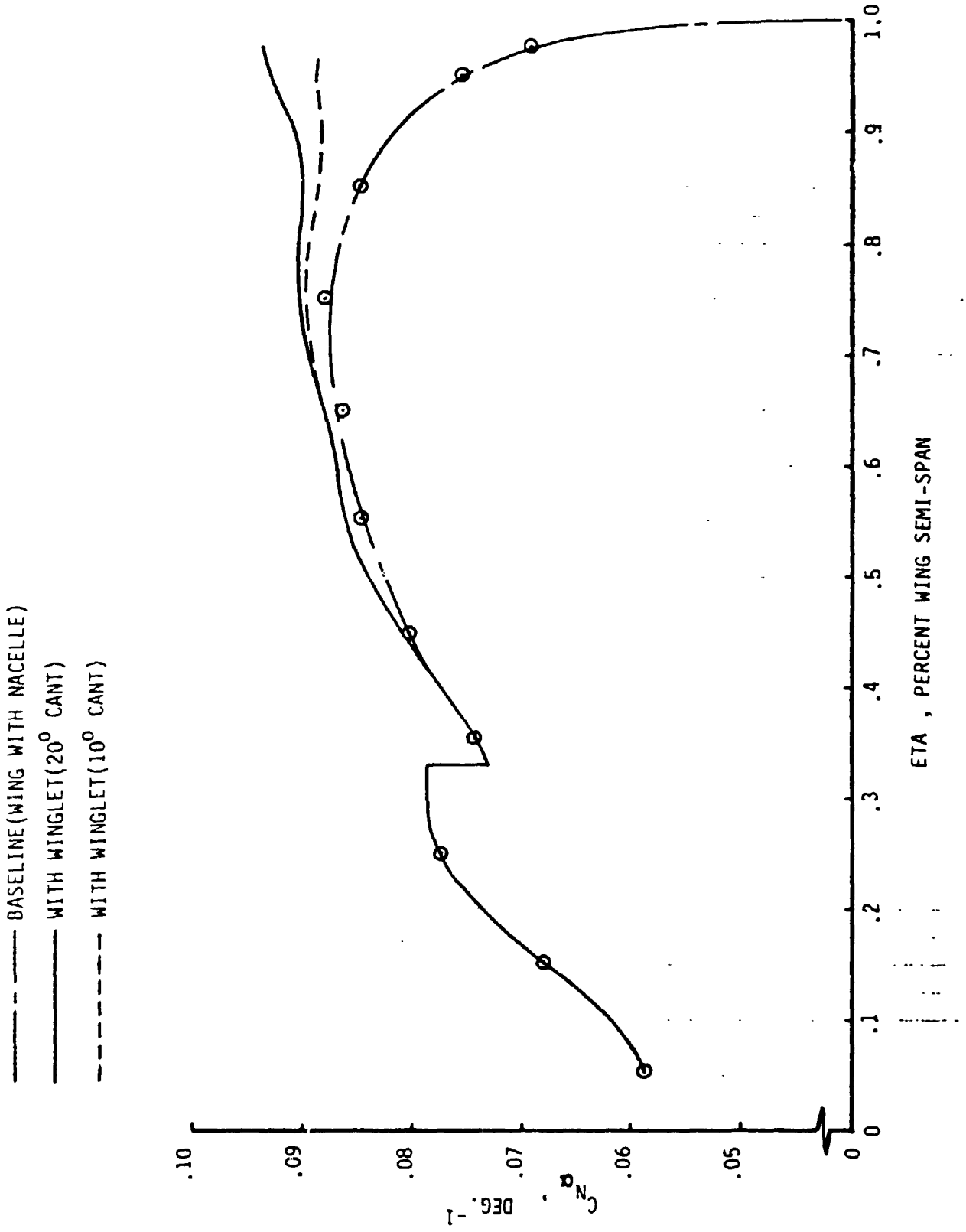

FIGURE B2 WING SECTIONAL C_{n_α} DISTRIBUTION AT M=0.4

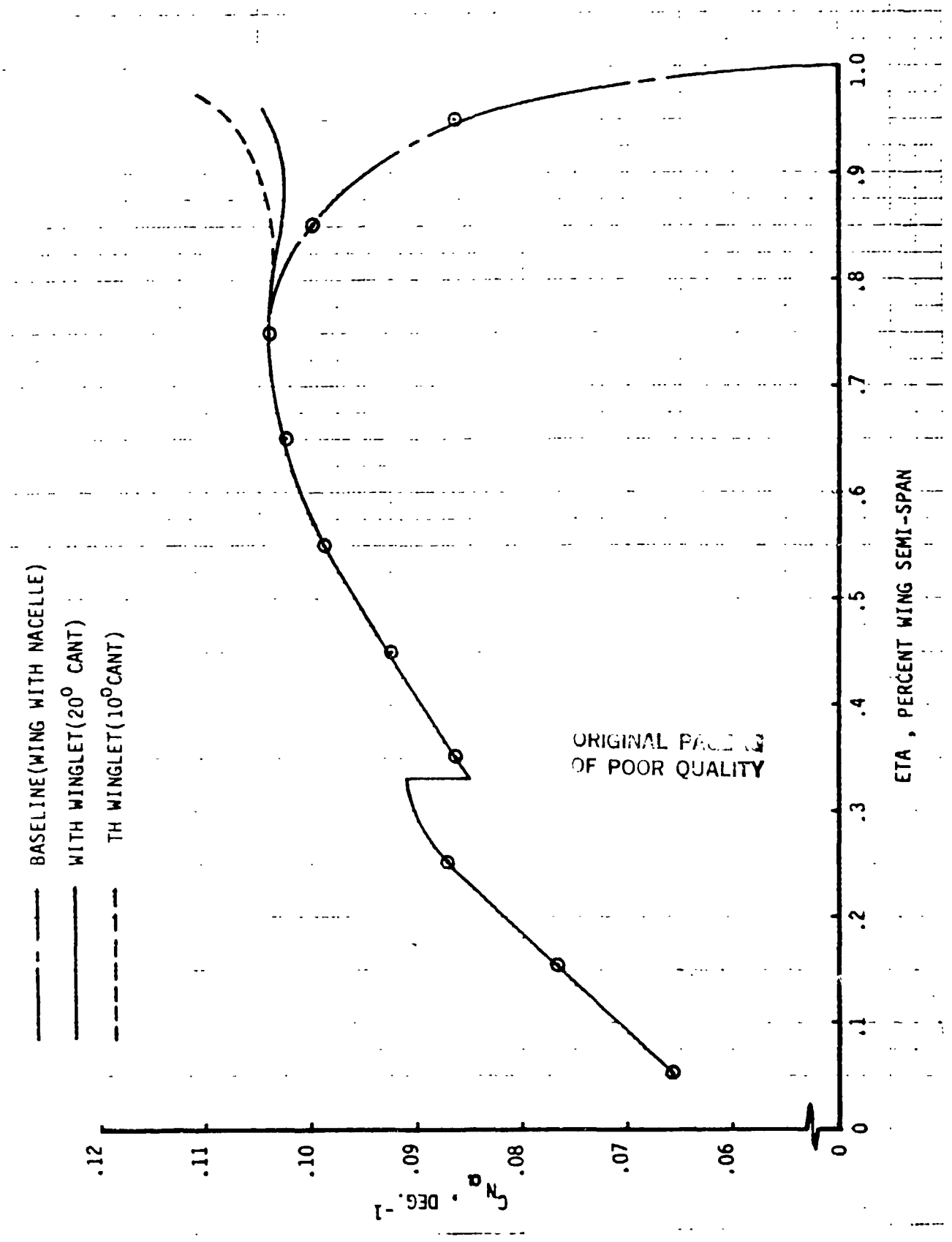

FIGURE B3 WING SECTIONAL C_{n_α} DISTRIBUTION AT M=0.65

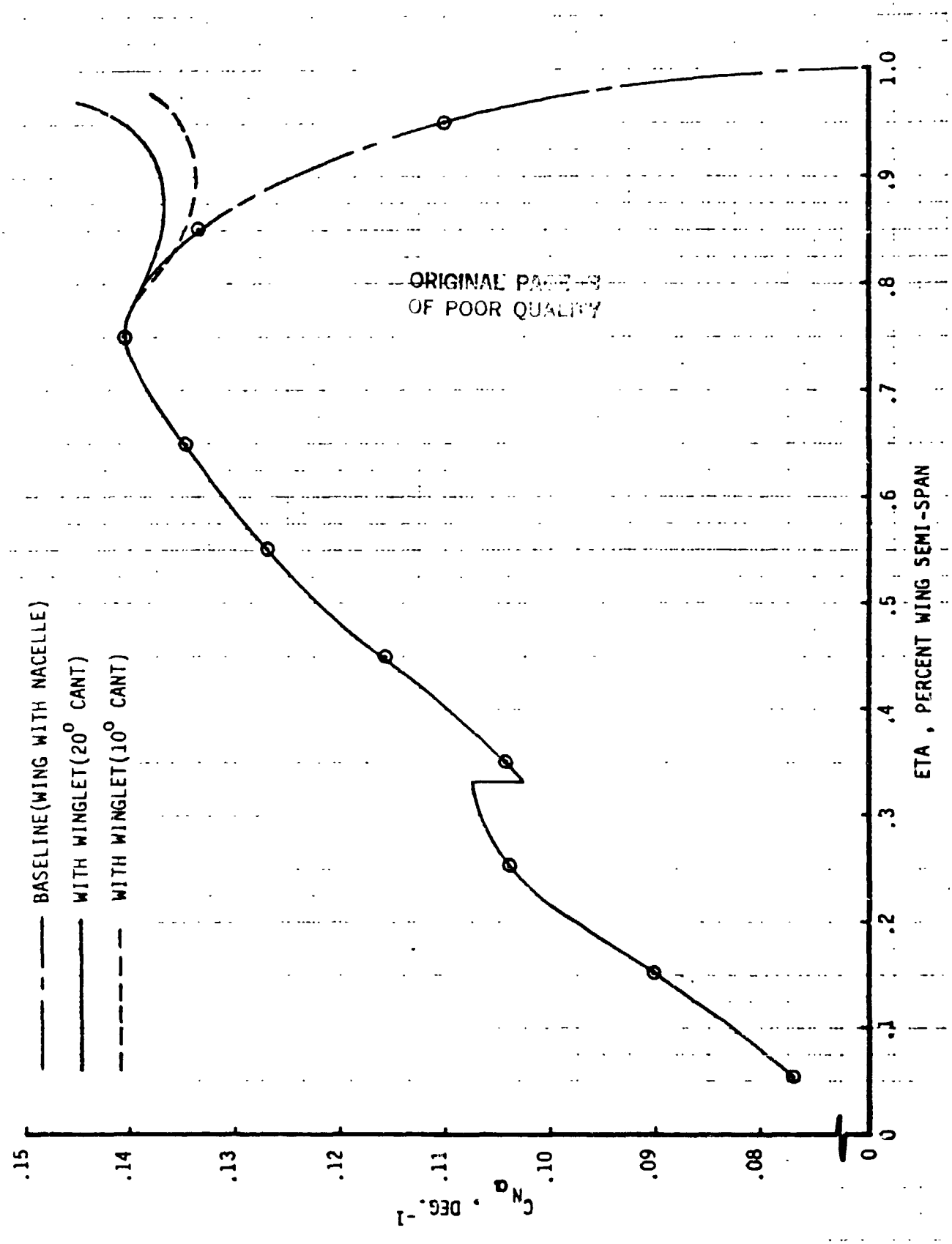

FIGURE B4 WING SECTIONAL C_{n_α} DISTRIBUTION AT M=0.80

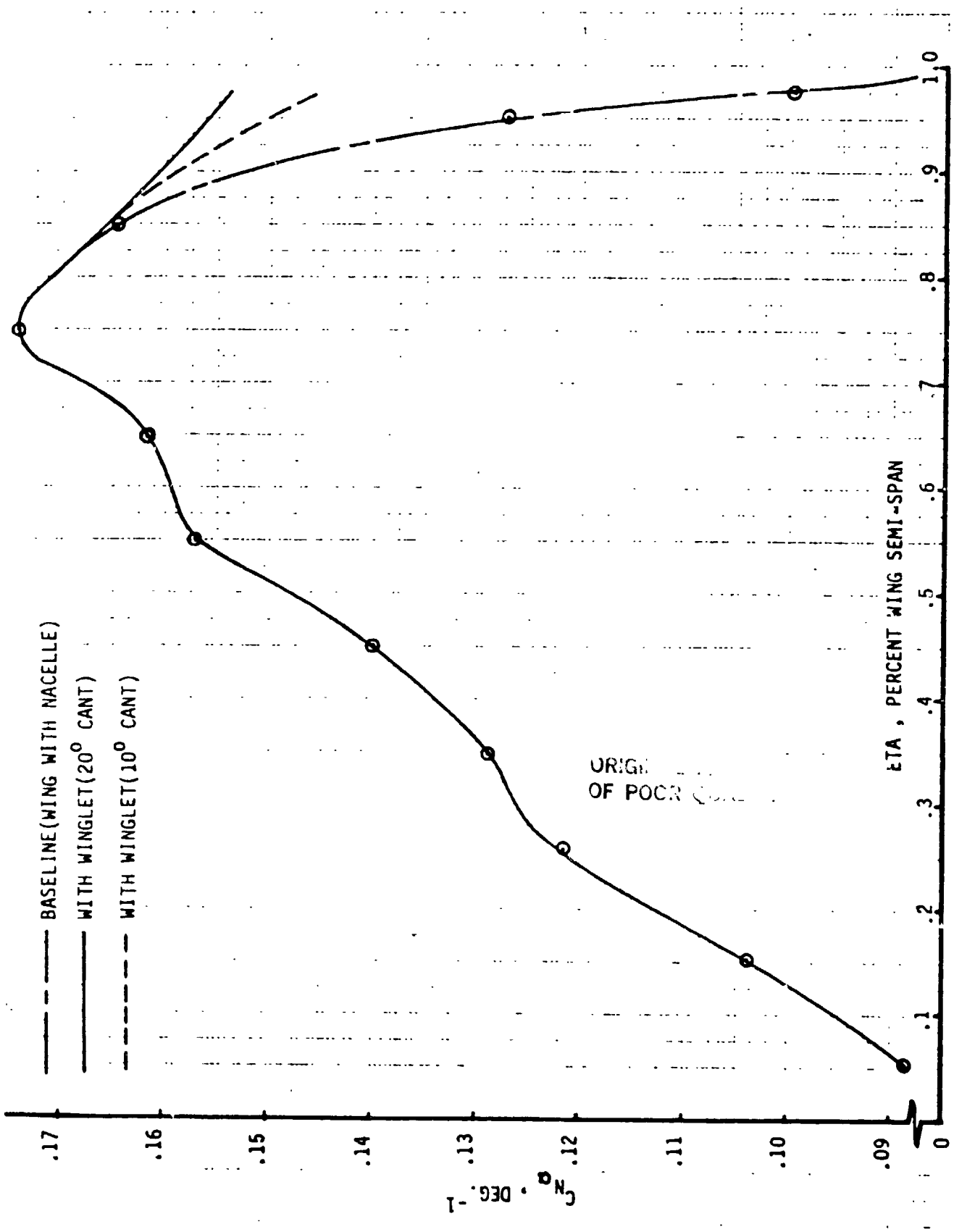

FIGURE B5 WING SECTIONAL C_{n_α} DISTRIBUTION AT M=0.88

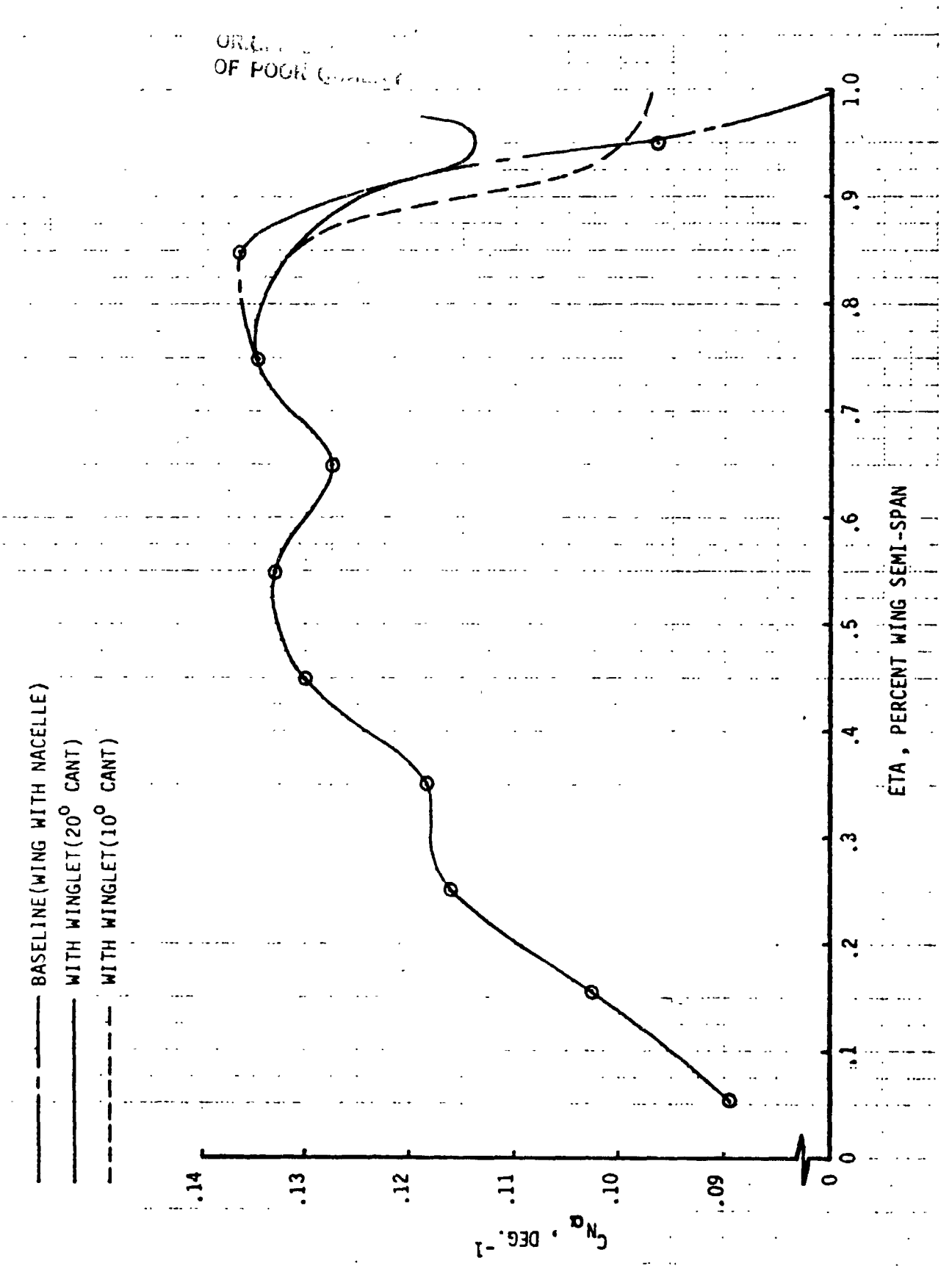

FIGURE B6 WING SECTIONAL C_{n_α} DISTRIBUTION AT M=0.91

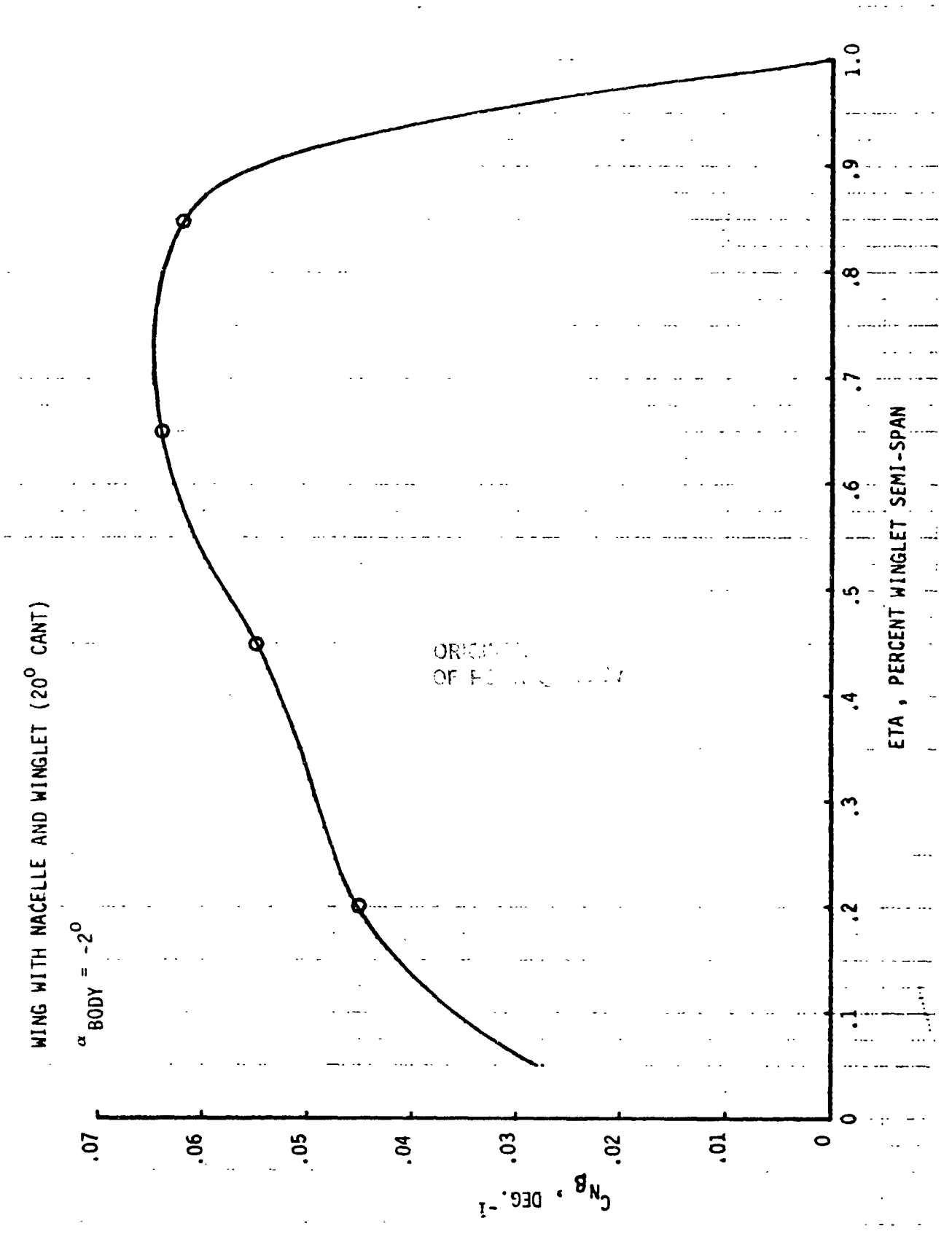

FIGURE B7 WINGLET SECTIONAL C_{n_β} DISTRIBUTION AT M=0.4

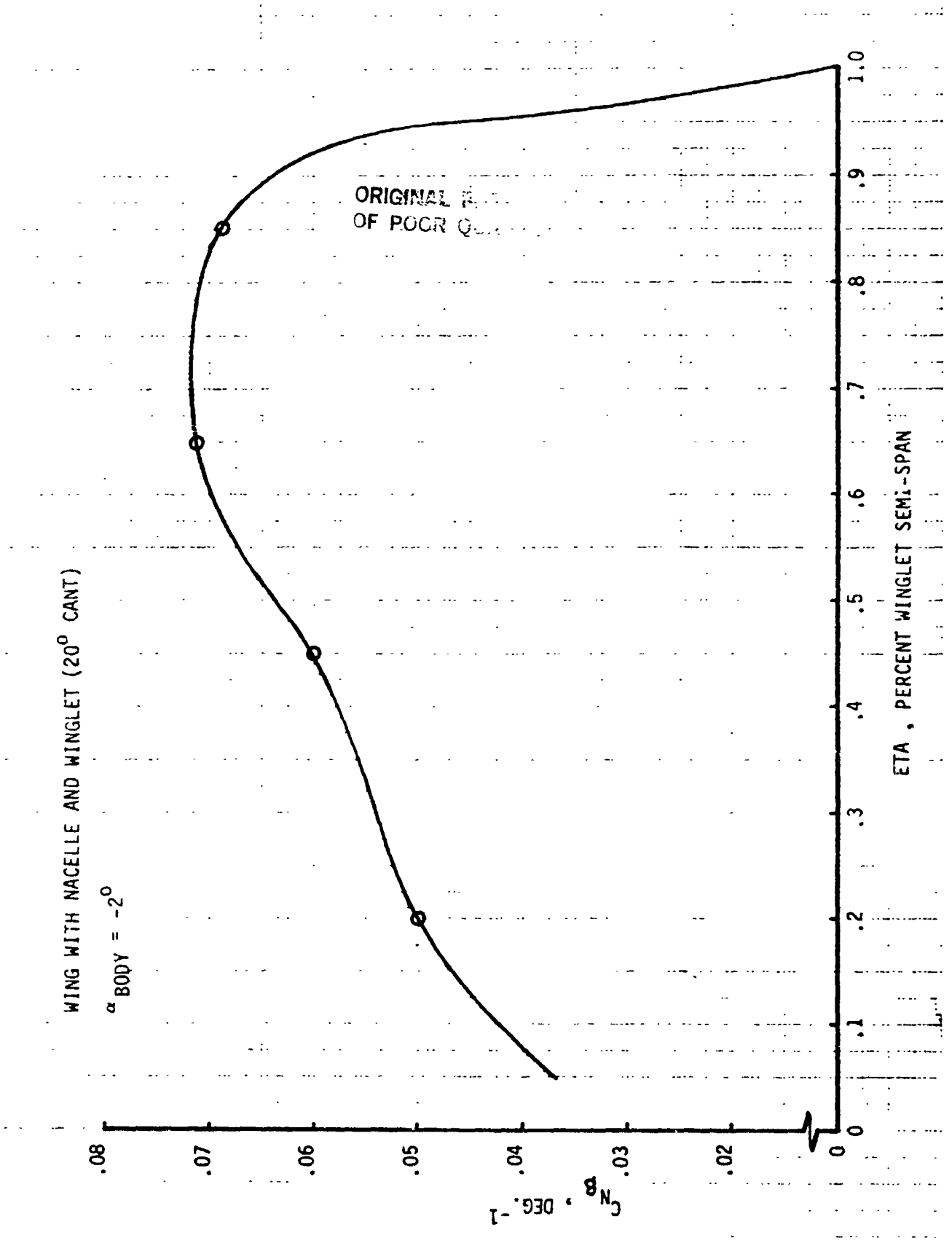

FIGURE B8 WINGLET SECTIONAL C_{n_β} DISTRIBUTION AT M=0.65

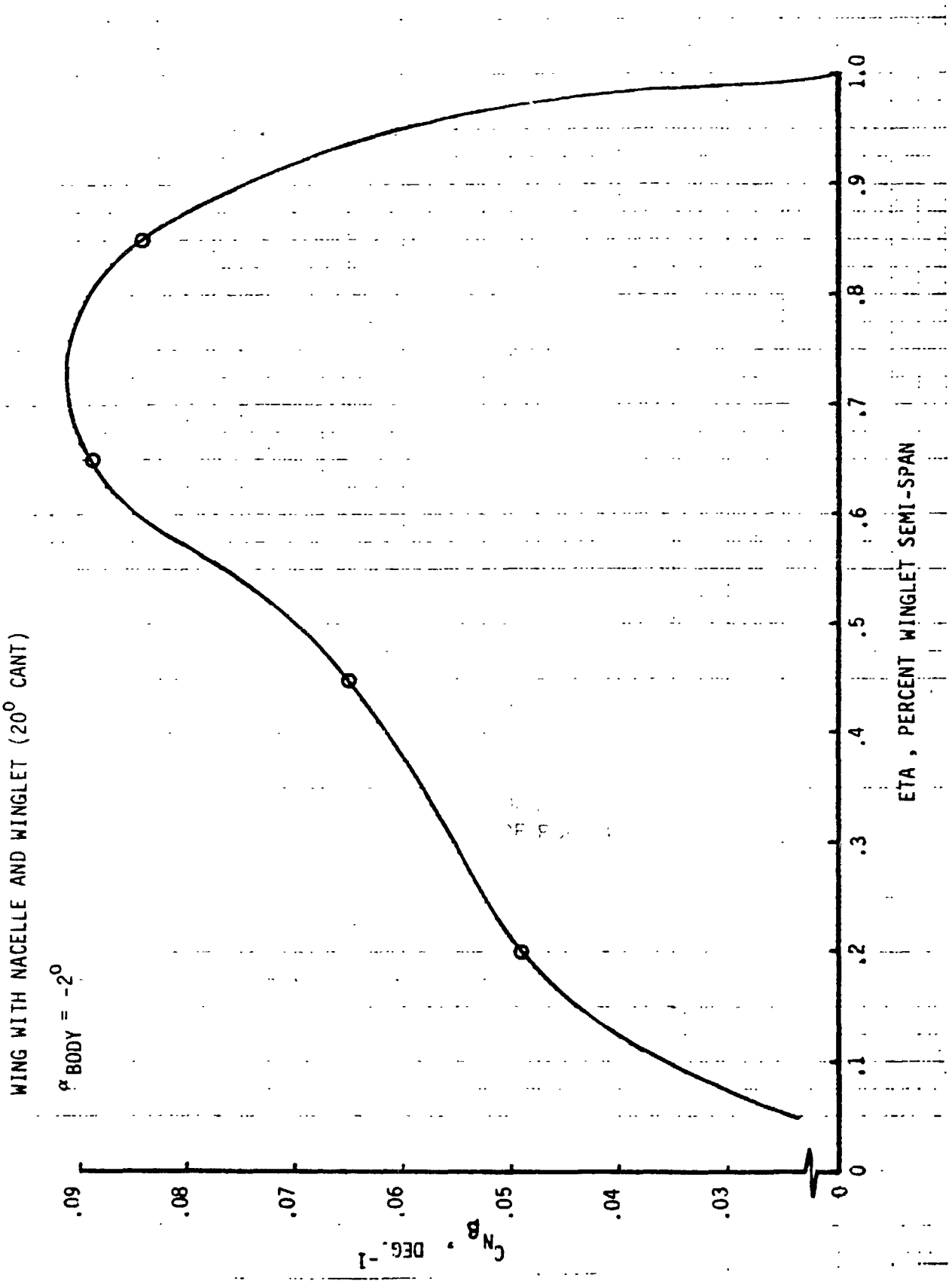

FIGURE B9 WINGLET SECTIONAL C_{n_β} DISTRIBUTION AT M=0.80

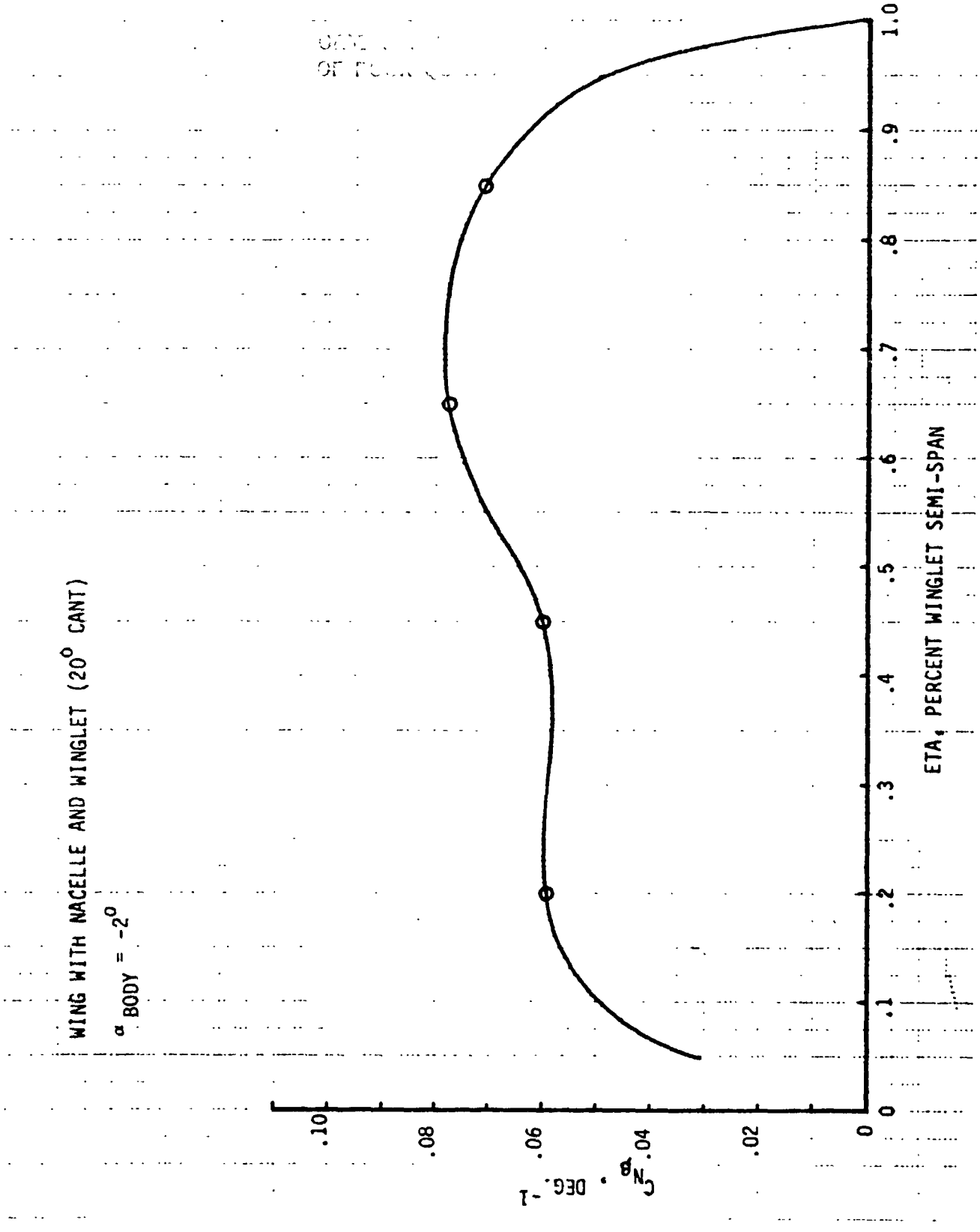

FIGURE B10 WINGLET SECTIONAL C_{n_β} DISTRIBUTION AT M=0.88

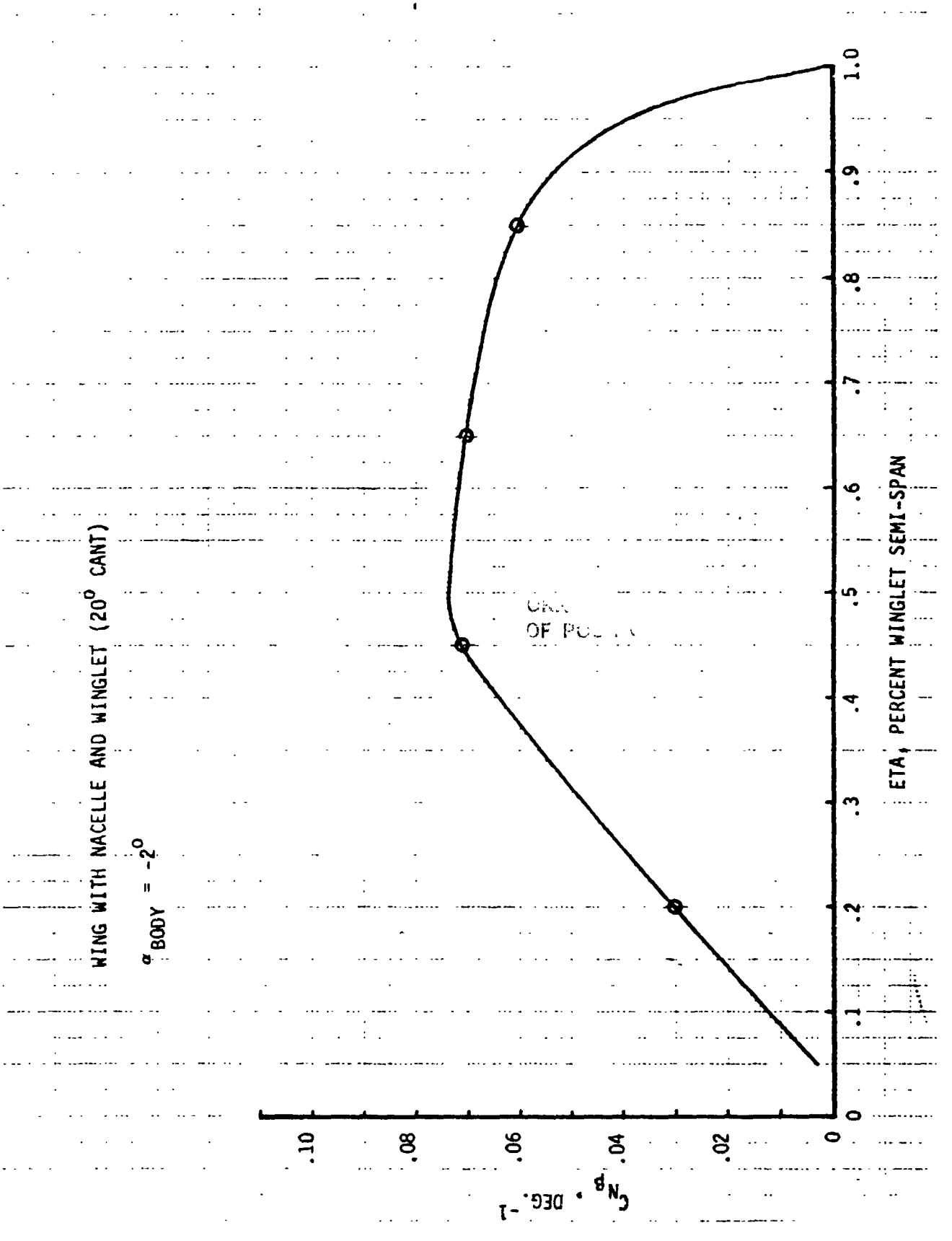

FIGURE B11 WINGLET SECTIONAL C_{n_β} DISTPIBUTION AT M=0.91

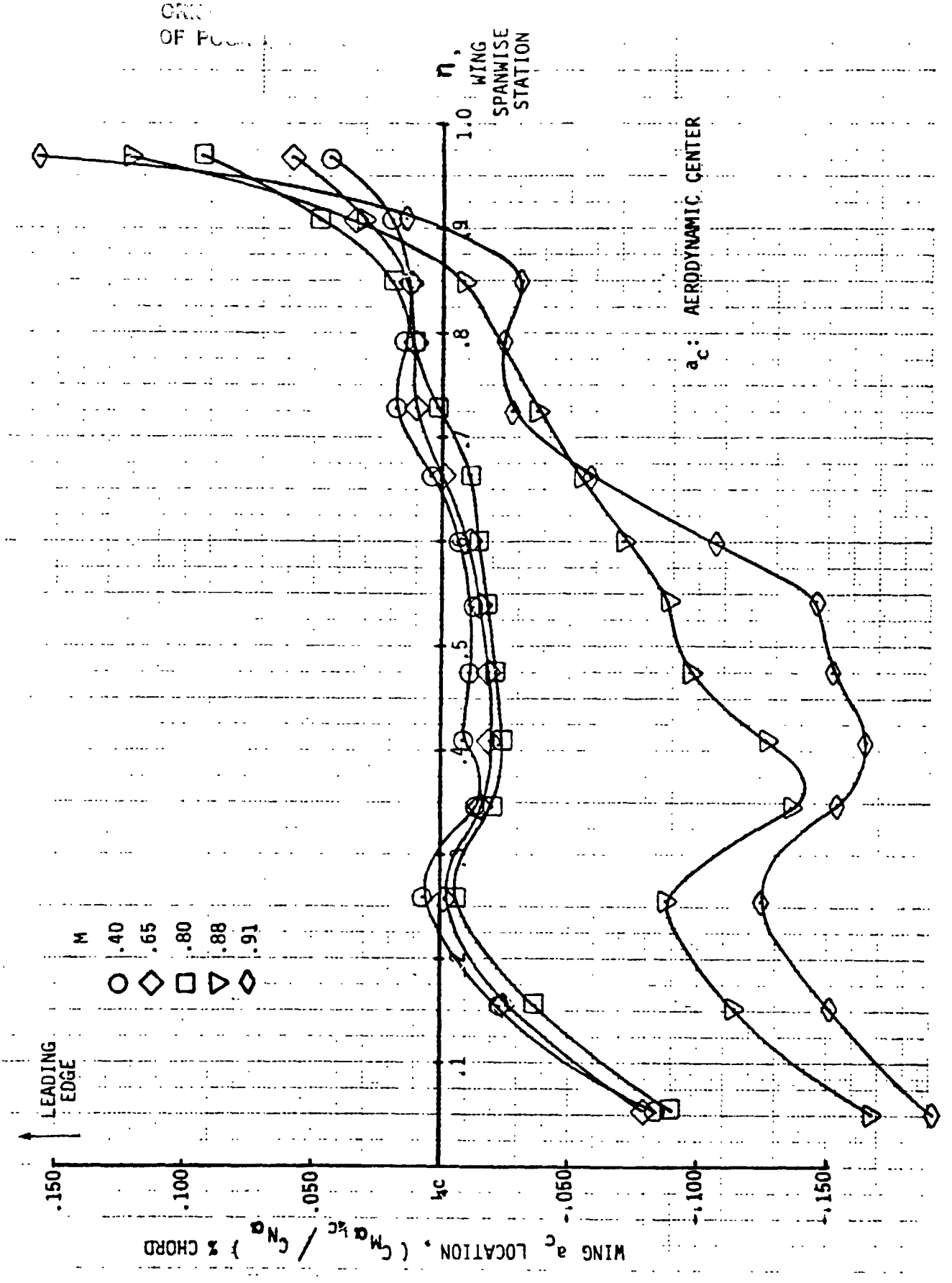

FIGURE B12 WING AERODYNAMIC CENTER DISTRIBUTION, WING-NACELLE

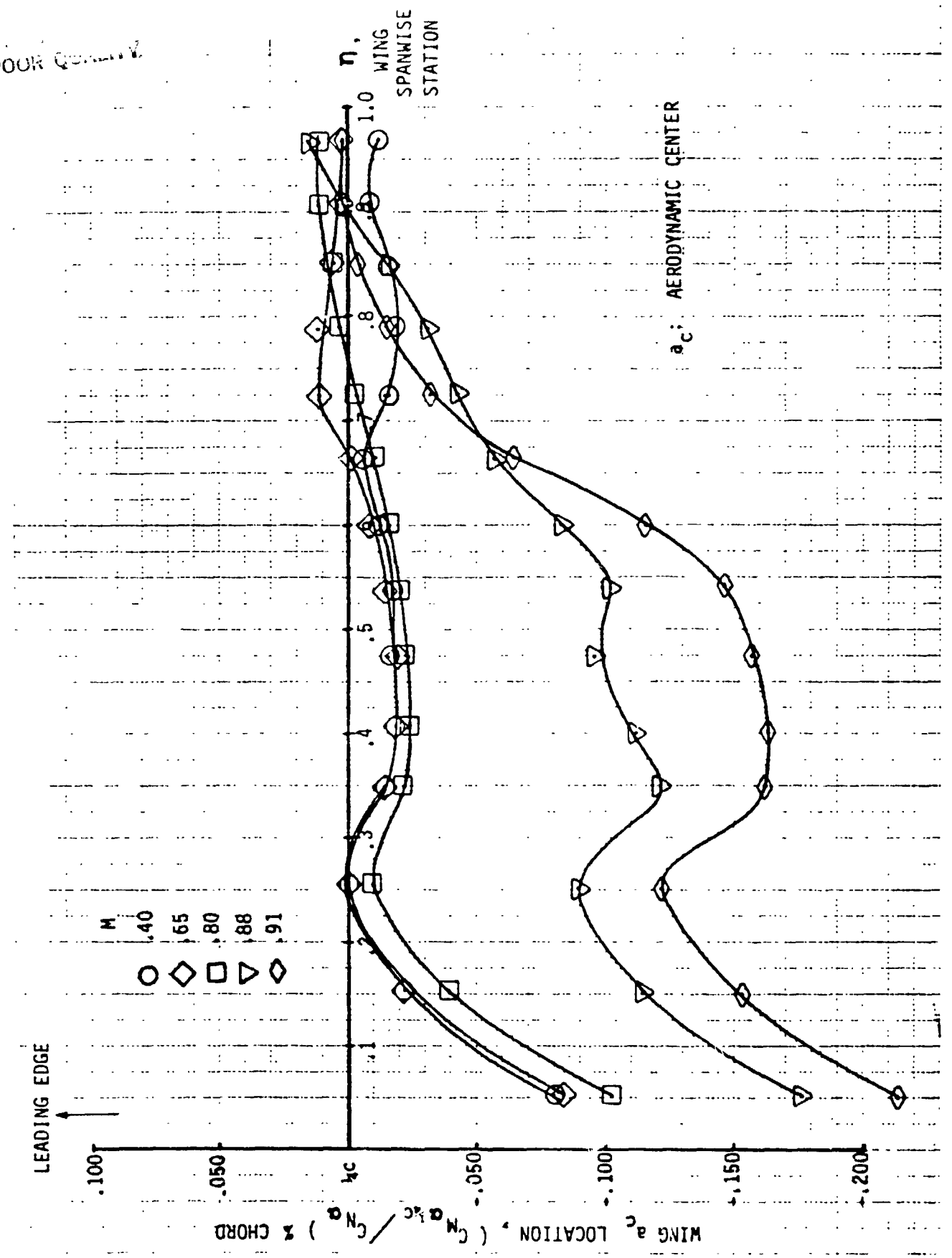

FIGURE B13 WING AERODYNAMIC CENTER DISTRIBUTION, WING-NACELLE- WINGLET (20 DEG.)

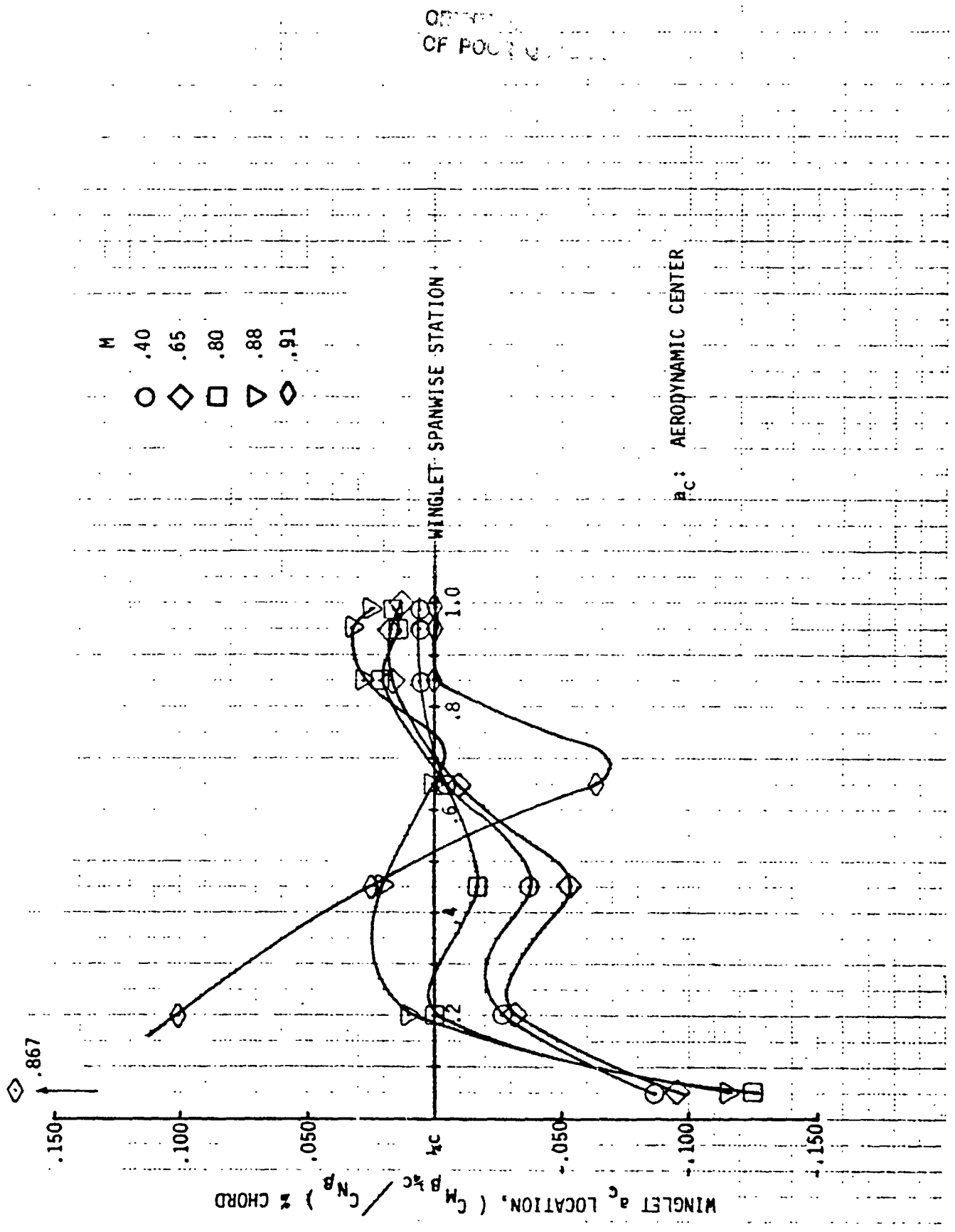

FIGURE B14 WINGLET AEPODYNAMIC CENTEP DISTRIBTUION, WING-NACELLE- WINGLET (20 DEG.)

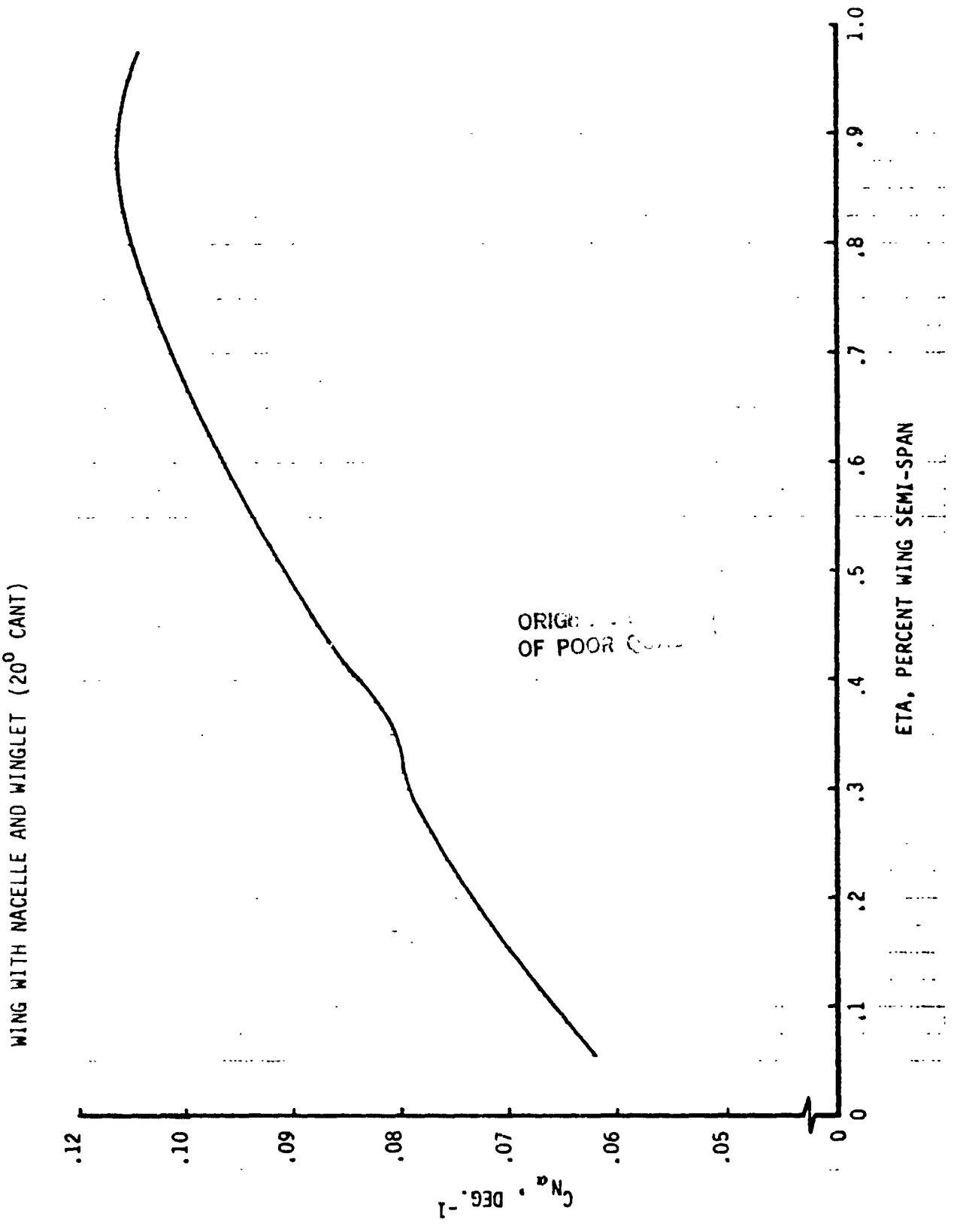

FIGURE B15a THEORETICAL WING C_{n_α} DISTRIBUTION, WING-NACELLE- WINGLET (20 DEG.)

M = 0.40

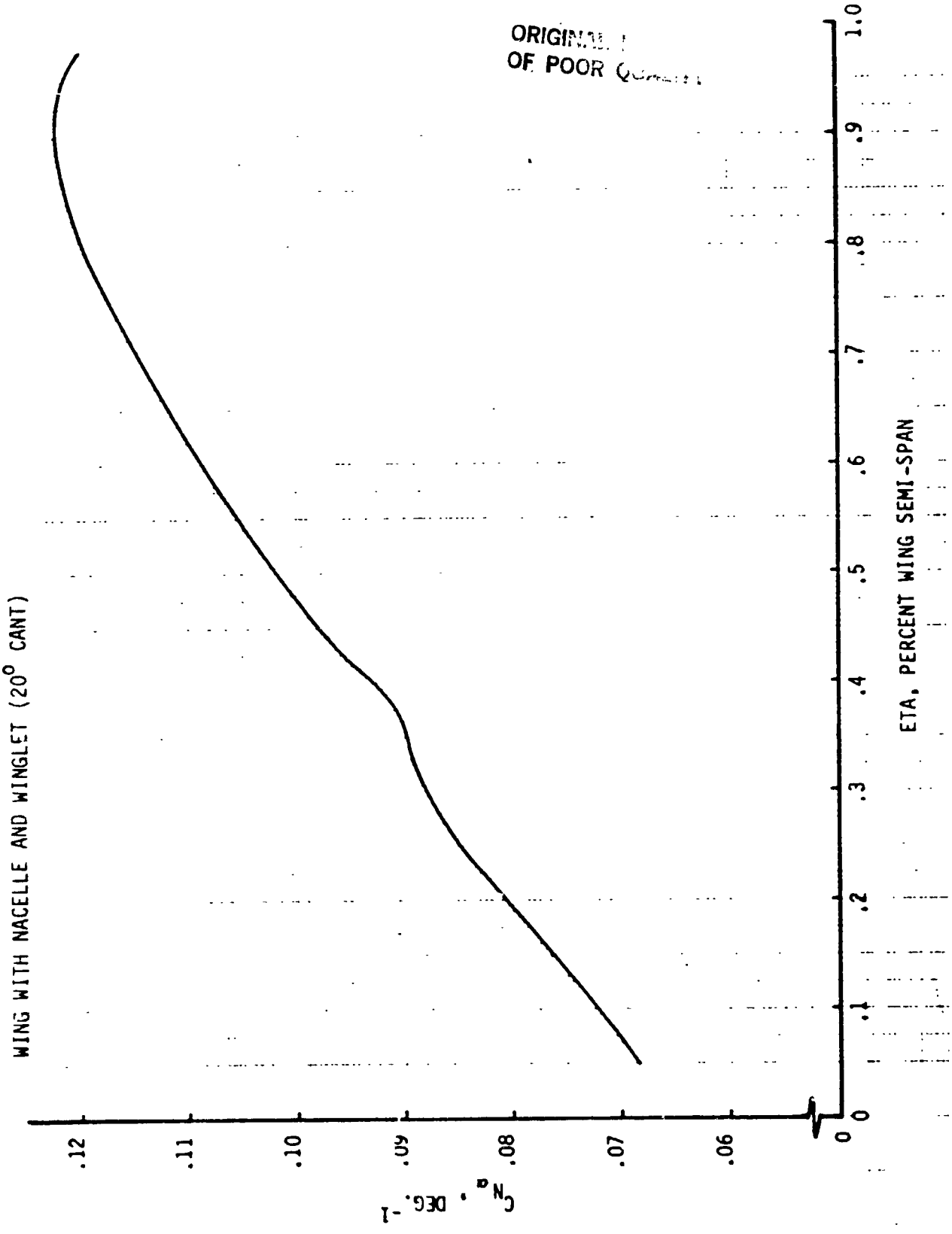

FIGURE B15b THEORETICAL WING C_{n_α} DISTRIBUTION, WING-NACELLE-WINGLET(20 DEG.)

M = 0.65

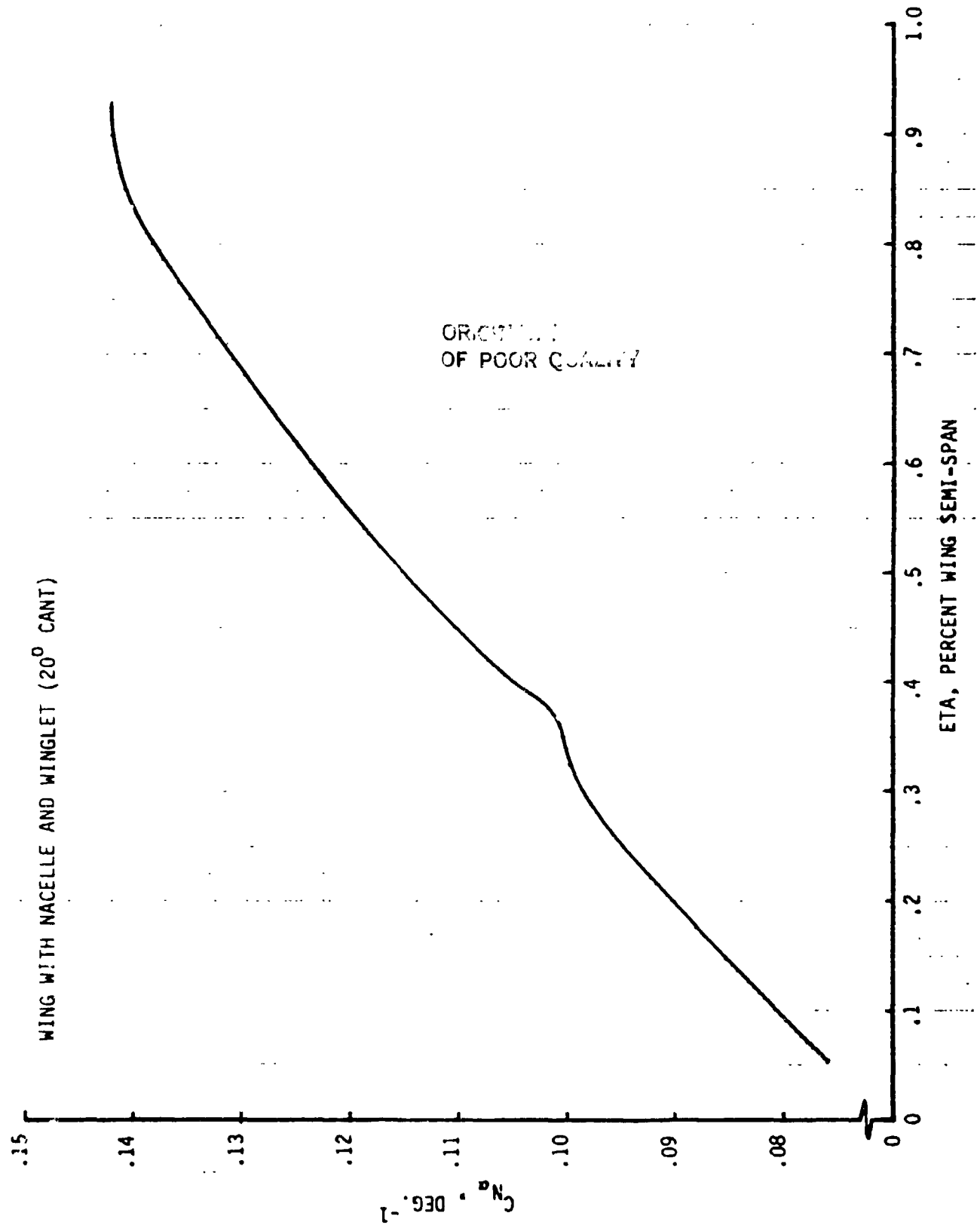

FIGURE B15c THEORETICAL WING C_{n_α} DISTRIBUTION, WING-NACELLE-WINGLET(20 DEG.)

M = 0.80

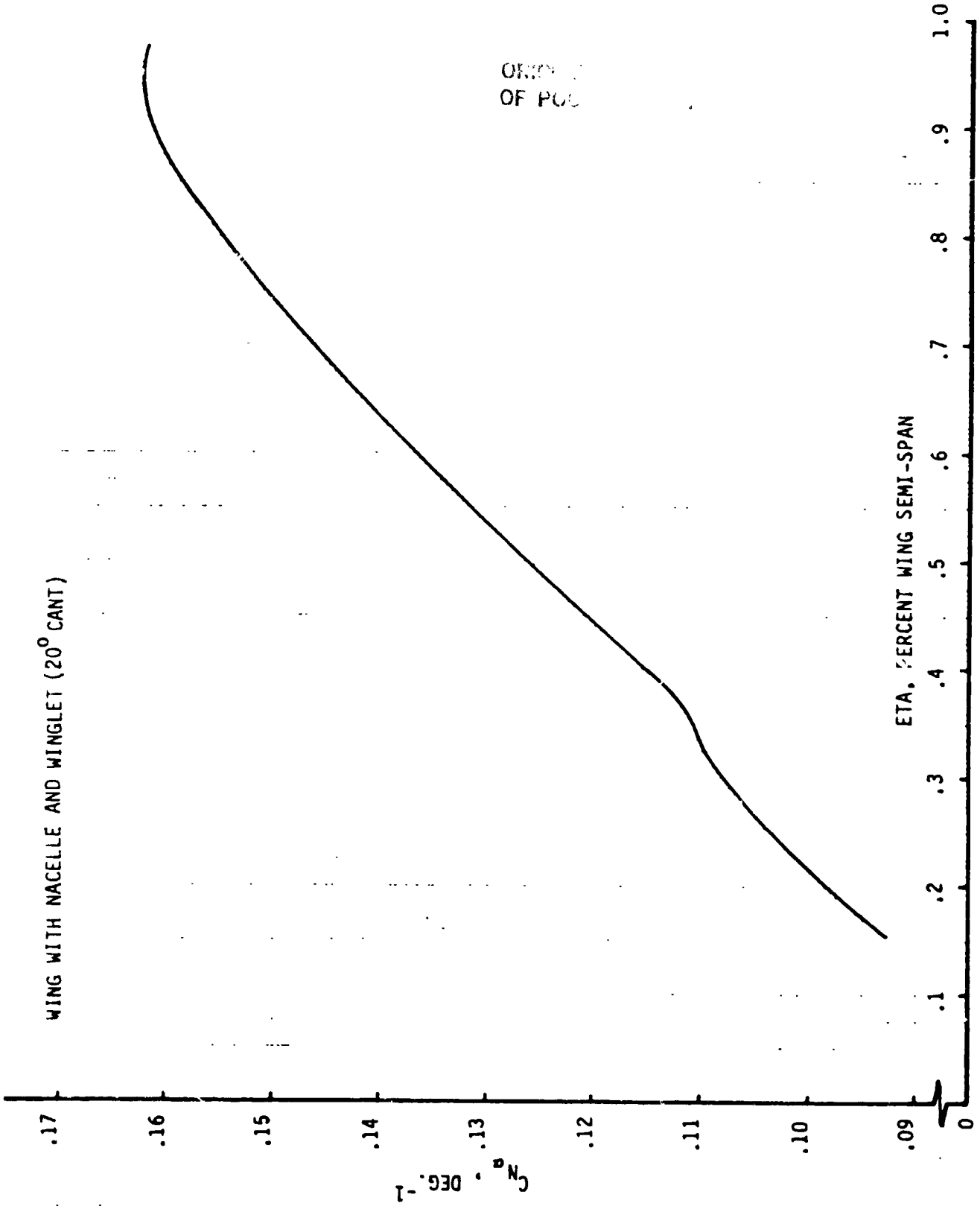

FIGURE B15d THEORETICAL WING C_{n_α} DISTRIBUTION, WING-NACELLE-WINGLET(20 DEG.)

M = 0.88

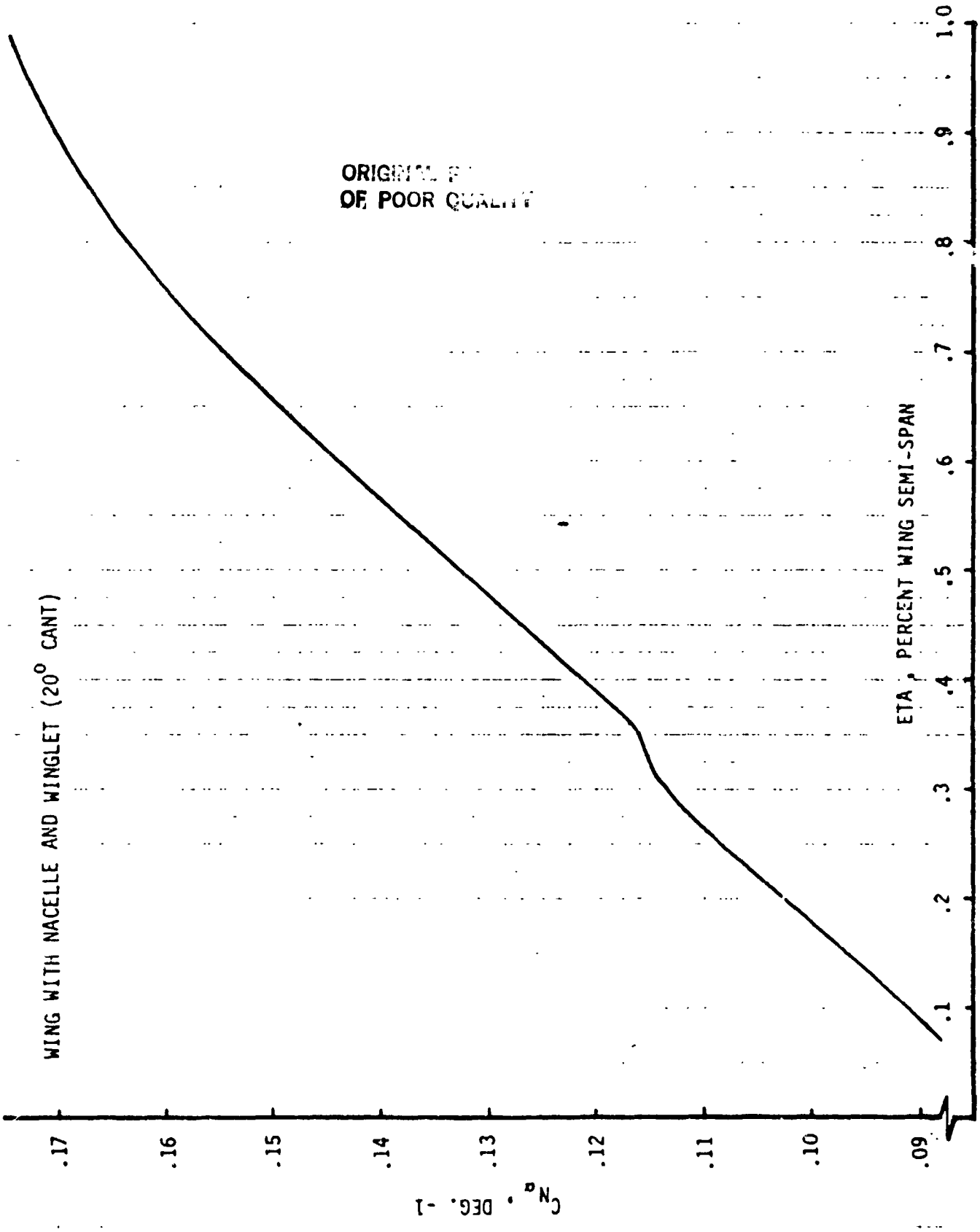

FIGURE B15e THEORETICAL WING C_{n_α} DISTRIBUTION, WING-NACELLE-WINGLET(20 DEG.)

M = 0.91

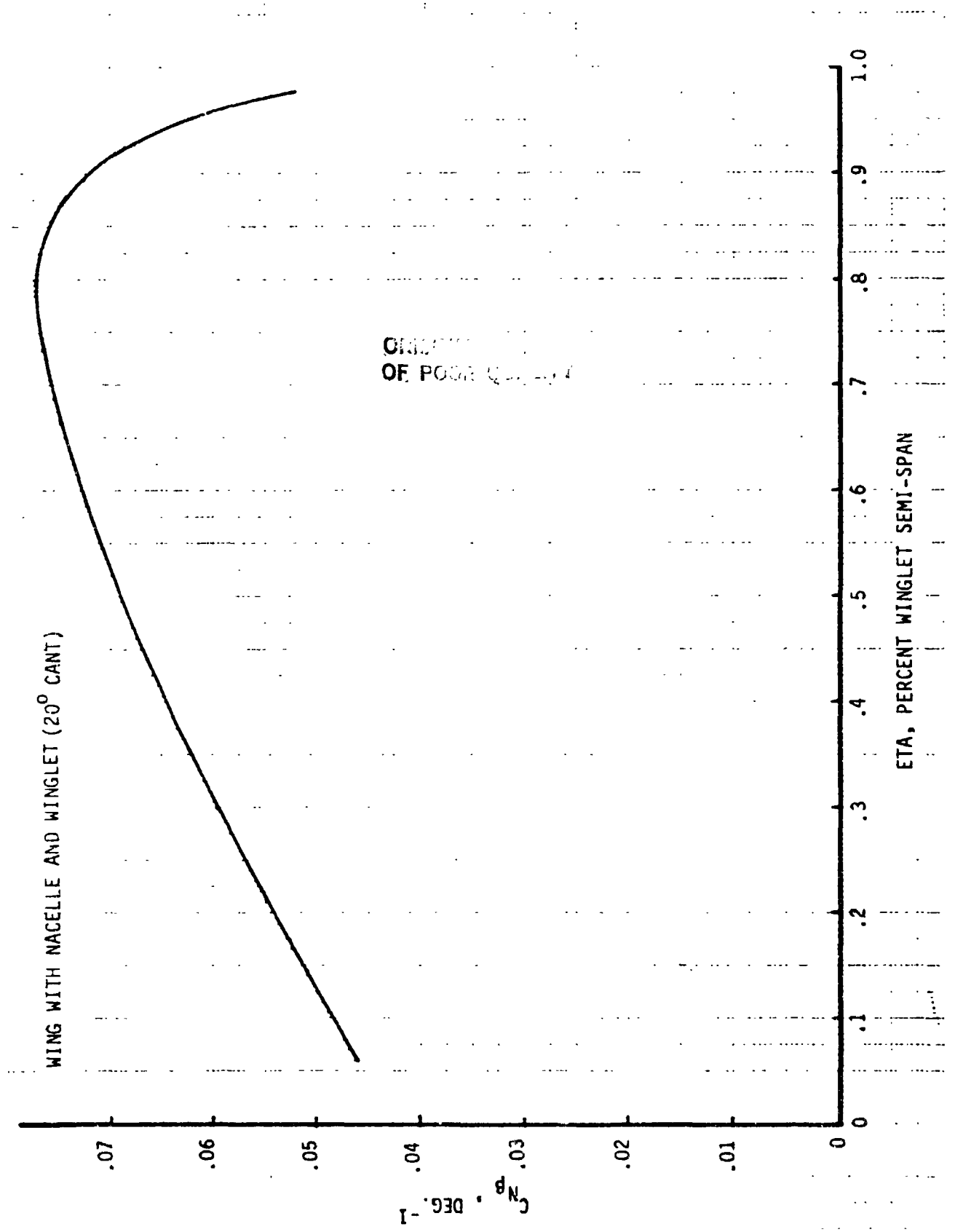

FIGURE B16a THEORETICAL WINGLET C_{n_β} DISTRIBUTION, WING-NACELLE-WINGLET(20 DEG.)

M = 0.40

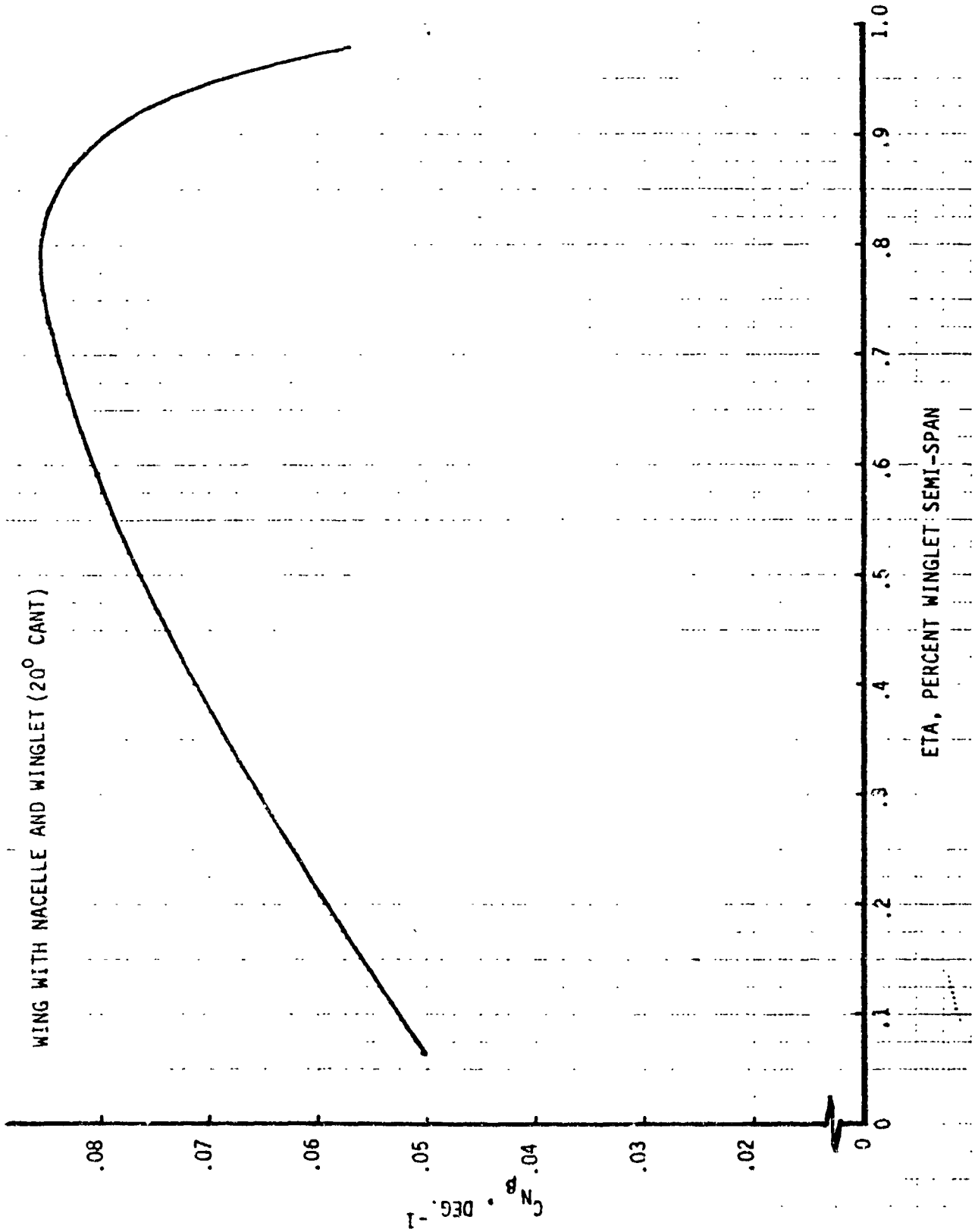

FIGURE B16b THEORETICAL WINGLET C_{n_β} DISTRIBUTION , WING-NACELLE-WINGLET(20 DEG.)

M = 0.65

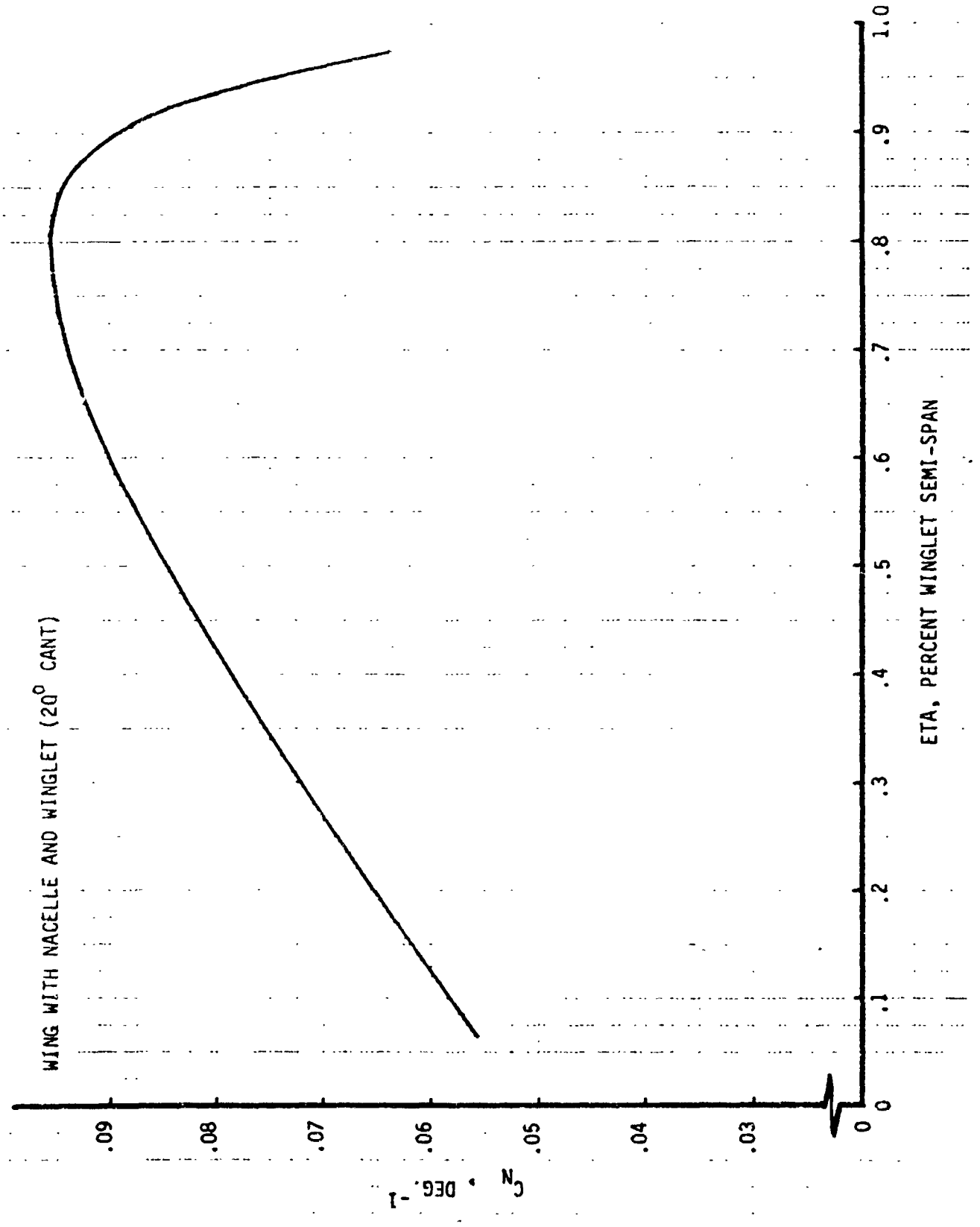

FIGURE B16c THEORETICAL WINGLET C_{n_β} DISTRIBUTION, WING-NACELLE-WINGLET(20 DEG.)

M = 0.80

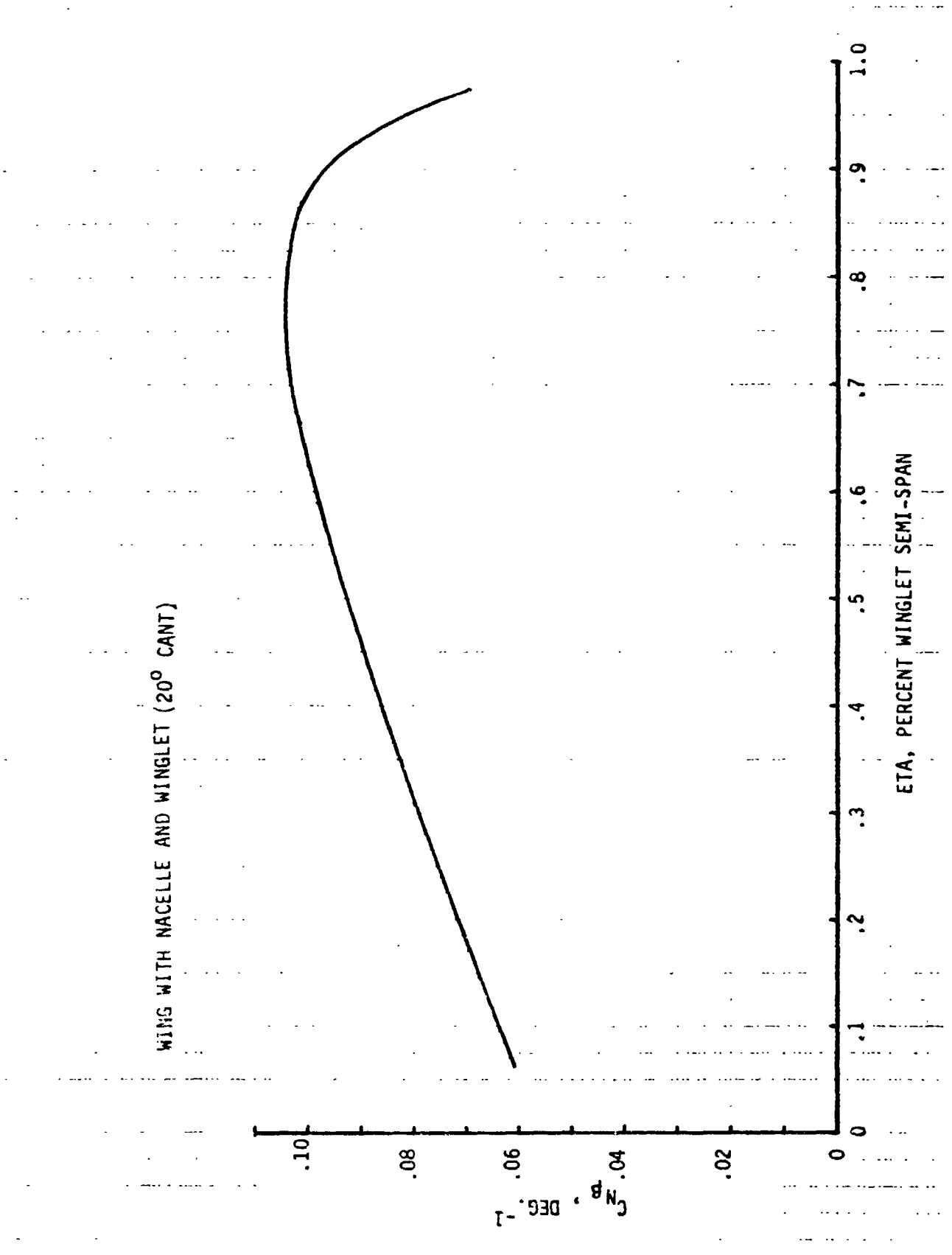

FIGURE B16d THEORETICAL WINGLET C_{n_β} DISTRIBUTION, WING-NACELLE-WINGLET(20 DEG.)

M = 0.88

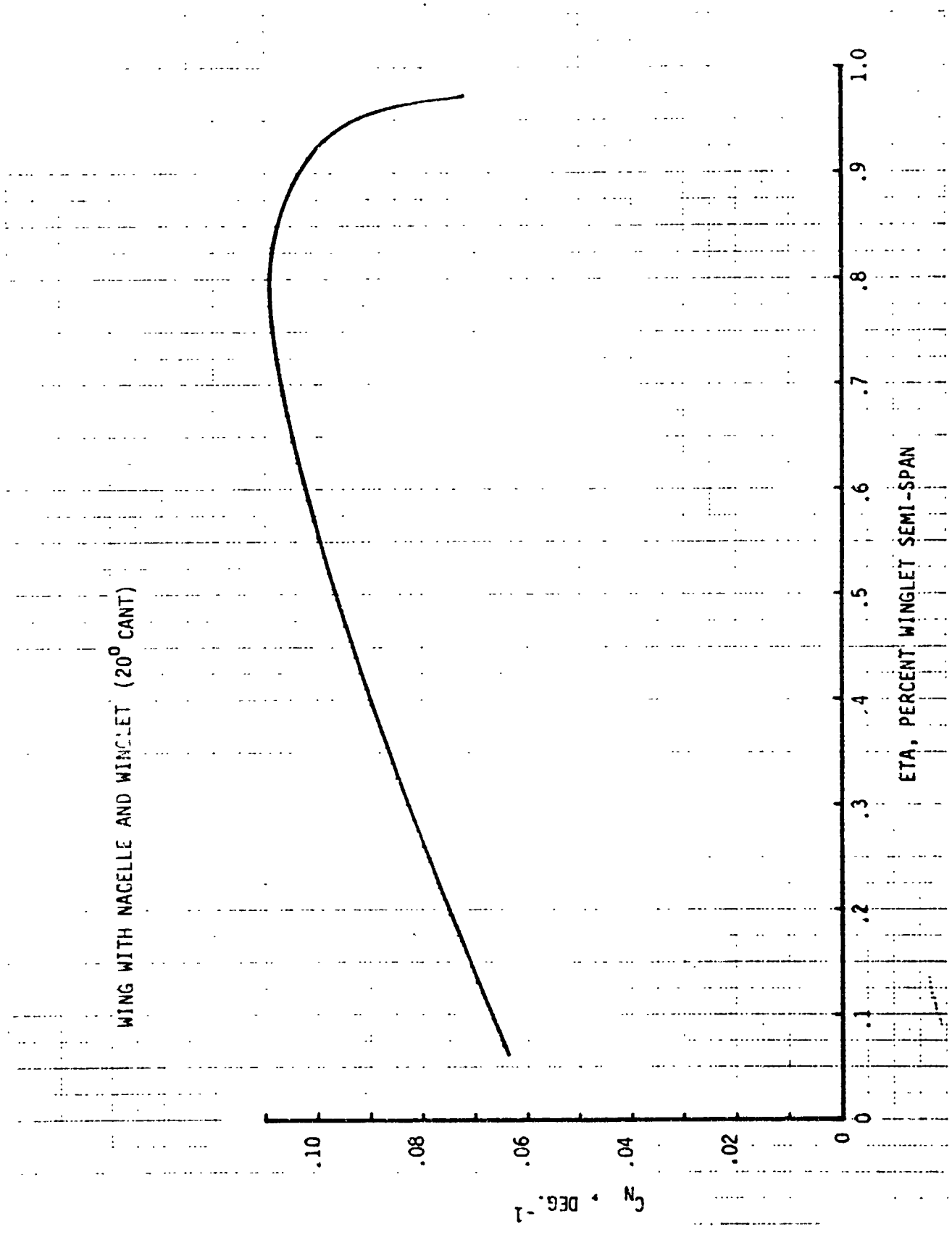

FIGURE B16e THEORETICAL WINGLET C_{n_β} DISTRIBUTION, WING-NACELLE-WINGLET(20 DEG.)

M = 0.91

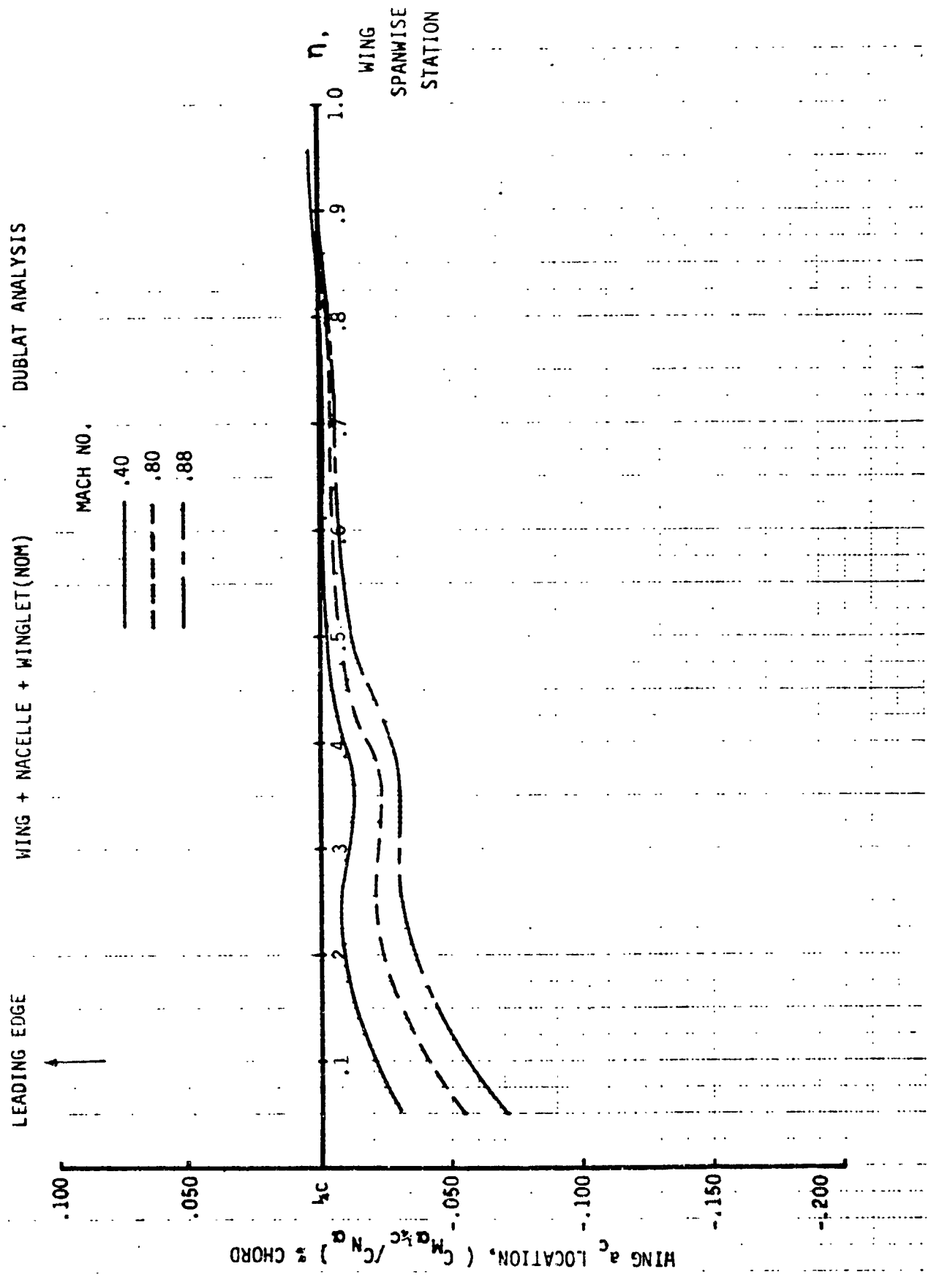

FIGURE B17 THEORETICAL WING AERODYNAMIC CENTER DISTRIBUTION, WING-NACELLE-WINGLET(20 DEG.)

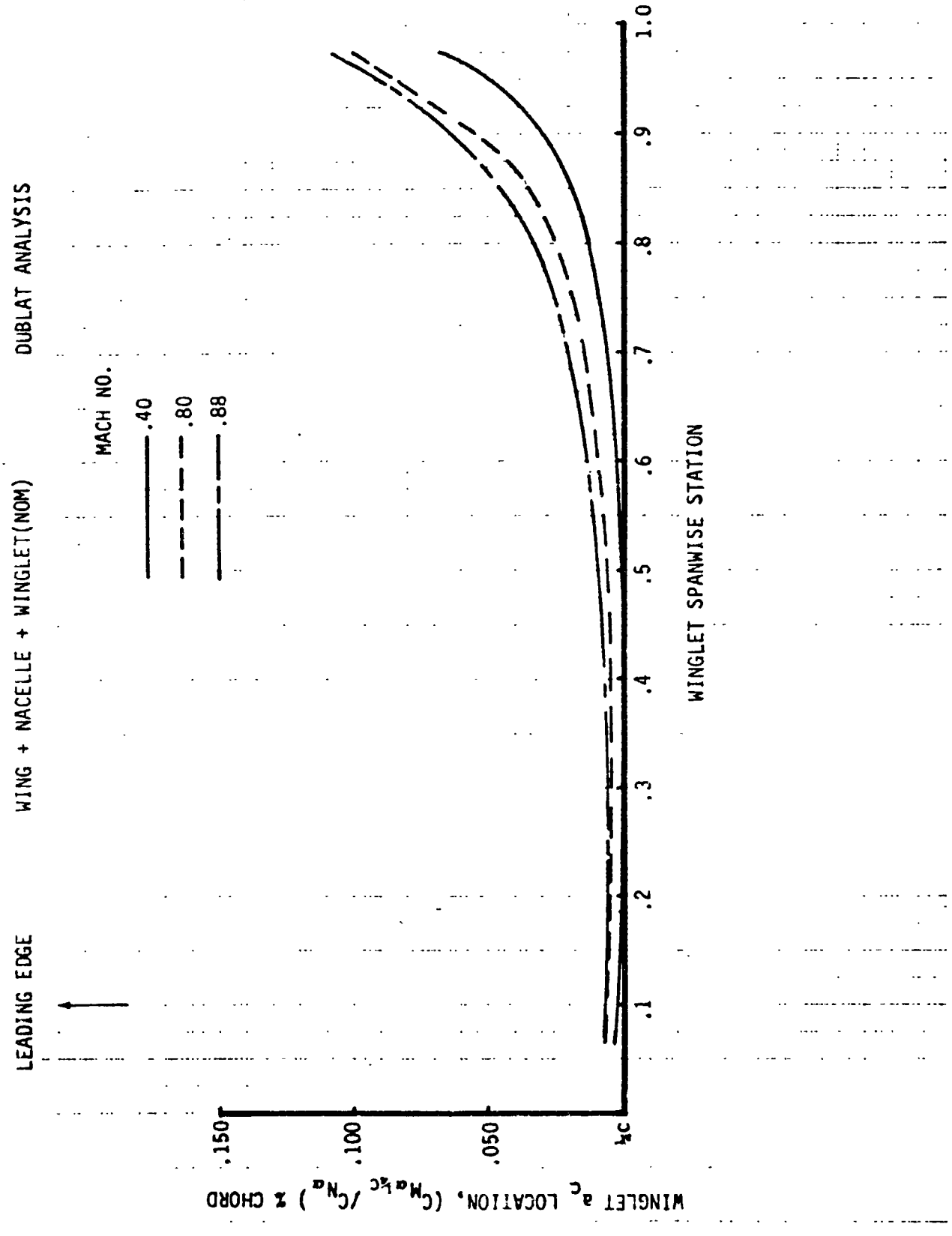

FIGURE B18 THEORETICAL WINGLET AERODYNAMIC CENTER DISTRIBUTION, WING-NACELLE-WINGLET(20 DEG.)

APPENDIX C

VIBRATION FREQUENCIES & NODE LINES

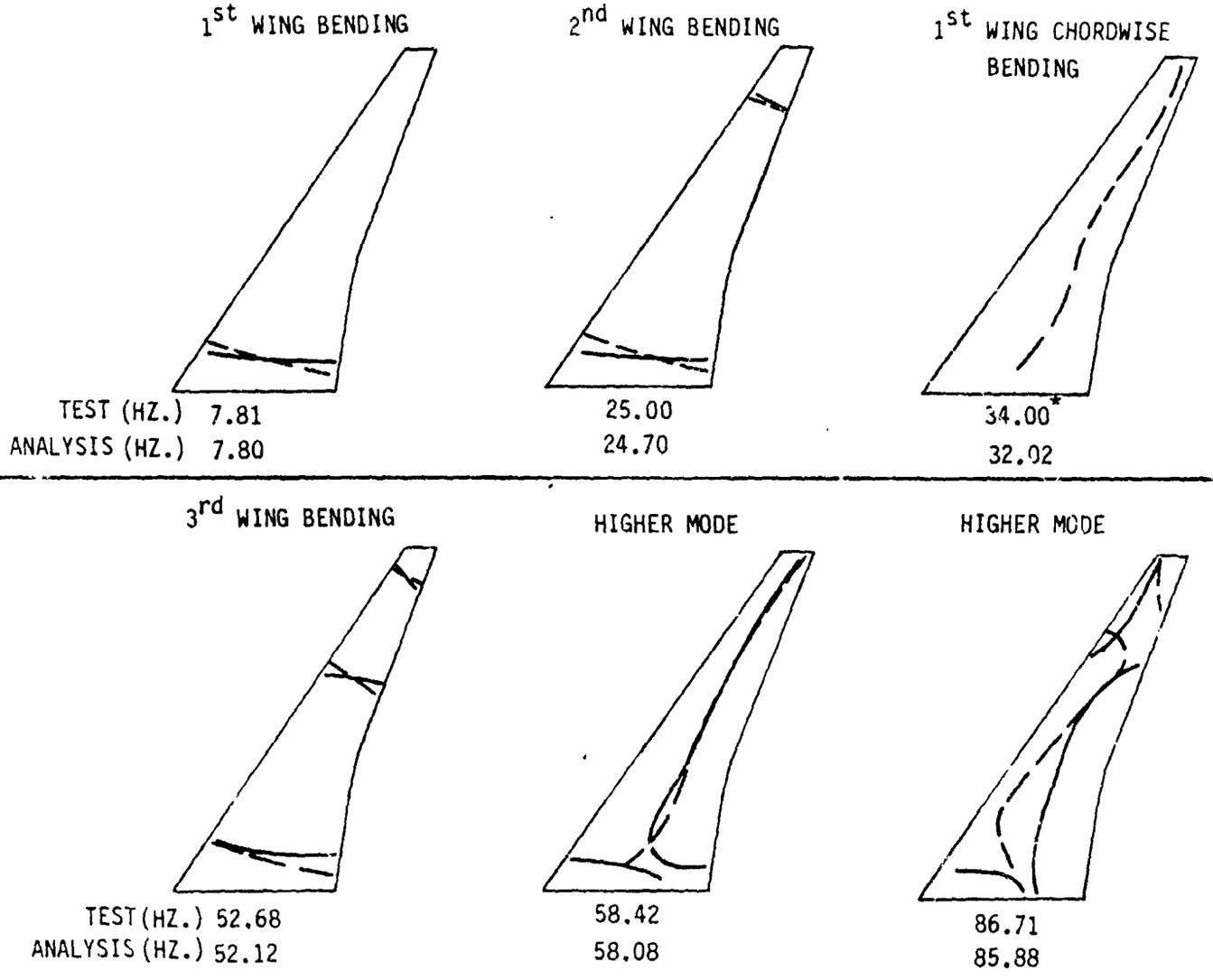

FIGURE C1 MEASURED & CALCULATED FREQUENCIES & NODE LINES FOR WING (EMPTY)

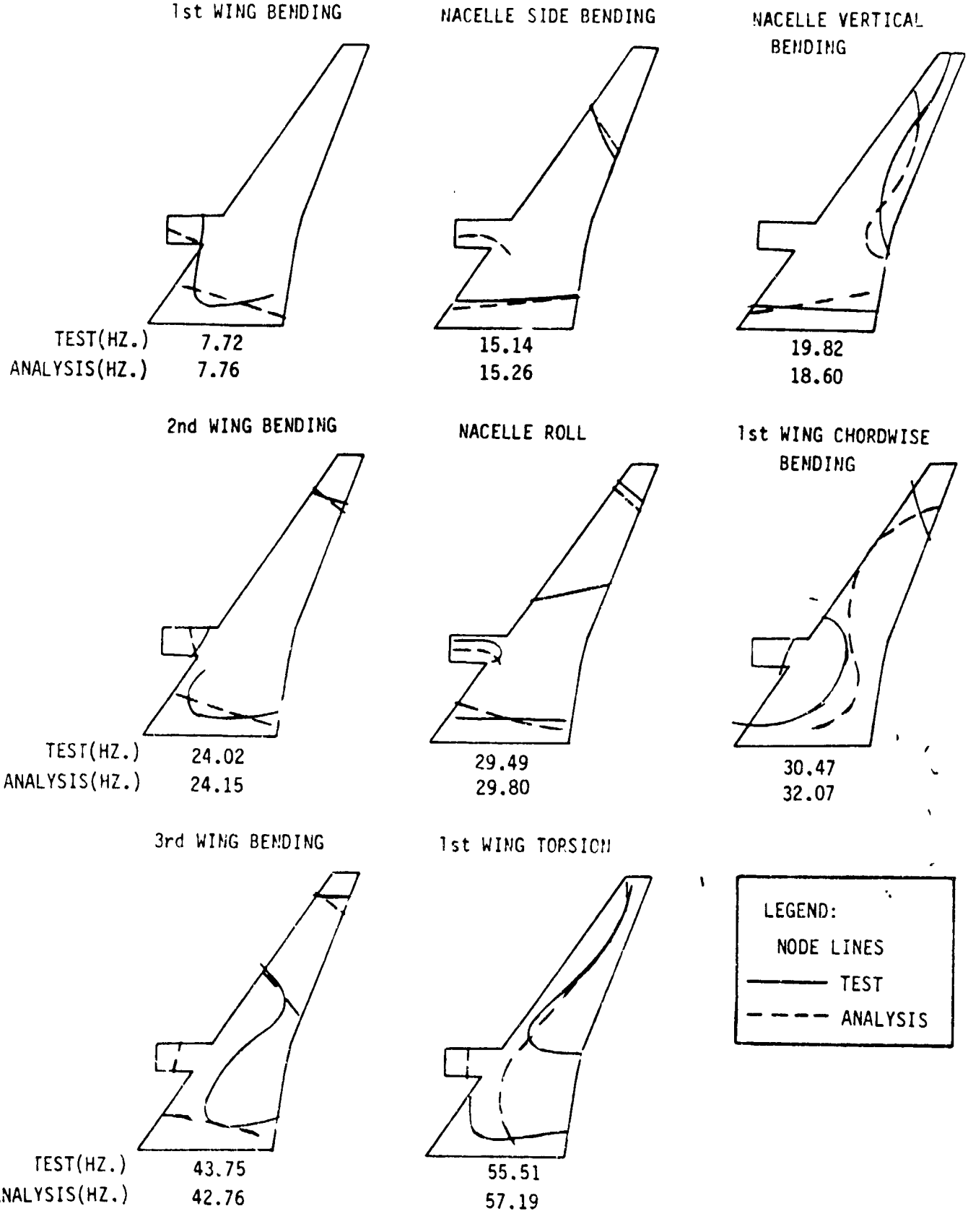

FIGURE 62 MEASURED & CALCULATED FREQUENCIES & NODE LINES FOR WING (EMPTY) - NACELLE(NOMINAL)

1st WING BENDING

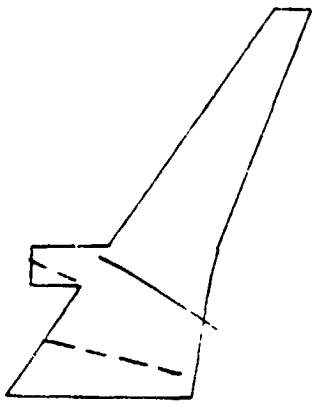

TEST(HZ.) 6.84
ANALYSIS(HZ.) 6.72

NACELLE SIDE BENDING

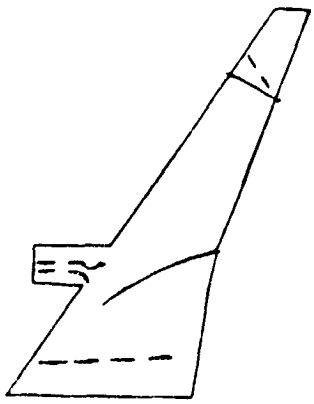

15.23
15.19

NACELLE VERTICAL BENDING

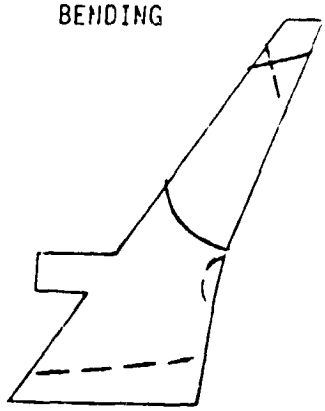

19.82
18.54

2nd WING BENDING

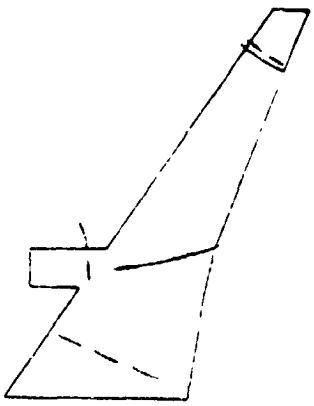

TEST(HZ.) 21.09
ANALYSIS(HZ.) 21.08

1st WING CHORDWISE BENDING

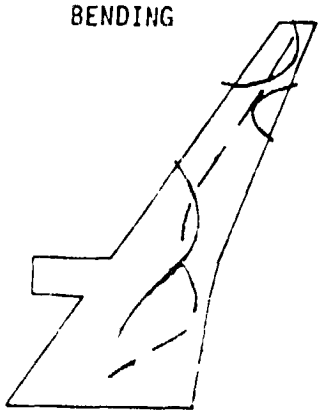

27.64
26.64

NACELLE ROLL

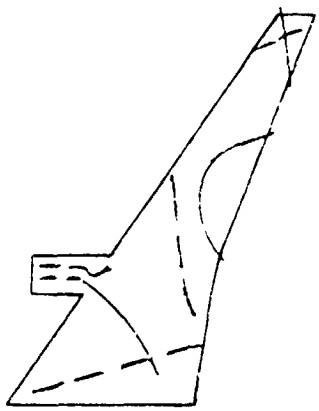

29.69
29.98

3rd WING BENDING

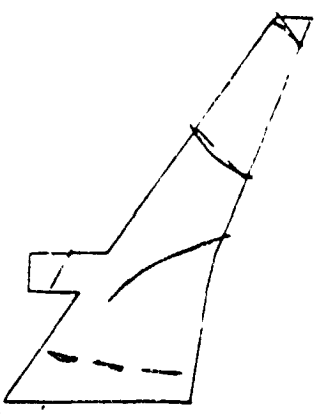

TEST(HZ.) 40.33
ANALYSIS(HZ.) 38.91

1st WING TORSION

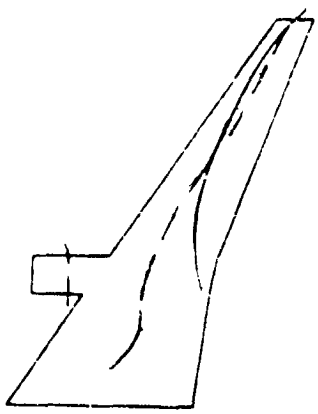

46.88
47.01

LEGEND:
NODE LINES
——— TEST
– – – ANALYSIS

FIGURE C3 MEASURED & CALCULATED FREQUENCIES & NODE LINES FOR WING (EMPTY) - NACELLE(NOMINAL)- WINGLET (20 DEG)

1st WING BENDING

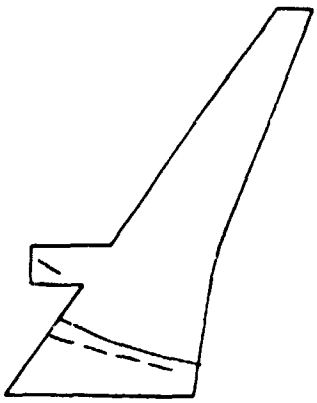

TEST(HZ.) 6.06
ANALYSIS(HZ.) 6.06

NACELLE SIDE BENDING

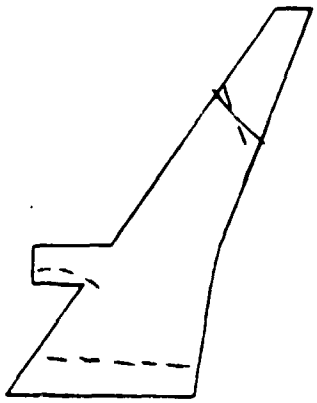

15.04
14.98

2nd WING BENDING

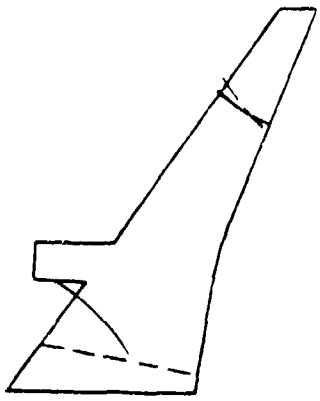

17.19
16.80

NACELLE VERTICAL BENDING

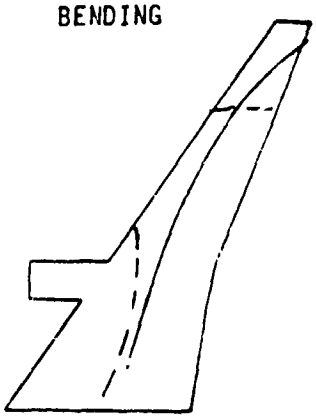

TEST(HZ.) 19.14
ANALYSIS(HZ.) 19.08

1ST WING CHORDWISE BENDING

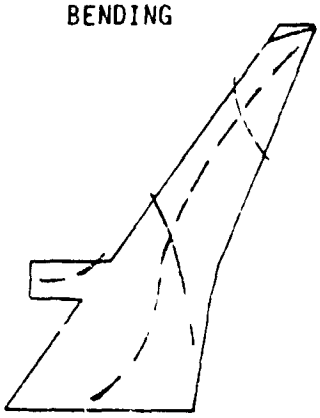

22.36
25.20

NACELLE ROLL

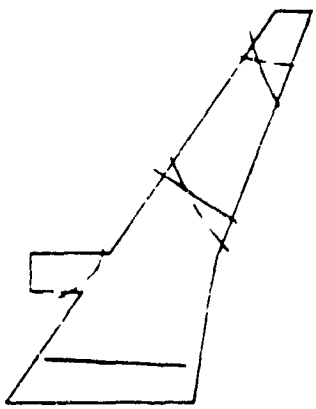

29.20
29.93

3rd WING BENDING

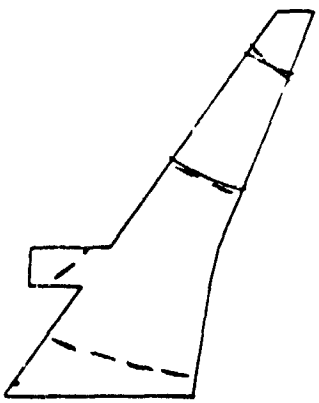

TEST(HZ.) 32.03
ANALYSIS(HZ.) 32.41

1st WING TORSION

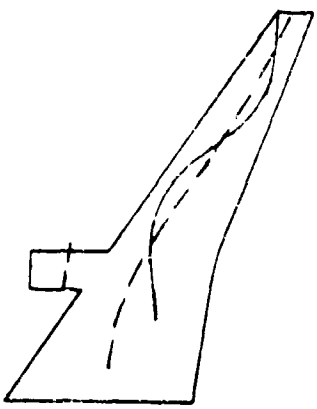

46.39
46.63

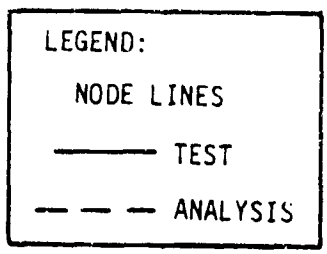

FIGURE C4 MEASURED & CALCULATED FREQUENCIES & NODE LINES FOR WING (FULL) - NACELLE(NOMINAL)

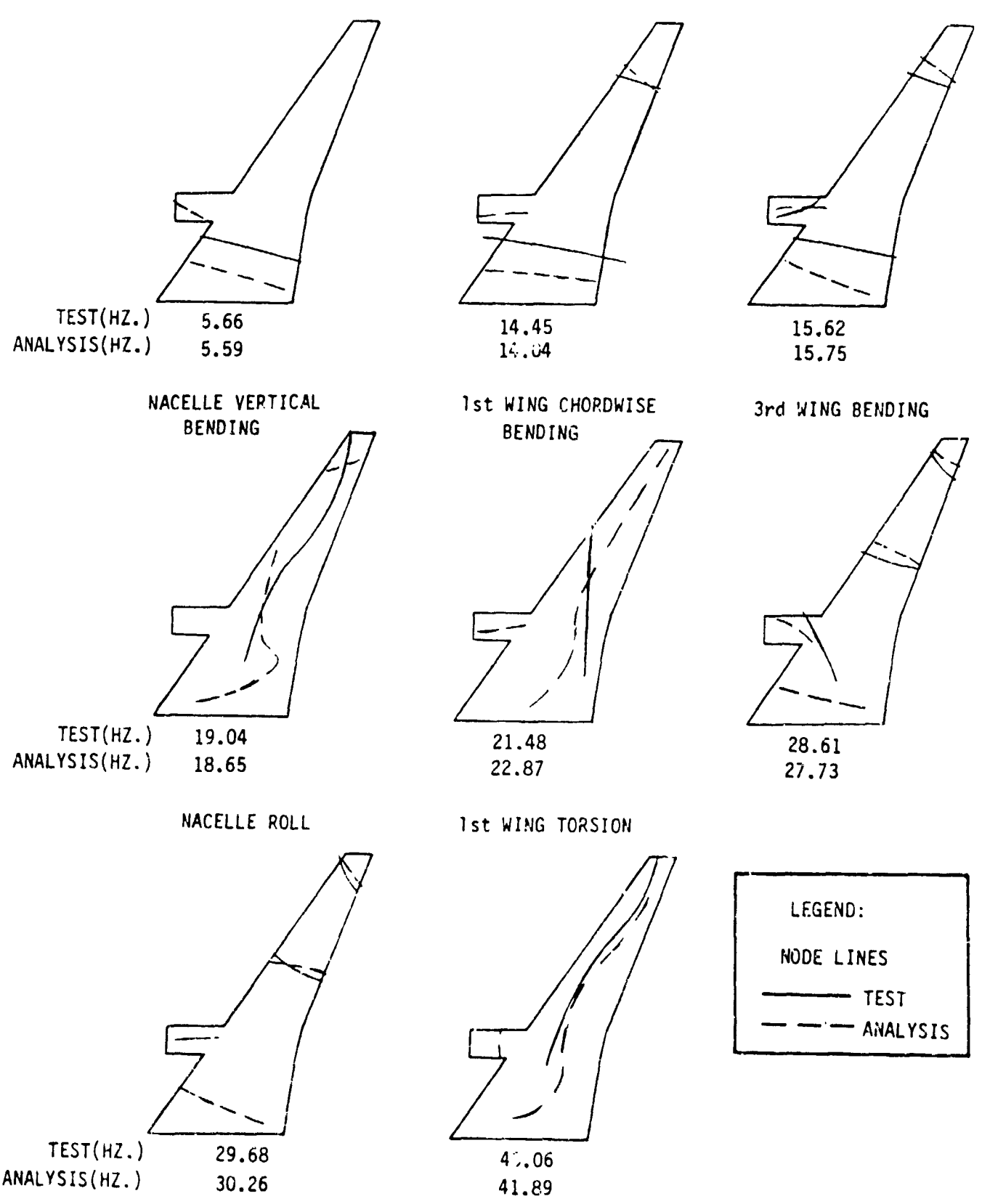

FIGURE C5 MEASURED & CALCULATED FREQUENCIES & NODE LINES FOR WING (FULL) - NACELLE(NOMINAL)-WINGLET (20 DEG)

APPENDIX D

PROCEDURE FOR MODIFYING STIFFNESS MATRIX

APPENDIX D - Procedure for Modifying Stiffness Matrix

The procedure is based on following assumptions:

1. The analytical mode shapes exactly match the test mode shapes.
2. The frequecies for modes m + 1 through n are exact where m lowest frequencies are available from the test and n is the total degrees-of-freedom of the analytical model.
3. The analytical mass distribution accurately describes the model.

$$([K] - \lambda_i [M])\{\phi_i\} = 0 \quad ; \quad i = 1, n$$

$$[\Phi] = [\Phi_m \mid \Phi_\ell] = [\phi_1 \; \phi_2 \cdots \phi_m \mid \phi_{m+1} \cdots \phi_n] \quad ; \quad m - \ell = n$$

$$[K_{g_m}] = [\Phi_m^T][K][\Phi_m] \quad ; \quad [K_{g_n}] = [\Phi^T][K][\Phi] \; ; \; [\Phi^T][M][\Phi] = [I]$$

$$[K] = [M]^T[\Phi][K_{g_n}][\Phi]^T[M]$$

$$= [M]^T [\Phi_m \mid \Phi_\ell] \begin{bmatrix} [K_{g_m}] & 0 \\ 0 & [K_{g_\ell}] \end{bmatrix} \begin{bmatrix} \Phi_m^T \\ \Phi_\ell^T \end{bmatrix} [M]$$

$$= [M]^T[\Phi_m][K_{g_m}][\Phi_m^T][M] + [M^T][\Phi_\ell][K_{g_\ell}][\Phi_\ell^T][M]$$

$[K^*]$ = Modified Stiffness Matrix

$$= [M]^T[\Phi_m][K_{g_m}^*][\Phi_m^T][M] + \left([K] - [M^T][\Phi_m][K_{g_m}][\Phi_m^T][M]\right)$$

$$[K_{g_m}^*] = (2\pi)^2 [f_T^2][M_{g_m}] \text{ where } [f_T] \text{ are test freqs.}$$

Thus $$[K^*] = [K] + (2\pi)^2 [M^T][\Phi_m][M_{g_m}]\left([f_T^2 - f_A^2]\right)[\Phi_m^T][M]$$

where f_A is the freq. from analysis using unmodified stiffness matrix $[K]$

The procedure was applied to correct the stiffness matrix based on the clean wing vibration test.

APPENDIX E

SUMMARY OF EXPERIMENTAL RESULTS - HIGH SPEED MODEL

APPENDIX E

SUMMARY OF EXPERIMENTAL RESULTS - HIGH SPEED MODEL

RUN NO.	WING	NACELLE	WINGTIP	BEHAVIOR*/f(HZ.)	DYNAMIC PRESSURE (LB/FT^2)	MACH	SPEED (FT/SEC)	DENSITY ($SLUGS/FT^3$)	REYNOLDS NUMBER/ FT X 10^{-6}
9	EMPTY	NOM	NOM	LOW DAMPING (16.0)	120.6	.890	441.4	.001228	2.130
10				NVB FLUTTER (17.5)	140.0	.830	411.8	.001633	2.637
11				NVB FLUTTER (18.0)	169.3	.780	385.6	.002244	3.366
2			WINGLET (20^o)	NVB FLUTTER (17.5)	124.4	.770	NOT AVAILABLE FROM TUNNEL COMPUTER SYSTEM		
3				WB2 FLUTTER (22.0,17.5)	157.0	.660			
4				BUFFET	85.1	.900			
5				NVB FLUTTER (17.5)	105.6	.828			
6			BALLAST	LOW DAMPING (14.5,17.0)	122.5	.900			
7				NVB FLUTTER, (16.0)	138.5	.820			
8				NVB FLUTTER, (17.5)	163.5	.745			
27		SOFT	NOM	LOW DAMPING (13.0)	86.5	.900	443.4	.000873	1.536
28				LOW DAMPING, HR (13.0,17.4,14.0)	122.6	.890	441.3	.001248	2 173
29				FLUTTER, HR (13.0,14,22)	139.9	.865	423.1	.001505	2.501
30				FLUTTER (21.5,17.0)	161.0	.823	398.2	.001906	2 950
31				FLUTTER (23.0)	190.0	.782	398.5	.001893	2.927
23			WINGLET (20^o)	FLUTTER (14.0,22.7)	85.3	.890	425.0	.000890	1.526
24				FLUTTER (17.5,19.0)	107.7	.844	417.2	.001227	2.019
25				FLUTTER (21.0,14.0)	136.1	.778	385.8	.001807	2.730
26				FLUTTER (23.0)	153.6	.710	353.7	.002422	3.324
32			BALLAST	LOW DAMPING (13)	131.0	.870	428.8	.001414	2.406
33				LOW DAMPING (16.5)	153.0	.820	408.7	.001815	2.884
34				FLUTTER (19.0)	69.0	.737	349.5	.002454	3.309
34R				FLUTTER (19.0)	173.0	.750	373.7	.002443	3.538

APPENDIX E (cont'd)

SUMMARY OF EXPERIMENTAL RESULTS - HIGH SPEED MODEL

RUN NO.	WING	NACELLE	WINGTIP	BEHAVIOR*/f (HZ.)	DYNAMIC PRESSURE (LB/FT^2)	MACH	SPEED (FT/SEC)	DENSITY ($SLUGS/FT^3$)	REYNOLDS NUMBER/ FT X 10^{-6}
12	FULL	NOM	NOM	NO FLUTTER	158.0	.900	442.3	.001596	2 816
13	↓	↓	↓	FLUTTER (23.5)	206.2	.840	411.4	.002350	3.732
14	↓	↓	WINGLET (20°)	FLUTTER (19.5,18.5)	97.2	.856	420.6	.001077	1 794
15	↓	↓	↓	LOW DAMPING (20.0,19.5)	128.5	.790	392.9	.001648	2 532
16	↓	↓	↓	FLUTTER (24.5)	161.7	.730	350.0	.002428	3.299
17	↓	↓	↓	FLUTTER (26.0)	171.7	.640	320.3	.003287	4.053
18	↓	↓	BALLAST	NO FLUTTER	164.1	.864	422.3	.001812	3.098
19	↓	↓	↓	LOW DAMPING (14.5)	189.7	.820	406.6	.002258	3.622
36	EMPTY	↓	WINGLET (0°)	NO FLUTTER	79.8	.860	426.6	.000370	1 468
37	↓	↓	↓	FLUTTER (18.0)	106.0	.815	404.8	.001283	2 030
38	↓	↓	↓	FLUTTER (18.0)	122.0	.760	374.1	.001685	2.440
39	↓	↓	↓	FLUTTER (17.8,20.0)	154.0	.640	322.3	.002915	3 602

* HR - HIGH RESPONSE
NVB - NACELLE VERTICAL BENDING
WB2 - 2ND WING BENDING

NOTE: COEFFICIENT OF VISCOSITY, μ(SLUGS/FT-SEC) VARIED FROM .24 X 10^{-6} TO .26 X 10^{-6}